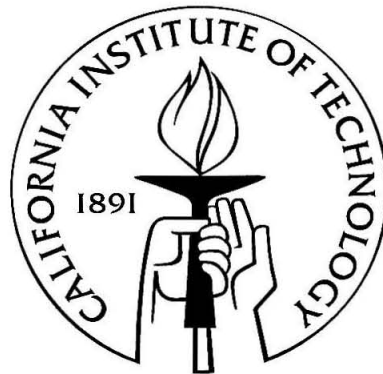


Topics in general relativity: binary black holes and hyperbolic formulations of Einstein's equations

Thesis by
Kashif Alvi

In Partial Fulfillment of the Requirements
for the Degree of
Doctor of Philosophy



California Institute of Technology
Pasadena, California

2002
(Defended 21 May 2002)

Acknowledgements

First and foremost, I would like to thank my parents Farhat and Mohammed Siddiq Alvi for their support and encouragement over the years, and especially for teaching me what is truly important in life. They have imprinted me with their high standards for personal conduct and achievement. They have always encouraged me to pursue my interests and dreams.

I am grateful to my advisor Kip Thorne for his guidance and support, and for providing a fruitful research environment. I am indebted to Lee Lindblom for suggesting the direction for the final research project in this thesis, and for guidance during its completion. I have collaborated with and benefited from discussions with Scott Hughes, Yuk Tung Liu, Arkadas Ozakin, Jongwon Park, and Mark Scheel.

For enriching my life with companionship, support, and sympathy, I would like to thank my brothers Rashid and Yasir, my sister Mariam, and my friends Paveljit Bindra, Dane Boysen, Nancy Chang, Lisa Cowan, Donhee Ham, Saleem Mukhtar, Ajit Pai, Florian Pintgen, Rajat Rohatgi, Pururav Thoutireddy, and Michele Vallisneri. The times we have shared are perhaps the most valuable part of my graduate experience.

Abstract

This thesis consists of three projects in general relativity on topics related to binary black holes and the gravitational waves they emit. The first project involves calculating a four-metric that is an approximate solution to Einstein's equations representing two widely separated nonrotating black holes in a circular orbit. This metric is constructed by matching a post-Newtonian metric to two tidally distorted Schwarzschild metrics using the framework of matched asymptotic expansions. The four-metric presented here provides physically realistic initial data that are tied to the binary's inspiral phase and can be evolved numerically to determine the gravitational wave output during the late stages of inspiral as well as the merger.

The second project is on the tidal interaction of binary black holes during the inspiral phase. The holes' tidal distortion results in the flow of energy and angular momentum into or out of the holes in a process analogous to Newtonian tidal friction in a planet-moon system. The changes in the black holes' masses, spins, and horizon areas during inspiral are calculated for a circular binary with holes of possibly comparable masses. The absorption or emission of energy and angular momentum by the holes is shown to have a negligible influence on the binary's orbital evolution when the holes have comparable masses. The tidal-interaction analysis presented in this thesis is applicable to a black hole in a binary with any companion body (e.g., a neutron star) that is well separated from the hole.

The final project is on first-order hyperbolic formulations of Einstein's equations, which are promising as a basis for numerical simulation of binary black holes. This thesis presents two first-order symmetrizable hyperbolic systems that include the lapse and shift as dynamical fields and have only physical characteristic speeds. The first system may be useful in numerical work; the second system allows one to show that any solution to Einstein's equations in any gauge can be obtained using hyperbolic evolution of the entire metric, including the gauge fields.

Contents

Acknowledgements	iii
Abstract	iv
1 Introduction	1
1.1 Bibliography	5
2 An approximate binary black hole metric	7
2.1 Introduction	7
2.2 Near zone and radiation zone metrics	9
2.2.1 Binary system parameters	9
2.2.2 Demarcation of four regions in spacetime	10
2.2.3 Near zone metric in harmonic coordinates	11
2.2.4 Near zone metric in corotating coordinates	12
2.2.5 Radiation zone metric in harmonic coordinates	13
2.2.6 Radiation zone metric in corotating coordinates	15
2.3 Tidal deformation of the first black hole	16
2.3.1 Tidal fields of the companion black hole	17
2.3.2 Schwarzschild perturbation	21
2.4 Distorted black hole metrics in corotating coordinates	24
2.4.1 Buffer zone coordinate transformation	24
2.4.2 Internal metric in corotating coordinates	29
2.4.3 Metric near the second black hole	31
2.5 Results and discussion	32
2.6 Bibliography	34
3 Ingoing coordinates for binary black holes	36
3.1 Introduction	36
3.2 Ingoing coordinates	37

3.3	Transformation to corotating coordinates	39
3.4	Bibliography	42
4	Energy and angular momentum flow into a black hole in a binary	43
4.1	Introduction	43
4.2	Framework	45
4.3	Stationary companion	46
4.4	Equatorial orbits	48
4.4.1	Instantaneous rates	49
4.4.2	Total changes during inspiral	50
4.4.3	Effect on orbital evolution	52
4.5	Non-equatorial orbits	54
4.5.1	Description of orbit	54
4.5.2	Approximation scheme	55
4.5.3	Orbit-averaged quantities	56
4.6	Discussion	57
4.7	Bibliography	58
5	First-order symmetrizable hyperbolic formulations of Einstein's equations including lapse and shift as dynamical fields	60
5.1	Introduction	60
5.2	System I	62
5.2.1	Fischer-Marsden system	62
5.2.2	Generalized harmonic coordinates	63
5.2.3	System I	65
5.2.4	Initial data	65
5.2.5	Hyperbolicity of system I	67
5.3	System II	68
5.4	Future directions	71
5.5	Bibliography	72

List of Figures

- 2.1 Schematic illustration of the various regions in the binary black hole spacetime. Regions I, II, III, and IV are demarcated by solid lines; the buffer zones are bounded by dashed lines. 11

List of Tables

2.1	Errors and discontinuities in the metric components in corotating coordinates. Numbers denote orders in $\epsilon = (m/b)^{1/2}$; e.g., 4 denotes $O(\epsilon^4)$. The last two columns contain normalized errors.	34
4.1	Normalized change $\Delta S_1/M_1^2$ in spin evaluated at $b/M=100, 20$, and 6 for an equal-mass binary with $\hat{\mathbf{L}}_N \cdot \hat{\mathbf{S}}_1 = 1$. For rapidly rotating holes ($\chi_1 = \chi_2 = 0.998$), this change is also evaluated at $b/M = 2$	52
4.2	Normalized change $\Delta M_1/M_1$ in mass evaluated at $b/M=100, 20$, and 6 for an equal-mass binary with $\hat{\mathbf{L}}_N \cdot \hat{\mathbf{S}}_1 = 1$. For rapidly rotating holes ($\chi_1 = \chi_2 = 0.998$), this change is also evaluated at $b/M = 2$	52
4.3	Normalized change $\Delta A_1/A_1$ in horizon area evaluated at $b/M=100, 20$, and 6 for an equal-mass binary with $\hat{\mathbf{L}}_N \cdot \hat{\mathbf{S}}_1 = 1$. For rapidly rotating holes ($\chi_1 = \chi_2 = 0.998$), this change is also evaluated at $b/M = 2$	52
4.4	Change ΔN in the number of gravitational-wave cycles due to black hole absorption/emission, for various values of total mass M and mass ratio M_1/M_2 . The initial separation is such that the wave frequency is 10 Hz and the spins satisfy $\chi_1 = \chi_2 = 0.998$ and $\hat{\mathbf{L}}_N \cdot \hat{\mathbf{S}}_1 = \hat{\mathbf{L}}_N \cdot \hat{\mathbf{S}}_2 = 1$. The numbers without parentheses are for a final separation b_f of $6M$; those with parentheses are for b_f equal to the larger of $2M$ or the separation at which the wave frequency is 1000 Hz.	53

Chapter 1

Introduction

The central theme in this thesis is binary black holes. The exact evolution of these binaries is still an unsolved problem in general relativity. Solution of this two-body problem is important not only as a matter of principle, but also as a practical concern. A full solution of the problem will not only give insights into Einstein's theory of gravitation, but also provide gravitational waveforms that will be used in several stages of data analysis for gravitational wave detectors such as the Laser Interferometer Gravitational-Wave Observatory (LIGO) and the Laser Interferometer Space Antenna (LISA). Since binary black holes are expected to be among the primary sources of gravitational waves for these interferometric detectors, it is important to try to solve this problem using all available techniques, including approximate analytical methods and numerical simulations.

One regime in which the evolution of binary black holes is well understood is the early inspiral phase. In this phase, the holes' separation is still much larger than the binary's total mass, and post-Newtonian expansions can be used to analyze the system. Eventually radiation reaction drives the holes together and the post-Newtonian approximation fails. The binary's subsequent evolution must be studied numerically. As the holes merge and begin to settle down into a stationary final state, black hole perturbation theory becomes increasingly effective in describing the dynamics. The approximate analytical techniques of post-Newtonian expansions and black hole perturbation theory, which are applicable before and after the merger, will have to be combined with numerical simulations of the merger to yield complete waveforms for binary black hole coalescences.

The research work done for this thesis is motivated by the need to calculate the gravitational wave output from binary black holes. The main chapters of this thesis deal with various aspects of these binaries. Chapter 2 is concerned with the interface between the post-Newtonian inspiral and the fully nonlinear merger. It has been argued [1] that post-Newtonian expansions begin to fail during the late stages of inspiral, before the black holes begin to merge. The gap between the failure of post-Newtonian expansions and merger has been called the intermediate binary black hole region. This gap consists of approximately 10–20 orbits and 100–250 radians of gravitational-wave phase [1]. For binaries with total mass approximately $20 M_{\odot}$, the intermediate binary black hole

region lies in the frequency band of optimal LIGO sensitivity [1]. Since binaries with total mass in the range $10\text{--}40 M_{\odot}$ are most likely to be the first detected by LIGO [1], it is important to come up with techniques to fill in the intermediate binary black hole gap.

Numerical solution of this problem will require initial data that accurately represent binary black holes that have spiraled in from large separation. Furthermore, these initial data will have to be linked to the early inspiral phase of the binary and to the binary's initial parameters (e.g., masses and spins) during this phase. Post-Newtonian expansions alone are not capable of providing such initial data because they treat the two bodies as point particles. These expansions do not take into account the spacetime structure near the black holes' horizons. Furthermore, the initial data being used currently in numerical simulations (see [2] for a recent review; see also [3]) are not astrophysically realistic: these data typically depend on unphysical assumptions on the metric such as conformal flatness for the spatial metric. As a result, these data contain spurious gravitational wave energy of the order of the total energy radiated to infinity during coalescence [3]. These data also contain spurious deformations of the black holes, which will lead to black hole pulsations. A different method is therefore required to provide initial data at the interface between the post-Newtonian inspiral and the fully nonlinear merger.

In Chapter 2, I present such a method. I derive a 4-metric that is an approximate solution to Einstein's equations representing two widely separated nonrotating black holes in a circular orbit. This metric is constructed by matching a post-Newtonian metric to two perturbed Schwarzschild metrics using the framework of matched asymptotic expansions. The spacetime metric is presented in a single corotating coordinate system that covers the radiation and near zones as well as the regions near the black holes, up to their apparent horizons. In Chapter 3, I define an ingoing coordinate transformation that extends this corotating coordinate system through the holes' horizons and into their interiors. The motivation for using ingoing coordinates is that numerical simulations of black holes require the computational grid to extend inside the horizons. Thus, the coordinate system used near the black holes in Chapter 2 is not suitable for numerical relativity.

Initial data extracted from the binary black hole 4-metric presented in Chapters 2 and 3 have the advantages of being linked to the early inspiral phase of the binary system, and of not containing spurious gravitational waves or spurious deformation of the black holes. Besides providing initial data, this 4-metric serves as a check on the early stages of numerical evolution of these data. Plans are underway to implement and evolve these initial data in collaboration with L. Kidder, H. Pfeiffer, and M. Scheel. These three individuals are developing a numerical platform, based on pseudospectral collocation methods, that includes a nonlinear elliptic solver [4] to handle the constraint equations (which are a subset of the Einstein equations that only involve the intrinsic and extrinsic geometry of a hypersurface of constant time) and a first-order hyperbolic evolution code [5] for the dynamical Einstein equations (which specify the time evolution of this intrinsic and extrinsic geometry).

Hyperbolic systems will be discussed in further detail below.

It should be kept in mind that the 4-metric presented in Chapters 2 and 3 is an approximate solution to Einstein's equation, and the approximation gets worse as the ratio of the binary's total mass to the holes' separation gets larger. A complete error analysis on the metric is given in Chapter 2. The accuracy of the metric can be improved by restricting to large separations relative to total mass (note that the code being developed by Kidder, Pfeiffer, and Scheel can handle these large separations because pseudospectral collocation techniques require far fewer spatial grid points than straightforward finite difference techniques), or by taking the calculation in Chapters 2 and 3 to higher order.

Chapter 4 examines the tidal interaction of binary black holes during the inspiral phase. As the holes spiral in, they distort each other with their tidal fields. This distortion causes the holes' horizon areas to increase slowly during inspiral, and results in the flow of energy and angular momentum into or out of the holes. This process is analogous to Newtonian tidal friction in a planet-moon system [6–9]. The tidal-interaction analysis of Chapter 4 is applicable to a black hole in a binary with any companion body (e.g., a neutron star) that is well separated from the hole. The changes in the black hole's mass, spin, and horizon area during inspiral are calculated for a hole in a circular binary with a companion body of possibly comparable mass.

The orbital evolution of binary black holes is affected by the absorption/emission of energy and angular momentum by the holes. In particular, the number of orbits—and hence the number of gravitational-wave cycles emitted to infinity—changes when black hole absorption/emission is accounted for. In Chapter 4, this effect is estimated for a circular, nearly Newtonian binary with spins aligned or anti-aligned with the orbital angular momentum. The binary is assumed to lose orbital energy and angular momentum to infinity via Newtonian quadrupole radiation, and to the black holes via tidal interaction. The conclusion in Chapter 4 is that black hole absorption/emission of energy and angular momentum during inspiral may not be an important effect for the detection (by LIGO) and analysis of gravitational waves from comparable-mass black holes. However, in the extreme-mass-ratio limit, black hole absorption/emission can strongly influence the binary's orbital evolution and thus is an important effect for LISA [10].

The results in Chapter 4 also provide some information on the interface between the inspiral and merger phases of binary evolution. As mentioned above, current numerical simulations of binary black holes use initial data that are not tied to the inspiral phase and to the post-Newtonian expansions used to describe it. Therefore, one needs to relate the masses, spins, and horizon areas of the black holes present in currently used initial data to the corresponding quantities when the holes were infinitely separated. For this purpose, it is necessary to know how these quantities change during inspiral. The changes in the holes' masses, spins, and horizon areas during inspiral are calculated for a circular binary in Chapter 4.

The final chapter of this thesis is concerned with first-order hyperbolic formulations of Einstein's equations, which are promising as a basis for numerical simulation of binary black holes. The basic framework for the theory of first-order hyperbolic systems is as follows. Consider a system of equations of the form

$$\partial_t u + A^i(t, x^j, u) \partial_i u = F(t, x^j, u),$$

where u is a column vector composed of the unknown fields (which could include metric components and extrinsic curvature components, for example), and the matrices A^i and column vector F can depend on space and time and on the fields but not their derivatives. Pick a unit spatial covector ξ_i and compute the eigenvalues λ of the matrix $A^i \xi_i$; λ are the characteristic speeds in the direction ξ_i . If all the eigenvalues are real for each ξ_i , then the system is called weakly hyperbolic. If in addition, $A^i \xi_i$ has a complete set of eigenvectors for each ξ_i , the system is called strongly hyperbolic. If the matrices A^i are symmetric, the system is called symmetric hyperbolic. If there is a positive definite symmetric matrix H such that HA^i are symmetric, the system is called symmetrizable hyperbolic. The initial value problem is well posed for strongly, symmetric, and symmetrizable hyperbolic systems—that is, for these systems the problem has a unique solution that depends continuously on the initial data [11]. The initial value problem is not well posed for weakly hyperbolic systems [11].

First-order hyperbolic systems have been used in the past to prove that general relativity has a well-posed initial value formulation [12, 13]. There has been considerable interest recently in these systems because of the advantages they offer to numerical simulations [14, 15]. The main advantage is that imposing physical boundary conditions is much easier in the framework of a hyperbolic system than a non-hyperbolic one. This is especially true for boundary conditions inside a black hole horizon [14, 15]. Indeed, if the hyperbolic system has only physical characteristic speeds—that is, if the characteristic fields propagate only on the light cones of spacetime or normal to the hypersurfaces of constant time—then the boundary condition inside the horizon on fields propagating into the numerical grid has no effect on the dynamics outside the horizon. Therefore, in this case, any convenient boundary condition can be imposed inside the horizon. This is a significant advantage when simulating black holes.

Numerical solution of Einstein's equations is typically done in the framework of a 3+1 split of spacetime (see, e.g., [16, 17]). In this framework, spacetime is foliated by spacelike hypersurfaces that represent constant time slices. The spacetime metric is expressed as

$$g_{\mu\nu} = \begin{pmatrix} -\alpha^2 + \beta_k \beta^k & \beta_j \\ \beta_i & \gamma_{ij} \end{pmatrix},$$

where α is the lapse, β^i is the shift, γ_{ij} is the spatial 3-metric on the constant time hypersurfaces,

and $\beta_i = \gamma_{ij}\beta^j$. The lapse and shift can be freely chosen when evolving initial data, and are therefore called gauge fields. Freedom in choosing these gauge fields, i.e., gauge freedom, corresponds to freedom in choosing coordinates for spacetime. This freedom can be used in numerical evolutions for a variety of purposes, e.g., to prevent the occurrence of coordinate singularities [18], to reduce coordinate shear [18], and to adapt the coordinate system to the particular problem under consideration. When simulating black holes, it is helpful to choose the shift so that numerical grid points do not fall into the holes. When simulating binary black holes, it may be advantageous to implement gauge conditions which generate corotating coordinates [1, 19].

In previous work, the gauge fields have typically not been considered part of the hyperbolic system and have been prescribed independently. Some of the favored gauge prescriptions in numerical relativity [18, 19] require solution of elliptic equations for the lapse and shift, which is expensive computationally. It would be more efficient to evolve the gauge fields as part of the hyperbolic system. However, it is important to keep some freedom in choosing the gauge in order to allow the coordinates to be adapted to fit specific needs. In Chapter 5, I present two first-order symmetrizable hyperbolic systems for Einstein's equations which include the lapse and shift as dynamical fields and allow four functions of spacetime to be specified freely in the gauge prescription. The first hyperbolic system is a modification and generalization of the work of Fischer and Marsden [12]; this system uses generalized harmonic coordinates and evolves 50 fields. It is promising as a basis for numerical work. The second system is based on the work of Kidder, Scheel, and Teukolsky [5] and Lindblom and Scheel [20]; it evolves 70 fields. This system is not practical for numerical implementation. Its main use is theoretical: it allows one to show that any solution to Einstein's equations in any gauge can be obtained using hyperbolic evolution of the entire metric, including the gauge fields. Both systems have only physical characteristic speeds.

An important future research direction is to study and understand the stability of numerical implementations of the first hyperbolic system presented in Chapter 5. It has been shown in previous work [5] that some hyperbolic systems are more stable than others when used to simulate black holes in three spatial dimensions. The reasons for this behavior are not yet understood. Another future research direction is to explore how to use the freedom in gauge choice in the first hyperbolic system of Chapter 5 to control the coordinate system.

1.1 Bibliography

- [1] P. R. Brady, J. D. E. Creighton, and K. S. Thorne, *Phys. Rev. D* **58**, 061501 (1998).
- [2] G. B. Cook, *Living Rev. Relativity* **3** (2000), [Online article]: cited on 3 May 2002, URL <http://www.livingreviews.org/Articles/Volume3/2000-5cook/>.

- [3] H. P. Pfeiffer, G. B. Cook, and S. A. Teukolsky, gr-qc/0203085.
- [4] H. P. Pfeiffer, L. E. Kidder, M. A. Scheel, and S. A. Teukolsky, gr-qc/0202096.
- [5] L. E. Kidder, M. A. Scheel, and S. A. Teukolsky, *Phys. Rev. D* **64**, 064017 (2001).
- [6] S. W. Hawking and J. B. Hartle, *Commun. Math. Phys.* **27**, 283 (1972).
- [7] J. B. Hartle, *Phys. Rev. D* **8**, 1010 (1973).
- [8] J. B. Hartle, *Phys. Rev. D* **9**, 2749 (1974).
- [9] *Black Holes: The Membrane Paradigm*, edited by K. S. Thorne, R. H. Price, and D. A. Macdonald (Yale University Press, New Haven, 1986).
- [10] S. A. Hughes, *Phys. Rev. D* **64**, 064004 (2001).
- [11] B. Gustafsson, H.-O. Kreiss, and J. Olinger, *Time Dependent Problems and Difference Methods* (Wiley, New York, 1995).
- [12] A. E. Fischer and J. E. Marsden, *Commun. Math. Phys.* **28**, 1 (1972).
- [13] H. Friedrich, *Commun. Math. Phys.* **100**, 525 (1985).
- [14] H. Friedrich, *Class. Quantum Grav.* **13**, 1451 (1996).
- [15] A. Anderson and J. W. York, *Phys. Rev. Lett.* **82**, 4384 (1999).
- [16] C. W. Misner, K. S. Thorne, and J. A. Wheeler, *Gravitation* (Freeman, San Francisco, 1973).
- [17] J. W. York, in *Sources of Gravitational Radiation*, edited by L. L. Smarr (Cambridge University Press, Cambridge, 1979), p. 83.
- [18] L. Smarr and J. W. York, *Phys. Rev. D* **17**, 2529 (1978).
- [19] D. Garfinkle, C. Gundlach, J. Isenberg, and N. ÓMurchadha, *Class. Quantum Grav.* **17**, 3899 (2000).
- [20] L. Lindblom and M. Scheel, in preparation.

Chapter 2

An approximate binary black hole metric

Published as K. Alvi, *Phys. Rev. D* **61**, 124013 (2000).

Abstract

An approximate solution to Einstein's equations representing two widely separated nonrotating black holes in a circular orbit is constructed by matching a post-Newtonian metric to two perturbed Schwarzschild metrics. The spacetime metric is presented in a single coordinate system valid up to the apparent horizons of the black holes. This metric could be useful in numerical simulations of binary black holes. Initial data extracted from this metric have the advantages of being linked to the early inspiral phase of the binary system, and of not containing spurious gravitational waves.

2.1 Introduction

One of the outstanding issues in gravitational wave research is calculating the wave output from the last stages of inspiral of binary black holes. This intermediate binary black hole problem has been discussed by Brady, Creighton, and Thorne [1]. The purpose of this paper is to provide an approximate four-dimensional binary black hole metric from which initial data can be extracted and evolved numerically into and through the intermediate binary black hole region.

The approach I take is based on the work of Manasse [2] and D'Eath [3, 4]. I consider two widely separated nonrotating black holes in a circular orbit. The black holes' mass ratio is not restricted—they can have comparable masses. However, the masses are assumed to be much smaller than the distance between them¹. As a result spacetime can be divided into four regions, each with its own approximation scheme to solve Einstein's equations. There is a strong-gravity region near each of the black holes which is described by the Schwarzschild solution plus a perturbation due to the companion's tidal field. This perturbation is constrained to satisfy the linearized Einstein equations

¹Throughout this paper I use geometrized units in which $G = c = 1$.

about the Schwarzschild metric. The companion black hole's electric-type and magnetic-type tidal fields are both taken into account in calculating the perturbation.

Outside the strong-gravity regions but within the near zone, the metric can be approximated by a post-Newtonian expansion. Further out is the radiation zone which contains outgoing gravitational waves and can be described by a post-Minkowski expansion of the metric.

There are overlap zones in this spacetime where the regions described above intersect in pairs. In the overlap zones, two different approximation schemes—one from each of the two intersecting regions—are both valid. The perturbative expansions produced by the two approximation schemes are matched in the overlap zones using the framework of matched asymptotic expansions. The post-Newtonian near-zone metric—taken from [5]—and the radiation-zone metric—taken from [6]—already match in their overlap region. In this paper, the post-Newtonian near-zone metric is matched to a perturbed Schwarzschild metric in the matching or buffer zone surrounding each black hole. This yields information on the asymptotic behavior of the Schwarzschild perturbation at large distances from the horizon, and on the coordinate transformation between the two buffer-zone coordinate systems.

The Schwarzschild perturbation and coordinate transformation are not uniquely determined. However, a different choice of transformation, and hence a different form of Schwarzschild perturbation, should still represent the same physical situation. In other words, different perturbations that match to the post-Newtonian near-zone metric are expected to be related via gauge transformations. For the purposes of this paper, it is sufficient to find one transformation and one Schwarzschild perturbation associated with each black hole that result in a match between the post-Newtonian near-zone metric and the distorted-black-hole metrics.

An approximate spacetime metric is put together by joining the regional metrics at some specific 3-surfaces in the matching zones. The final 4-metric is written in a single coordinate system valid up to (but not inside) the apparent horizons of the black holes. This metric is useful not only as a source of initial data for numerical evolution, but also as a check on the early stages of such an evolution.

It has been suggested that numerical simulation of binary black holes should be performed in corotating coordinates [1]. For this reason the metric in final form is given in corotating coordinates. The binary black hole spacetime can be sliced and spatial coordinates chosen in any convenient way when extracting initial data from the metric. (Asymptotically inertial coordinates can be used, for example.)

Initial data generated by the method presented in this paper have the advantage of being connected to the early inspiral phase of the binary black holes. Detailed gravitational waveforms from this early inspiral phase have already been calculated using post-Newtonian expansions. These waveforms will be easily linked to the waveforms obtained by evolving initial data extracted from

the metric presented here.

Initial data from this metric have the additional advantages of not containing spurious gravitational waves and of reliably describing the physical situation of coalescing binary black holes. The accuracy of this description can be improved by taking the calculation in this paper to higher orders.

In Sec. 2.2, the near-zone and radiation-zone metrics are written down. In Sec. 2.3, the first black hole’s tidal deformation is calculated. In Sec. 2.4, the buffer-zone coordinate transformations are determined, and the distorted-black-hole metrics are written in corotating post-Newtonian coordinates. The full spacetime metric is summarized in Sec. 2.5.

2.2 Near zone and radiation zone metrics

Blanchet and collaborators ([7] and references therein) and Will and Wiseman [6] have calculated in detail the near-zone and radiation-zone gravitational fields of compact binary systems. The approach taken by Will and Wiseman is particularly useful here because they use a single coordinate system—harmonic coordinates—to cover both the near zone and the radiation zone. As a result, expressions for the radiation-zone metric components taken from [6] automatically match (to some finite order) the harmonic-coordinate, post-Newtonian, near-zone metric components calculated in [5]. For this reason I work initially in harmonic coordinates (t', x', y', z') with the origin of the spatial coordinates placed at the binary system’s center of mass. I use only the first post-Newtonian (1PN) metric, not the full 2.5PN metric given in [5]². Consistently with this, I put the black holes on Newtonian trajectories: they are taken to be in circular orbits with Keplerian orbital angular velocities. Moreover, I use the post-Newtonian metric for point-like particles; in the near zone, I ignore the black holes’ internal structure. The near-zone gravitational effects of the black holes’ multipole moments can in principle be computed by matching out to the near zone the tidally-distorted Schwarzschild metrics obtained in this paper. However, these effects are too small to be included in this paper; this is discussed further in Sec. 2.4.2.

2.2.1 Binary system parameters

Label the black holes BH1 and BH2, and let m_1 and m_2 be their respective masses. Define

$$m = m_1 + m_2, \quad \delta m = m_1 - m_2, \quad \mu = \frac{m_1 m_2}{m}. \quad (2.1)$$

Denote the harmonic-coordinate trajectories of the black holes by $x_A^j(t')$ for $A = 1, 2$ and $j = 1, 2, 3$. In other words, $x_A^j(t')$ are the spatial coordinates at time t' of the center of attraction of the gravitational field of black hole A .

²Higher order versions of this calculation will presumably use higher order post-Newtonian metrics.

In this section, boldface letters are used to denote spatial coordinates. For example $\mathbf{x}_A = (x_A^1, x_A^2, x_A^3) = (x_A, y_A, z_A)$. The notation $\mathbf{a} \cdot \mathbf{b}$ is used for the quantity $\delta_{jk} a^j b^k$, and $|\mathbf{a}|$ is by definition $(\mathbf{a} \cdot \mathbf{a})^{1/2}$.

Denote the black holes' separation $|\mathbf{x}_1 - \mathbf{x}_2|$ by b . The circular, Newtonian trajectories of the black holes are

$$\mathbf{x}_1(t') = \frac{m_2}{m} \mathbf{b}(t'), \quad \mathbf{x}_2(t') = -\frac{m_1}{m} \mathbf{b}(t'), \quad (2.2)$$

where

$$\mathbf{b}(t') = \mathbf{x}_1(t') - \mathbf{x}_2(t') = b(\cos \omega t', \sin \omega t', 0) \quad (2.3)$$

and

$$\omega = \sqrt{\frac{m}{b^3}} \quad (2.4)$$

is the Keplerian orbital angular velocity. Define

$$\begin{aligned} \epsilon &= \sqrt{\frac{m}{b}}, & r &= (x'^2 + y'^2 + z'^2)^{1/2}, \\ r_A &= |\mathbf{x}' - \mathbf{x}_A|, & \mathbf{n}_A &= \frac{\mathbf{x}' - \mathbf{x}_A}{r_A}, \\ \mathbf{v}_A &= \frac{d\mathbf{x}_A}{dt'}, & v_A &= |\mathbf{v}_A|, \\ \mathbf{v} &= \mathbf{v}_1 - \mathbf{v}_2 = \epsilon(-\sin \omega t', \cos \omega t', 0), \end{aligned} \quad (2.5)$$

for $A = 1, 2$. By assumption, $\epsilon \ll 1$.

2.2.2 Demarcation of four regions in spacetime

Let us first fix precisely four regions in this binary black hole spacetime; each of these regions will receive a metric calculated as an approximate solution to the Einstein equations. With such a partition of spacetime in mind, define the inner limits $r_1^{in} = \sqrt{m_1 b}$ and $r_2^{in} = \sqrt{m_2 b}$. These are just convenient choices for the inner limits. The important property r_1^{in} has is that both $r_1^{in}/b \rightarrow 0$ and $m_1/r_1^{in} \rightarrow 0$ as $m_1/b \rightarrow 0$. Similarly $r_2^{in}/b \rightarrow 0$ and $m_2/r_2^{in} \rightarrow 0$ as $m_2/b \rightarrow 0$. Also define the outer limit $r^{out} = \lambda_c/2\pi = b/2\epsilon$, where $\lambda_c = \pi/\omega$ is the characteristic wavelength of gravitational radiation emitted by the binary system.

Divide spacetime into four regions that are bounded by the black holes' apparent horizons and the surfaces $r_1 = r_1^{in}$, $r_2 = r_2^{in}$, and $r = r^{out}$: (i) the region $r_1 < r_1^{in}$ (but outside the apparent horizon of BH1), labeled region I; (ii) the region $r_2 < r_2^{in}$ (but outside the apparent horizon of BH2), labeled region II; (iii) the subset of the near zone specified by $r_1 > r_1^{in}$, $r_2 > r_2^{in}$, and $r < r^{out}$, labeled region III; and (iv) the region $r > r^{out}$, labeled region IV. The near zone contains region

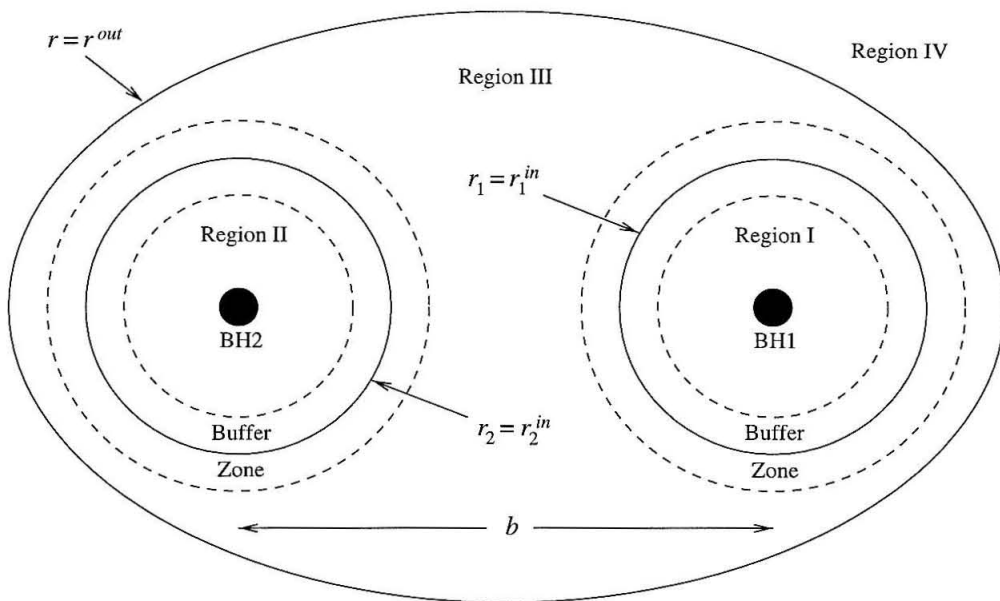


Figure 2.1: Schematic illustration of the various regions in the binary black hole spacetime. Regions I, II, III, and IV are demarcated by solid lines; the buffer zones are bounded by dashed lines.

III and overlaps with regions I and II; the radiation zone corresponds to region IV. The buffer zone around black hole A contains $r_A = r_A^{in}$ and satisfies $m_A \ll r_A \ll b$. These regions of spacetime are illustrated in Fig. 2.1.

2.2.3 Near zone metric in harmonic coordinates

In the near zone, the 1PN harmonic-coordinate metric with two point-like particles representing the black holes is [5]

$$\begin{aligned}
 g_{0'0'} &= -1 + \frac{2m_1}{r_1} + \frac{2m_2}{r_2} - 2 \left(\frac{m_1}{r_1} + \frac{m_2}{r_2} \right)^2 + \frac{m_1}{r_1} [4v_1^2 - (\mathbf{n}_1 \cdot \mathbf{v}_1)^2] + \frac{m_2}{r_2} [4v_2^2 - (\mathbf{n}_2 \cdot \mathbf{v}_2)^2] \\
 &\quad - 2 \frac{m_1 m_2}{b} \left(\frac{1}{r_1} + \frac{1}{r_2} \right) + \frac{m_1 m_2}{b^3} \mathbf{b} \cdot (\mathbf{n}_1 - \mathbf{n}_2), \\
 g_{0'i'} &= -4 \left(\frac{m_1}{r_1} v_1^i + \frac{m_2}{r_2} v_2^i \right), \\
 g_{i'j'} &= \delta_{ij} \left(1 + \frac{2m_1}{r_1} + \frac{2m_2}{r_2} \right). \tag{2.6}
 \end{aligned}$$

This metric presumably differs in the near zone by a small amount from an exact solution to the Einstein equations representing binary black holes. I take the neglected terms in the 2.5PN metric [5] to be an estimate of the errors in the 1PN metric (2.6).

The largest neglected terms in $g_{0'0'}$ are of the form $m^3/b^2 r_A$, $m^3/b r_A^2$, m_A^3/r_A^3 , m^3/b^3 , and $\epsilon m^3 r^2/b^5$. (The last term represents a radiation reaction potential.) Let us compute the orders of

magnitude of these terms at various places in region III. If $r_A \gtrsim r_A^{in} \sim b\epsilon$ (here and henceforth “ \sim ” means “is of the order of” and $a \gtrsim b$ means $a > b$ and $a \sim b$) for $A = 1$ or 2 , then the error in $g_{0'0'}$ (denoted $\delta g_{0'0'}$) is of $O(\epsilon^3)$ and comes from neglecting a term of the form m_A^3/r_A^3 . If both $r_1 \sim b$ and $r_2 \sim b$, then $\delta g_{0'0'} \sim \epsilon^6$. Finally, if $r \lesssim r^{out} \sim b/\epsilon$ (so that $r_A \sim b/\epsilon$ for $A = 1$ and 2), then the error $\delta g_{0'0'} \sim \epsilon^5$ arises from neglecting the radiation reaction potential. Note that it is reasonable to consider the “absolute” errors $\delta g_{\mu'\nu'}$ in the metric components since the coordinate system being used is asymptotically inertial and the errors are only calculated in regions of weak gravity where deviations from a flat metric are small.

A similar analysis for $g_{0'i'}$ yields $\delta g_{0'i'} \sim \epsilon^3$ if $r_A \gtrsim r_A^{in}$ for $A = 1$ or 2 , $\delta g_{0'i'} \sim \epsilon^5$ if both $r_1 \sim b$ and $r_2 \sim b$, and $\delta g_{0'i'} \sim \epsilon^5$ if $r \lesssim r^{out}$. Lastly, $\delta g_{i'j'}$ $\sim \epsilon^2$ if $r_A \gtrsim r_A^{in}$ for $A = 1$ or 2 (this comes from neglecting a term of the form m_A^2/r_A^2 in $g_{i'j'}$), $\delta g_{i'j'} \sim \epsilon^4$ if both $r_1 \sim b$ and $r_2 \sim b$, and $\delta g_{i'j'} \sim \epsilon^5$ if $r \lesssim r^{out}$.

2.2.4 Near zone metric in corotating coordinates

The metric (2.6) is transformed to corotating coordinates (t, x, y, z) defined by

$$\begin{aligned} t' &= t, & x' &= x \cos \omega t - y \sin \omega t, \\ y' &= x \sin \omega t + y \cos \omega t, & z' &= z. \end{aligned} \quad (2.7)$$

In terms of the new coordinates,

$$r = (x^2 + y^2 + z^2)^{1/2}. \quad (2.8)$$

Putting the expressions (2.2)–(2.5) in Eq. (2.6) and transforming to corotating coordinates gives

$$\begin{aligned} ds^2 &= dt^2 \left[-1 + \frac{2m_1}{r_1} + \frac{2m_2}{r_2} - 2 \left(\frac{m_1}{r_1} + \frac{m_2}{r_2} \right)^2 + \frac{3\mu}{b} \left(\frac{m_2}{r_1} + \frac{m_1}{r_2} \right) - \frac{\mu}{b} \left(\frac{m_2}{r_1^3} + \frac{m_1}{r_2^3} \right) y^2 \right. \\ &\quad \left. - 2\mu\epsilon^2 \left(\frac{1}{r_1} + \frac{1}{r_2} \right) - 7\mu\epsilon^2 \left(\frac{1}{r_1} - \frac{1}{r_2} \right) \frac{x}{b} + \omega^2 \left(1 + \frac{2m_1}{r_1} + \frac{2m_2}{r_2} \right) (x^2 + y^2) \right] \\ &\quad + 2\omega \left(1 + \frac{2m_1}{r_1} + \frac{2m_2}{r_2} \right) dt(xdy - ydx) - 8\mu\epsilon \left(\frac{1}{r_1} - \frac{1}{r_2} \right) dt dy \\ &\quad + \left(1 + \frac{2m_1}{r_1} + \frac{2m_2}{r_2} \right) (dx^2 + dy^2 + dz^2), \end{aligned} \quad (2.9)$$

where, in terms of the new coordinates, the quantities r_A are

$$\begin{aligned} r_1 &= [(x - m_2 b/m)^2 + y^2 + z^2]^{1/2}, \\ r_2 &= [(x + m_1 b/m)^2 + y^2 + z^2]^{1/2}. \end{aligned} \quad (2.10)$$

This is the final form of the metric in region III. (Note, however, that this metric is valid

throughout the near zone, which includes the buffer zones around the black holes.) It remains to specify the metric in regions I, II, and IV. I postpone until Sec. 2.2.6 discussion of the errors $\delta g_{\mu\nu}$ in the metric components in the new, rotating coordinate system (t, x, y, z) .

2.2.5 Radiation zone metric in harmonic coordinates

The radiation-zone metric can be extracted from [6]. In that paper, a potential $h^{\mu'\nu'}$ is defined by

$$h^{\mu'\nu'} = \eta^{\mu'\nu'} - (-g')^{1/2} g^{\mu'\nu'}, \quad (2.11)$$

where $\eta^{\mu'\nu'} = \text{diag}(-1, 1, 1, 1)$, $g_{\mu'\nu'}$ is the spacetime metric, and $g' = \det(g_{\mu'\nu'})$. Equation (5.5) of [6] gives $h^{\mu'\nu'}$ in the radiation zone in harmonic coordinates (t', x', y', z') for a system of several bodies. After correcting a typo in that equation,³ I specialize to a system of two bodies of masses m_1 and m_2 in a circular orbit specified by Eqs. (2.2)–(2.5). This yields⁴

$$\begin{aligned} h^{0'o'}(t', x', y', z') &= \frac{4\tilde{m}}{r} + \frac{7m^2}{r^2} + 2 \left[\frac{1}{r} Q^{ij}(u') \right]_{,ij} - \frac{2}{3} \left[\frac{1}{r} Q^{ijk}(u') \right]_{,ijk}, \\ h^{0'i'}(t', x', y', z') &= -2 \left\{ \frac{1}{r} \left[\dot{Q}^{ij}(u') - \epsilon^{ijl} J^l(u') \right] \right\}_{,j} + \frac{2}{3} \left\{ \frac{1}{r} \left[\dot{Q}^{ijk}(u') - 2\epsilon^{ikl} J^{lj}(u') \right] \right\}_{,jk}, \\ h^{i'j'}(t', x', y', z') &= \frac{m^2}{r^2} n'^i n'^j + \frac{2}{r} \ddot{Q}^{ij}(u') - \frac{2}{3} \left\{ \frac{1}{r} \left[\ddot{Q}^{ijk}(u') - 4\epsilon^{(i|kl} \dot{J}^{l|j)}(u') \right] \right\}_{,k}, \end{aligned} \quad (2.12)$$

where

$$\tilde{m} = m(1 - \mu/2b), \quad u' = t' - r, \quad \mathbf{n}' = \mathbf{x}'/r \quad (2.13)$$

and

$$\begin{aligned} Q^{ij} &= \sum_{A=1}^2 m_A x_A^i x_A^j = \mu b^i b^j, & Q^{ijk} &= \sum_{A=1}^2 m_A x_A^i x_A^j x_A^k = -\mu(\delta m/m) b^i b^j b^k, \\ J^i &= \sum_{A=1}^2 m_A \epsilon^{ilm} x_A^l v_A^m = \mu \epsilon^{ilm} b^l v^m, & J^{ij} &= \sum_{A=1}^2 m_A \epsilon^{ilm} x_A^l v_A^m x_A^j = -\mu(\delta m/m) \epsilon^{ilm} b^l v^m b^j. \end{aligned} \quad (2.14)$$

Putting the expressions (2.14) in Eq. (2.12) and using Eqs. (2.2)–(2.5) gives

$$\begin{aligned} h^{0'o'} &= \frac{4\tilde{m}}{r} + \frac{7m^2}{r^2} + \frac{2\mu}{r} \left\{ 2(\mathbf{n}' \cdot \mathbf{v})^2 - \frac{2m}{b^3} (\mathbf{n}' \cdot \mathbf{b})^2 + \frac{6}{r} (\mathbf{n}' \cdot \mathbf{b})(\mathbf{n}' \cdot \mathbf{v}) + \frac{1}{r^2} [3(\mathbf{n}' \cdot \mathbf{b})^2 - b^2] \right\} \\ &+ \frac{2\mu}{r} \frac{\delta m}{m} \left\{ \frac{7m}{b^3} (\mathbf{n}' \cdot \mathbf{b})^2 (\mathbf{n}' \cdot \mathbf{v}) - 2(\mathbf{n}' \cdot \mathbf{v})^3 + \frac{1}{r} (\mathbf{n}' \cdot \mathbf{b}) \left[\frac{6m}{b^3} (\mathbf{n}' \cdot \mathbf{b})^2 - 12(\mathbf{n}' \cdot \mathbf{v})^2 - \frac{m}{b} \right] \right. \\ &\left. + \frac{3}{r^2} (\mathbf{n}' \cdot \mathbf{v}) [b^2 - 5(\mathbf{n}' \cdot \mathbf{b})^2] + \frac{1}{r^3} (\mathbf{n}' \cdot \mathbf{b}) [3b^2 - 5(\mathbf{n}' \cdot \mathbf{b})^2] \right\}, \end{aligned}$$

³The term $4m/r'$ in the expression for h^{00} should instead be $4\tilde{m}/r'$.

⁴Note that I have replaced r' in Eq. (5.5) of [6] by r .

$$\begin{aligned}
h^{0'i'} &= \frac{4\mu}{r} \left\{ \left[(\mathbf{n}' \cdot \mathbf{v}) + \frac{1}{r}(\mathbf{n}' \cdot \mathbf{b}) \right] v^i - \frac{m}{b^3}(\mathbf{n}' \cdot \mathbf{b})b^i \right\} \\
&\quad - \frac{2\mu}{r} \frac{\delta m}{m} \left\{ -\frac{m}{b^3}(\mathbf{n}' \cdot \mathbf{b}) [3(\mathbf{n}' \cdot \mathbf{b})v^i + 4(\mathbf{n}' \cdot \mathbf{v})b^i] + 2(\mathbf{n}' \cdot \mathbf{v})^2 v^i \right. \\
&\quad \left. + \frac{1}{r} \left[6(\mathbf{n}' \cdot \mathbf{b})(\mathbf{n}' \cdot \mathbf{v})v^i - \frac{3m}{b^3}(\mathbf{n}' \cdot \mathbf{b})^2 b^i + \frac{m}{b} b^i \right] + \frac{1}{r^2} [3(\mathbf{n}' \cdot \mathbf{b})^2 - b^2] v^i \right\}, \\
h^{i'j'} &= \frac{m^2}{r^2} n'^i n'^j + \frac{4\mu}{r} \left[v^i v^j - \frac{m}{b^3} b^i b^j \right] + \frac{2\mu}{r} \frac{\delta m}{m} \left\{ \frac{6m}{b^3} (\mathbf{n}' \cdot \mathbf{b}) v^{(i} b^{j)} \right. \\
&\quad \left. + \left[(\mathbf{n}' \cdot \mathbf{v}) + \frac{1}{r}(\mathbf{n}' \cdot \mathbf{b}) \right] \left(\frac{m}{b^3} b^i b^j - 2v^i v^j \right) \right\}, \tag{2.15}
\end{aligned}$$

where \mathbf{v} and \mathbf{b} are evaluated at the retarded time $u' = t' - r$.

The metric $g_{\mu'\nu'}$ can be gotten from Eq. (2.15) as follows: from Eq. (2.11) we have

$$g^{\mu'\nu'} = (-g')^{-1/2} (\eta^{\mu'\nu'} - h^{\mu'\nu'}). \tag{2.16}$$

Take the determinant of both sides of Eq. (2.16); this yields $g' = \det(\eta^{\mu'\nu'} - h^{\mu'\nu'})$. So g' can be calculated once $h^{\mu'\nu'}$ is known, and then $g^{\mu'\nu'}$ can be gotten from Eq. (2.16). Inverting the matrix $g^{\mu'\nu'}$ gives the spacetime metric $g_{\mu'\nu'}$.

When performing these calculations, I keep all terms of the form $m^{3-p/2} b^{-3(1-p/2)} r^{-p}$ for integer $p > 0$. I also keep—at each order in r —all terms that are of lower order in m/b than this, and throw away terms of higher order in m/b . This means in particular that no terms of $O(r^{-5})$ are kept. This scheme of organizing terms is consistent with the ordering of terms in Eq. (5.5) of [6].

The result of these calculations is the following radiation-zone metric in harmonic coordinates:

$$\begin{aligned}
g_{0'0'} &= -1 + \frac{2\tilde{m}}{r} - \frac{2m^2}{r^2} + \frac{\mu}{r} \left\{ 2(\mathbf{n}' \cdot \mathbf{v})^2 - \frac{2m}{b^3}(\mathbf{n}' \cdot \mathbf{b})^2 + \frac{6}{r}(\mathbf{n}' \cdot \mathbf{b})(\mathbf{n}' \cdot \mathbf{v}) \right. \\
&\quad \left. + \frac{1}{r^2} [3(\mathbf{n}' \cdot \mathbf{b})^2 - b^2] \right\} + \frac{\mu}{r} \frac{\delta m}{m} \left\{ (\mathbf{n}' \cdot \mathbf{v}) \left[\frac{7m}{b^3}(\mathbf{n}' \cdot \mathbf{b})^2 - 2(\mathbf{n}' \cdot \mathbf{v})^2 - \frac{m}{b} \right] \right. \\
&\quad \left. + \frac{2}{r}(\mathbf{n}' \cdot \mathbf{b}) \left[\frac{3m}{b^3}(\mathbf{n}' \cdot \mathbf{b})^2 - 6(\mathbf{n}' \cdot \mathbf{v})^2 - \frac{m}{b} \right] \right. \\
&\quad \left. + \frac{3}{r^2}(\mathbf{n}' \cdot \mathbf{v}) [b^2 - 5(\mathbf{n}' \cdot \mathbf{b})^2] + \frac{1}{r^3}(\mathbf{n}' \cdot \mathbf{b}) [3b^2 - 5(\mathbf{n}' \cdot \mathbf{b})^2] \right\}, \\
g_{0'i'} &= -\frac{4\mu}{r} \left\{ \left[(\mathbf{n}' \cdot \mathbf{v}) + \frac{1}{r}(\mathbf{n}' \cdot \mathbf{b}) \right] v^i - \frac{m}{b^3}(\mathbf{n}' \cdot \mathbf{b})b^i \right\} \\
&\quad + \frac{2\mu}{r} \frac{\delta m}{m} \left(\left\{ 2(\mathbf{n}' \cdot \mathbf{v})^2 - \frac{3m}{b^3}(\mathbf{n}' \cdot \mathbf{b})^2 + \frac{6}{r}(\mathbf{n}' \cdot \mathbf{b})(\mathbf{n}' \cdot \mathbf{v}) + \frac{1}{r^2} [3(\mathbf{n}' \cdot \mathbf{b})^2 - b^2] \right\} v^i \right. \\
&\quad \left. + \left\{ -\frac{4m}{b^3}(\mathbf{n}' \cdot \mathbf{b})(\mathbf{n}' \cdot \mathbf{v}) + \frac{m}{rb} \left[1 - \frac{3}{b^2}(\mathbf{n}' \cdot \mathbf{b})^2 \right] \right\} b^i \right), \\
g_{i'j'} &= \delta_{ij} \left(\frac{\mu}{r} \left\{ 2(\mathbf{n}' \cdot \mathbf{v})^2 - \frac{2m}{b^3}(\mathbf{n}' \cdot \mathbf{b})^2 + \frac{6}{r}(\mathbf{n}' \cdot \mathbf{b})(\mathbf{n}' \cdot \mathbf{v}) + \frac{1}{r^2} [3(\mathbf{n}' \cdot \mathbf{b})^2 - b^2] \right\} \right.
\end{aligned}$$

$$\begin{aligned}
& + \frac{\mu}{r} \frac{\delta m}{m} \left\{ (\mathbf{n}' \cdot \mathbf{v}) \left[\frac{7m}{b^3} (\mathbf{n}' \cdot \mathbf{b})^2 - 2(\mathbf{n}' \cdot \mathbf{v})^2 + \frac{m}{b} \right] + \frac{6}{r} (\mathbf{n}' \cdot \mathbf{b}) \left[\frac{m}{b^3} (\mathbf{n}' \cdot \mathbf{b})^2 - 2(\mathbf{n}' \cdot \mathbf{v})^2 \right] \right. \\
& + \left. \frac{3}{r^2} (\mathbf{n}' \cdot \mathbf{v}) [b^2 - 5(\mathbf{n}' \cdot \mathbf{b})^2] + \frac{1}{r^3} (\mathbf{n}' \cdot \mathbf{b}) [3b^2 - 5(\mathbf{n}' \cdot \mathbf{b})^2] \right\} \\
& + \delta_{ij} \left(1 + \frac{2\tilde{m}}{r} + \frac{m^2}{r^2} \right) + \frac{m^2}{r^2} n'^i n'^j + \frac{4\mu}{r} \left(v^i v^j - \frac{m}{b^3} b^i b^j \right) \\
& + \frac{2\mu}{r} \frac{\delta m}{m} \left\{ \frac{6m}{b^3} (\mathbf{n}' \cdot \mathbf{b}) v^{(i} b^{j)} + \left[(\mathbf{n}' \cdot \mathbf{v}) + \frac{1}{r} (\mathbf{n}' \cdot \mathbf{b}) \right] \left(\frac{m}{b^3} b^i b^j - 2v^i v^j \right) \right\}, \tag{2.17}
\end{aligned}$$

where \mathbf{v} and \mathbf{b} are evaluated at the retarded time $u' = t' - r$.

The errors $\delta g_{\mu'\nu'}$ in these metric components in region IV can be estimated by computing the orders of magnitude of neglected terms, which are of the form $m^{3-p/2} b^{-3(1-p/2)} r^{-p} (m/b)^{n/2}$ for integers $p > 0$ and $n > 0$. These terms include $m^3/b^2 r$, $\epsilon m^2/r^2$, $m^2 b/r^3$, etc. This gives $\delta g_{\mu'\nu'} \sim \epsilon^7$ for $r \gtrsim r^{out} \sim b/\epsilon$, $\delta g_{\mu'\nu'} \sim \epsilon^8$ for $r \sim b/\epsilon^2 \gg r^{out}$, and $\delta g_{\mu'\nu'} \ll \epsilon^8$ for $r \gg b/\epsilon^2$.

2.2.6 Radiation zone metric in corotating coordinates

Substituting the expressions (2.2)–(2.5) into the metric (2.17) and transforming this metric to corotating coordinates (t, x, y, z) [defined in Eq. (2.7)] gives

$$\begin{aligned}
ds^2 &= dt^2 \left[-1 + \frac{2m}{r} \left(1 - \frac{\mu}{2b} \right) - \frac{2m^2}{r^2} + A + \frac{2\epsilon^2}{b} \mathcal{L} B - 2\epsilon \mathcal{M} D \right. \\
& + \left. \omega^2 (x^2 + y^2) E + \frac{\epsilon^4}{b^2} \mathcal{L}^2 N + \epsilon^2 \mathcal{M}^2 S - \frac{12\mu\epsilon^5}{r^2 b^2} \frac{\delta m}{m} \mathcal{L}^2 \mathcal{M} \right] \\
& + 2dt \left(\epsilon [\sin(\omega r) dx + \cos(\omega r) dy] B + b [\cos(\omega r) dx - \sin(\omega r) dy] D + \omega (x dy - y dx) E \right. \\
& + \left. \frac{\epsilon^3}{b} \mathcal{L} [\sin(\omega r) dx + \cos(\omega r) dy] N - \epsilon b \mathcal{M} [\cos(\omega r) dx - \sin(\omega r) dy] S \right. \\
& + \left. \frac{6\mu\epsilon^4}{r^2 b} \frac{\delta m}{m} \mathcal{L} [(x \cos 2\omega r - y \sin 2\omega r) dx - (x \sin 2\omega r + y \cos 2\omega r) dy] \right) \\
& + E(dx^2 + dy^2 + dz^2) + \frac{m^2}{r^4} (x dx + y dy + z dz)^2 + \epsilon^2 [\sin(\omega r) dx + \cos(\omega r) dy]^2 N \\
& + b^2 [\cos(\omega r) dx - \sin(\omega r) dy]^2 S \\
& + \frac{12\mu\epsilon^3}{r^2} \frac{\delta m}{m} \mathcal{L} [\cos(\omega r) dx - \sin(\omega r) dy] [\sin(\omega r) dx + \cos(\omega r) dy], \tag{2.18}
\end{aligned}$$

where

$$\begin{aligned}
A &= \frac{\mu}{r^3} \left\{ 2\epsilon^2 [\mathcal{M}^2 - \mathcal{L}^2] + \frac{6b\epsilon}{r} \mathcal{M} \mathcal{L} + \frac{b^2}{r^2} [3\mathcal{L}^2 - r^2] \right\} + \frac{\mu}{r^4} \frac{\delta m}{m} \left\{ \frac{b^3}{r^3} \mathcal{L} [3r^2 - 5\mathcal{L}^2] \right. \\
& + \left. \frac{3b^2\epsilon}{r^2} \mathcal{M} [r^2 - 5\mathcal{L}^2] + \frac{2m}{r} \mathcal{L} [3\mathcal{L}^2 - 6\mathcal{M}^2 - r^2] + \epsilon^3 \mathcal{M} [7\mathcal{L}^2 - 2\mathcal{M}^2 - r^2] \right\}, \\
B &= -\frac{4\mu}{r^2} \left[\epsilon \mathcal{M} + \frac{b}{r} \mathcal{L} \right] + \frac{2\mu}{r^3} \frac{\delta m}{m} \left\{ \epsilon^2 [2\mathcal{M}^2 - 3\mathcal{L}^2] + \frac{6b\epsilon}{r} \mathcal{M} \mathcal{L} + \frac{b^2}{r^2} [3\mathcal{L}^2 - r^2] \right\},
\end{aligned}$$

$$\begin{aligned}
D &= \frac{2\mu\epsilon^2}{r^2} \left(\frac{2}{b}\mathcal{L} - \frac{1}{r} \frac{\delta m}{m} \left\{ \frac{4\epsilon}{b}\mathcal{L}\mathcal{M} + \frac{1}{r} [3\mathcal{L}^2 - r^2] \right\} \right), \\
E &= 1 + \frac{2m}{r} \left(1 - \frac{\mu}{2b} \right) + \frac{m^2}{r^2} + A + \frac{2\mu\epsilon^2}{r^2} \frac{\delta m}{m} \left[\frac{b}{r}\mathcal{L} + \epsilon\mathcal{M} \right], \\
N &= \frac{4\mu}{r} \left\{ 1 - \frac{\delta m}{m} \left[\frac{\epsilon}{r}\mathcal{M} + \frac{b}{r^2}\mathcal{L} \right] \right\}, \\
S &= \frac{2\mu\epsilon^2}{rb} \left\{ -\frac{2}{b} + \frac{1}{r} \frac{\delta m}{m} \left[\frac{\epsilon}{b}\mathcal{M} + \frac{1}{r}\mathcal{L} \right] \right\}, \tag{2.19}
\end{aligned}$$

and

$$\mathcal{L} = x \cos \omega r - y \sin \omega r, \quad \mathcal{M} = x \sin \omega r + y \cos \omega r.$$

This is the final form of the metric in region IV.

It is now necessary to evaluate the errors $\delta g_{\mu\nu}$ in the metric components in the corotating coordinate system (t, x, y, z) . Since this coordinate system is not asymptotically inertial, it no longer makes sense to compute absolute errors. The rotation of the coordinates introduces terms of $O(\omega r)$ and $O[(\omega r)^2]$ in g_{00} and terms of $O(\omega r)$ in g_{0i} . For this reason, I define the “normalized” errors $\overline{\delta g}_{00} = \delta g_{00}/(\omega r)^2$, $\overline{\delta g}_{0i} = \delta g_{0i}/\omega r$, and $\overline{\delta g}_{ij} = \delta g_{ij}$ in region IV. It follows that $\overline{\delta g}_{\mu\nu} \sim \epsilon^7$ for $r \gtrsim r^{out} \sim b/\epsilon$, $\overline{\delta g}_{\mu\nu} \sim \epsilon^8$ for $r \sim b/\epsilon^2 \gg r^{out}$, and $\overline{\delta g}_{\mu\nu} \ll \epsilon^8$ for $r \gg b/\epsilon^2$.

In region III, ωr is less than 1 (and in the buffer zones, $\omega r \ll 1$). So rotation of the coordinates is not important in analyzing errors in the metric (2.9) in region III. I continue to use absolute errors in that region. The errors $\delta g_{\mu\nu}$ in the metric components (2.9) in corotating coordinates in region III are the same as the errors in harmonic coordinates (see Sec. 2.2.3): (i) $\delta g_{00} \sim \epsilon^3$, $\delta g_{0i} \sim \epsilon^3$, and $\delta g_{ij} \sim \epsilon^2$ if $r_A \gtrsim r_A^{in}$ for $A = 1$ or 2 ; (ii) $\delta g_{00} \sim \epsilon^6$, $\delta g_{0i} \sim \epsilon^5$, and $\delta g_{ij} \sim \epsilon^4$ if both $r_1 \sim b$ and $r_2 \sim b$; and (iii) $\delta g_{\mu\nu} \sim \epsilon^5$ if $r \lesssim r^{out}$.

Since the analysis by Will and Wiseman [6] of compact binary systems uses a single coordinate chart to cover both the near and radiation zones, the near-zone metric (2.9) automatically matches (to some finite order; see below) the radiation-zone metric (2.18) at $r = r^{out}$. The match is not perfect because I have truncated the relevant perturbative expansions at finite order. As a result, there are discontinuities in the metric components at $r = r^{out}$. The orders of magnitude of these discontinuities can be estimated as follows: first expand r_A^{-1} in powers of b/r for $r > b$ and substitute this expansion in Eq. (2.9); then expand Eq. (2.18) in powers of ωr for $r < r^{out}$; finally, compare the two. The result is that the discontinuities in $g_{\mu\nu}$, denoted $[g_{\mu\nu}]$, are $[g_{\mu\nu}] \sim \epsilon^5$ at $r = r^{out}$.

2.3 Tidal deformation of the first black hole

The metric (2.9) is valid not only in region III but also in the buffer zones around the black holes. The next step is to match this metric to a tidally distorted black-hole metric in the buffer zone

around BH1. There are two coordinate systems which overlap in the buffer zone. The first is the corotating post-Newtonian coordinate system (t, x, y, z) defined in Eq. (2.7). The second—to be called the internal coordinate system—covers the strong-gravity region near the first black hole and is valid from the black hole’s apparent horizon up into (and through) the buffer zone. The internal coordinates are chosen to be isotropic coordinates (T, X, Y, Z) in which the unperturbed Schwarzschild metric is

$$ds^2 = - \left(\frac{1 - m_1/2R}{1 + m_1/2R} \right)^2 dT^2 + \left(1 + \frac{m_1}{2R} \right)^4 (dX^2 + dY^2 + dZ^2), \quad (2.20)$$

where

$$R = (X^2 + Y^2 + Z^2)^{1/2}. \quad (2.21)$$

The region these coordinates cover will be called the internal region; it contains region I in particular.

The first step in matching the near-zone metric (2.9) to the internal metric [which is the Schwarzschild metric (2.20) plus tidal perturbations] is to write the metric (2.9) in internal coordinates. Then the near-zone metric and the internal metric are both expanded in positive powers of m_1/R and R/b in the buffer zone. Finally, corresponding terms in the two asymptotic expansions are equated. The near-zone metric determines in this way the asymptotic form of the tidal perturbations on BH1. These perturbations are further constrained to solve the linearized Einstein equations about the Schwarzschild metric (2.20) and to be finite at the horizon $R = m_1/2$.

The asymptotic form of the Schwarzschild perturbations in internal coordinates can be determined independently of the matching procedure described above by calculating the electric- and magnetic-type tidal fields of BH2 in the buffer zone surrounding BH1. Once this asymptotic form is known, the matching procedure can be used to constrain the coordinate transformation taking corotating coordinates (t, x, y, z) to internal coordinates (T, X, Y, Z) . This is the approach to matching taken in this paper. In the next two sections, I calculate the second black hole’s tidal fields and the perturbations they induce on the first black hole.

2.3.1 Tidal fields of the companion black hole

Thorne and Hartle [8] have analyzed the motion of an isolated black hole in an arbitrary surrounding spacetime. They define and discuss the black hole’s local asymptotic rest frame. In the first black hole’s local asymptotic rest frame, the metric can be expanded in powers of the black hole’s mass m_1 as follows⁵:

$$g = g^{(0)} + m_1 g^{(1)} + m_1^2 g^{(2)} + \dots \quad (2.22)$$

⁵This expansion is written in Eq. (2.5) of [8]; I have substituted m_1 for M in that equation.

Here the metric $g^{(0)}$ represents the external universe without BH1; the rest of the terms represent the black hole's internal gravitational field and the nonlinear interaction between internal and external fields. In this section, I will focus on the external metric $g^{(0)}$ and use it to constrain internal perturbations. Throughout this section and in the rest of this paper, boldface letters denote spacetime tensors of all ranks (including 4-vectors).

In the case of binary black holes, the external metric is simply that of a single black hole; it is the metric of the companion black hole BH2 of mass m_2 . This metric must be expressed in local asymptotic rest frame coordinates. With this goal in mind, consider first a freely falling observer in a circular, equatorial orbit around a Kerr black hole of mass m_2 . (I will later specialize to a nonrotating black hole.) The Kerr black hole represents BH2 while the observer's local Lorentz frame (same as proper reference frame) represents the local asymptotic rest frame of BH1.

The metric near the observer's world line is determined by the Kerr black hole's electric-type and magnetic-type tidal fields as seen in the observer's local Lorentz frame. These tidal fields can be evaluated by taking components of the Kerr spacetime's Weyl tensor \mathbf{C} in a parallel-propagated orthonormal tetrad along the observer's world line. The vectors in this tetrad form the coordinate basis of the local Lorentz frame at the location of the geodesic orbit.

The electric-type tidal field as seen by such an observer has been calculated by Fishbone [9] and Marck [10]. Marck has computed a parallel-propagated orthonormal tetrad $(\lambda_0, \lambda_1, \lambda_2, \lambda_3)$ along arbitrary geodesics of the Kerr spacetime, with λ_0 equal to the 4-velocity of the geodesic. He obtains the electric-type tidal field by evaluating

$$R_{0i0j} = \mathbf{C}(\lambda_0, \lambda_i, \lambda_0, \lambda_j). \quad (2.23)$$

I specialize his tetrad to circular, equatorial geodesics; I also label the tetrad vectors (and hence coordinate axes) differently. Initially (that is, at proper time $\mathcal{T} = 0$), I choose λ_1 to be radially outward (in Boyer-Lindquist coordinates); λ_2 is chosen so that the projections of λ_0 and λ_2 on a constant-Boyer-Lindquist-time- t surface are parallel; and λ_3 is then chosen to give $(\lambda_1, \lambda_2, \lambda_3)$ positive (i.e., right-handed) orientation. With this choice of tetrad, I obtain the magnetic-type tidal field using Marck's work by evaluating

$$R_{0ijk} = \mathbf{C}(\lambda_0, \lambda_i, \lambda_j, \lambda_k). \quad (2.24)$$

The results of the calculations (2.23) and (2.24) with the above choice of tetrad are

$$\begin{aligned} R_{0101} &= \frac{m_2}{d^3} \left[1 - 3 \left(1 + \frac{\mathcal{W}^2}{d^2} \right) \cos^2 \bar{\Omega} \mathcal{T} \right], & R_{0202} &= \frac{m_2}{d^3} \left[1 - 3 \left(1 + \frac{\mathcal{W}^2}{d^2} \right) \sin^2 \bar{\Omega} \mathcal{T} \right], \\ R_{0303} &= \frac{m_2}{d^3} \left(1 + \frac{3\mathcal{W}^2}{d^2} \right), & R_{0102} = R_{0201} &= -\frac{3m_2}{d^3} \left(1 + \frac{\mathcal{W}^2}{d^2} \right) \cos \bar{\Omega} \mathcal{T} \sin \bar{\Omega} \mathcal{T}, \end{aligned}$$

$$\begin{aligned}
R_{0112} &= -R_{0121} = R_{0323} = -R_{0332} = \frac{3m_2\mathcal{W}}{d^4} \left(1 + \frac{\mathcal{W}^2}{d^2}\right)^{1/2} \cos \bar{\Omega}\mathcal{T}, \\
R_{0212} &= -R_{0221} = R_{0331} = -R_{0313} = \frac{3m_2\mathcal{W}}{d^4} \left(1 + \frac{\mathcal{W}^2}{d^2}\right)^{1/2} \sin \bar{\Omega}\mathcal{T},
\end{aligned} \tag{2.25}$$

and the rest of the Weyl-tensor components are zero. Here \mathcal{T} is proper time along the geodesic, m_2 is the mass of the Kerr black hole, d is the Boyer-Lindquist radial coordinate of the circular, equatorial orbit, and

$$\bar{\Omega} = \sqrt{\frac{m_2}{d^3}} \tag{2.26}$$

is the (exact) rotation rate of the black hole's tidal field as seen in the local Lorentz frame. The quantity \mathcal{W} is given by

$$\frac{\mathcal{W}}{d} = \frac{\sqrt{m_2/d} \pm a/d}{\left(1 - 3m_2/d \mp 2a\sqrt{m_2/d^3}\right)^{1/2}}, \tag{2.27}$$

where $m_2 a$ is the black hole's angular momentum. The upper sign in Eq. (2.27) is for a retrograde orbit while the lower one is for a direct or prograde orbit.

Notice that for $d \gg m_2$, the electric- and magnetic-type tidal field components at $\mathcal{T} = 0$ are simply related via a Lorentz boost with low velocity $(m_2/d)^{1/2}$. For example,

$$R_{0112}|_{\mathcal{T}=0} = -(m_2/d)^{1/2} [R_{0101} + R_{1212}]_{\mathcal{T}=0} = -(m_2/d)^{1/2} [2R_{0101} + R_{0202}]_{\mathcal{T}=0} \tag{2.28}$$

to lowest order in m_2/d . This fact will be used later in this section.

In the local Lorentz frame, the spacetime metric can be written as an expansion in powers of distance \mathcal{R} from the observer's geodesic world line [11]. The two types of tidal field (2.23) and (2.24) determine the metric up to and including terms of $O(\mathcal{R}^2)$. After exploiting some gauge freedom (see Sec. V.A.2 of [12] and Eq. (2.7) of [8]), the metric can be written in local coordinates $(\mathcal{T}, \mathcal{X}, \mathcal{Y}, \mathcal{Z})$ as

$$\begin{aligned}
g_{00} &= -1 - R_{0i0j}(\mathcal{T})\mathcal{X}^i\mathcal{X}^j + O(\mathcal{R}^3), \\
g_{0i} &= -\frac{2}{3}R_{0jik}(\mathcal{T})\mathcal{X}^j\mathcal{X}^k + O(\mathcal{R}^3), \\
g_{ij} &= \delta_{ij} [1 - R_{0k0m}(\mathcal{T})\mathcal{X}^k\mathcal{X}^m] + O(\mathcal{R}^3),
\end{aligned} \tag{2.29}$$

where $\mathcal{R} = (\mathcal{X}^2 + \mathcal{Y}^2 + \mathcal{Z}^2)^{1/2}$. Substituting the expressions (2.25) in Eq. (2.29) gives

$$\begin{aligned}
g_{00} &= -1 + \frac{m_2}{d^3} \left[3 \left(1 + \frac{\mathcal{W}^2}{d^2}\right) (\mathcal{X} \cos \bar{\Omega}\mathcal{T} + \mathcal{Y} \sin \bar{\Omega}\mathcal{T})^2 - \mathcal{R}^2 - \frac{3\mathcal{W}^2}{d^2} \mathcal{Z}^2 \right], \\
g_{0\mathcal{X}} &= \frac{2m_2\mathcal{W}}{d^4} \left(1 + \frac{\mathcal{W}^2}{d^2}\right)^{1/2} [(\mathcal{Z}^2 - \mathcal{Y}^2) \sin \bar{\Omega}\mathcal{T} - \mathcal{X}\mathcal{Y} \cos \bar{\Omega}\mathcal{T}],
\end{aligned}$$

$$\begin{aligned}
g_{0\mathcal{Y}} &= \frac{2m_2\mathcal{W}}{d^4} \left(1 + \frac{\mathcal{W}^2}{d^2}\right)^{1/2} [(\mathcal{X}^2 - \mathcal{Z}^2) \cos \bar{\Omega}\mathcal{T} + \mathcal{X}\mathcal{Y} \sin \bar{\Omega}\mathcal{T}], \\
g_{0\mathcal{Z}} &= \frac{2m_2\mathcal{W}}{d^4} \left(1 + \frac{\mathcal{W}^2}{d^2}\right)^{1/2} (\mathcal{Y} \cos \bar{\Omega}\mathcal{T} - \mathcal{X} \sin \bar{\Omega}\mathcal{T})\mathcal{Z}, \\
g_{ij} &= \delta_{ij} \left\{ 1 + \frac{m_2}{d^3} \left[3 \left(1 + \frac{\mathcal{W}^2}{d^2}\right) (\mathcal{X} \cos \bar{\Omega}\mathcal{T} + \mathcal{Y} \sin \bar{\Omega}\mathcal{T})^2 - \mathcal{R}^2 - \frac{3\mathcal{W}^2}{d^2} \mathcal{Z}^2 \right] \right\} \quad (2.30)
\end{aligned}$$

up to and including terms of $O(\mathcal{R}^2)$.

The rotation rate $\bar{\Omega}$ is only correct for test-particle orbits and is exact in that case. The correct rotation rate Ω of the second black hole's tidal field—measured in a local inertial frame in the first black hole's local asymptotic rest frame—is actually determined by the post-Newtonian metric (2.9) and by the requirements that (i) this metric match the local asymptotic rest frame metric [given in Eq. (2.43) in Sec. 2.3.2 below]; and (ii) the local asymptotic rest frame coordinate system be nonrotating relative to local inertial frames. The rotation rate Ω is calculated in Sec. 2.4.1 by transforming the metric (2.9) to internal coordinates and requiring a match to the local asymptotic rest frame metric (2.43). There it will be seen that the rotation rate is⁶

$$\Omega = \omega \left[1 - \frac{\mu}{b} + O(\epsilon^3) \right]. \quad (2.31)$$

Note that post-Newtonian corrections to the orbital angular velocity ω of $O(\epsilon^2\omega)$ have not been included in this paper.

The metric (2.30) is valid for all radii d which allow a circular, equatorial, geodesic orbit. To apply Eq. (2.30) to the situation of widely separated nonrotating binary black holes, I specialize to a Schwarzschild black hole by setting $a = 0$ and take the limit of small m_2/d , keeping only lowest-order terms in m_2/d . [In particular, I replace \mathcal{W}/d with $(m_2/d)^{1/2}$.] I then replace d with b , $\bar{\Omega}$ with Ω , and local coordinates $(\mathcal{T}, \mathcal{X}, \mathcal{Y}, \mathcal{Z})$ with internal coordinates (T, X, Y, Z) [which are described above Eq. (2.20)]. The result is

$$\begin{aligned}
g_{00} &= -1 + \frac{m_2}{b^3} [3(X \cos \Omega T + Y \sin \Omega T)^2 - R^2], \\
g_{0X} &= \frac{2m_2}{b^3} \sqrt{\frac{m_2}{b}} [(Z^2 - Y^2) \sin \Omega T - XY \cos \Omega T], \\
g_{0Y} &= \frac{2m_2}{b^3} \sqrt{\frac{m_2}{b}} [(X^2 - Z^2) \cos \Omega T + XY \sin \Omega T], \\
g_{0Z} &= \frac{2m_2}{b^3} \sqrt{\frac{m_2}{b}} (Y \cos \Omega T - X \sin \Omega T) Z, \\
g_{ij} &= \delta_{ij} \left\{ 1 + \frac{m_2}{b^3} [3(X \cos \Omega T + Y \sin \Omega T)^2 - R^2] \right\}, \quad (2.32)
\end{aligned}$$

where $R = (X^2 + Y^2 + Z^2)^{1/2}$ as defined in Eq. (2.21).

⁶This rotation rate can also be calculated by looking at geodetic precession of parallel-propagated vectors in the local asymptotic rest frame [13].

The metric (2.32) is still not applicable to binary black holes since the observer was taken to be massless [there are no factors of m_1 in Eq. (2.32)]. This can be fixed easily. As mentioned above, the factors of $(m_2/b)^{1/2}$ in g_{0i} in Eq. (2.32) arise from a Lorentz boost with low velocity $(m_2/b)^{1/2}$. But the correct (Newtonian) relative velocity between the black holes is $\epsilon = [(m_1 + m_2)/b]^{1/2}$. So I replace the factors of $(m_2/b)^{1/2}$ in Eq. (2.32) by $(m/b)^{1/2}$. The resulting metric includes the second black hole's tidal fields but does not include the first black hole's gravitational field:

$$\begin{aligned}
g_{00} &= -1 + \frac{m_2}{b^3} [3(X \cos \Omega T + Y \sin \Omega T)^2 - R^2], \\
g_{0X} &= \frac{2m_2}{b^3} \sqrt{\frac{m}{b}} [(Z^2 - Y^2) \sin \Omega T - XY \cos \Omega T], \\
g_{0Y} &= \frac{2m_2}{b^3} \sqrt{\frac{m}{b}} [(X^2 - Z^2) \cos \Omega T + XY \sin \Omega T], \\
g_{0Z} &= \frac{2m_2}{b^3} \sqrt{\frac{m}{b}} (Y \cos \Omega T - X \sin \Omega T) Z, \\
g_{ij} &= \delta_{ij} \left\{ 1 + \frac{m_2}{b^3} [3(X \cos \Omega T + Y \sin \Omega T)^2 - R^2] \right\}. \tag{2.33}
\end{aligned}$$

In the buffer zone around BH1, this metric provides the asymptotic form of the perturbation on BH1.

2.3.2 Schwarzschild perturbation

The next stage is to solve the linearized Einstein equations about the Schwarzschild metric for a perturbation which is finite at the horizon $R = m_1/2$ and asymptotes to the form (2.33) as $R/m_1 \rightarrow \infty$. For ease in dealing with the linearized Einstein equations, I transform to spherical, isotropic, internal coordinates (T, R, θ, ϕ) by letting

$$X = R \sin \theta \cos \phi, \quad Y = R \sin \theta \sin \phi, \quad Z = R \cos \theta. \tag{2.34}$$

The unperturbed Schwarzschild metric in these coordinates is

$$ds^2 = - \left(\frac{1 - m_1/2R}{1 + m_1/2R} \right)^2 dT^2 + \left(1 + \frac{m_1}{2R} \right)^4 [dR^2 + R^2(d\theta^2 + \sin^2 \theta d\phi^2)]. \tag{2.35}$$

The metric (2.33) in these coordinates is

$$\begin{aligned}
ds^2 &= -dT^2 + dR^2 + R^2(d\theta^2 + \sin^2 \theta d\phi^2) \\
&\quad - 4 \frac{m_2 R^3}{b^3} \sqrt{\frac{m}{b}} dT [\cos \theta \sin(\phi - \Omega T) d\theta + \sin \theta \cos(2\theta) \cos(\phi - \Omega T) d\phi] \\
&\quad + \frac{m_2 R^2}{b^3} [3 \sin^2 \theta \cos^2(\phi - \Omega T) - 1] [dT^2 + dR^2 + R^2(d\theta^2 + \sin^2 \theta d\phi^2)]. \tag{2.36}
\end{aligned}$$

The linearity of the linearized Einstein equations allows me to look separately for solutions corresponding to the electric-type and magnetic-type tidal fields. First I look for a perturbation $\mathbf{h}_1 = \mathbf{g} - \mathbf{g}_s$ (where \mathbf{g}_s is the unperturbed Schwarzschild metric and \mathbf{g} is the full metric including the perturbation) of BH1 which corresponds to the electric-type tidal field of BH2 and is of the form

$$\mathbf{h}_1 = \frac{m_2 R^2}{b^3} [3 \sin^2 \theta \cos^2(\phi - \Omega T) - 1] [f_1(R) dT^2 + f_2(R) dR^2 + f_3(R) R^2 (d\theta^2 + \sin^2 \theta d\phi^2)], \quad (2.37)$$

as suggested by Eq. (2.36). In this notation, dT , dR , $d\theta$, and $d\phi$ are coordinate one-forms and dT^2 denotes the tensor product $dT \otimes dT$. The functions f_1 , f_2 , and f_3 are to be determined by solving the linearized Einstein equations with the following boundary conditions: (i) $f_1(R)$, $f_2(R)$, and $f_3(R)$ are required to approach 1 as $R/m_1 \rightarrow \infty$ so that the perturbation (2.37) matches the electric-type tidal field in Eq. (2.36); and (ii) \mathbf{h}_1 is required to be finite at $R = m_1/2$.

Consider solving the linearized Einstein equations order by order in $\epsilon = (m/b)^{1/2}$. Time derivatives of the components of \mathbf{h}_1 produce factors of $m_1 \Omega \sim \epsilon^3$ in the linearized Einstein equations and can thus be neglected. A solution for \mathbf{h}_1 can then be found using the Regge-Wheeler formalism [14] for analysis of stationary Schwarzschild perturbations. Regge and Wheeler decompose perturbations into even- and odd-parity modes and analyze them in a particular gauge chosen to simplify computations. In their classification \mathbf{h}_1 is a superposition of static⁷ even-parity modes with angular numbers $l = 2$ and $m = -2, 0, 2$. The general solution of the linearized Einstein equations for static even-parity modes with $l \geq 2$ is well known in Schwarzschild coordinates and is given in Sec. IV of [15], for example. A particular solution with $l = 2$ that is finite at the black hole's horizon and contains an arbitrary multiplicative constant is easily obtained from the general solution, and is given in Eqs. (6.5) and (6.7) of [3], for example⁸. After transforming this solution to isotropic coordinates, the multiplicative constant is determined by imposing the boundary condition (i) (given at the end of the previous paragraph). This yields the following solution for the radial factors $f_1(R)$, $f_2(R)$, and $f_3(R)$ in isotropic coordinates:

$$\begin{aligned} f_1(R) &= \left(1 - \frac{m_1}{2R}\right)^4, \\ f_2(R) &= \left(1 - \frac{m_1}{2R}\right)^2 \left(1 + \frac{m_1}{2R}\right)^6, \\ f_3(R) &= \left(1 + \frac{m_1}{2R}\right)^4 \left[\left(1 + \frac{m_1}{2R}\right)^4 - \frac{2m_1^2}{R^2} \right]. \end{aligned} \quad (2.38)$$

Next I look for a perturbation $\mathbf{h}_2 = \mathbf{g} - \mathbf{g}_s$ of BH1 corresponding to the magnetic-type tidal field

⁷Time dependence in Eq. (2.37) is to be ignored, as explained above.

⁸The notation in Sec. VI of [3] may be confusing: R there denotes a dimensionless quantity obtained from the Schwarzschild radial coordinate r_s by $R = r_s/M$ where M —in my notation m_1 —is the mass of the black hole being perturbed.

of BH2 and of the form

$$\mathbf{h}_2 = -\frac{4m_2}{b^3} \sqrt{\frac{m}{b}} R^3 F(R) dT [\cos \theta \sin(\phi - \Omega T) d\theta + \sin \theta \cos 2\theta \cos(\phi - \Omega T) d\phi], \quad (2.39)$$

as suggested by Eq. (2.36). The function F is to be determined by solving the linearized Einstein equations with the following boundary conditions: (i) $F(R) \rightarrow 1$ as $R/m_1 \rightarrow \infty$ so that the perturbation (2.39) matches the magnetic-type tidal field in Eq. (2.36); and (ii) \mathbf{h}_2 finite at $R = m_1/2$. As was done for \mathbf{h}_1 , time dependence is ignored in \mathbf{h}_2 since time derivatives produce higher-order terms. In the Regge-Wheeler classification, \mathbf{h}_2 is a superposition of stationary odd-parity modes with angular numbers $l = 2$ and $m = -1, 1$. The general solution of the linearized Einstein equations for stationary odd-parity modes that are finite at the horizon and have $l \geq 2$ is given in Schwarzschild coordinates in Eq. (38) of [14]. This solution is only determined up to a multiplicative constant. The particular case $l = 2$ is easily obtained from the general solution, and is given in Eq. (6.10) of [3], for example⁸. After transforming this solution to isotropic coordinates, the multiplicative constant is determined by imposing the boundary condition (i) [given below Eq. (2.39)]. This yields the following solution for the radial factor $F(R)$ in isotropic coordinates:

$$F(R) = \left(1 - \frac{m_1}{2R}\right)^2 \left(1 + \frac{m_1}{2R}\right)^4. \quad (2.40)$$

The metric in the internal region near BH1 is now complete. It is given by the Schwarzschild metric (2.35) plus the perturbations (2.37) and (2.39) with radial factors given in Eqs. (2.38) and (2.40); in other words, $\mathbf{g} = \mathbf{g}_s + \mathbf{h}_1 + \mathbf{h}_2$. In spherical isotropic coordinates (T, R, θ, ϕ) , this internal metric is

$$\begin{aligned} ds^2 = & -\left(\frac{1 - m_1/2R}{1 + m_1/2R}\right)^2 dT^2 + \left(1 + \frac{m_1}{2R}\right)^4 [dR^2 + R^2(d\theta^2 + \sin^2 \theta d\phi^2)] \\ & - \frac{4m_2}{b^3} \sqrt{\frac{m}{b}} \left(1 - \frac{m_1}{2R}\right)^2 \left(1 + \frac{m_1}{2R}\right)^4 R^3 dT [\cos \theta \sin(\phi - \Omega T) d\theta \\ & + \sin \theta \cos(2\theta) \cos(\phi - \Omega T) d\phi] \\ & + \frac{m_2 R^2}{b^3} [3 \sin^2 \theta \cos^2(\phi - \Omega T) - 1] \left\{ \left(1 - \frac{m_1}{2R}\right)^4 dT^2 + \left(1 - \frac{m_1}{2R}\right)^2 \left(1 + \frac{m_1}{2R}\right)^6 dR^2 \right. \\ & \left. + \left(1 + \frac{m_1}{2R}\right)^4 \left[\left(1 + \frac{m_1}{2R}\right)^4 - \frac{2m_1^2}{R^2} \right] R^2 (d\theta^2 + \sin^2 \theta d\phi^2) \right\}. \end{aligned} \quad (2.41)$$

In isotropic coordinates (T, X, Y, Z) , this metric is

$$\begin{aligned} g_{00} &= -\left(\frac{1 - m_1/2R}{1 + m_1/2R}\right)^2 + \frac{m_2}{b^3} \left(1 - \frac{m_1}{2R}\right)^4 [3(X \cos \Omega T + Y \sin \Omega T)^2 - R^2], \\ g_{0X} &= \frac{2m_2}{b^3} \sqrt{\frac{m}{b}} \left(1 - \frac{m_1}{2R}\right)^2 \left(1 + \frac{m_1}{2R}\right)^4 [(Z^2 - Y^2) \sin \Omega T - XY \cos \Omega T], \end{aligned}$$

$$\begin{aligned}
g_{0Y} &= \frac{2m_2}{b^3} \sqrt{\frac{m}{b}} \left(1 - \frac{m_1}{2R}\right)^2 \left(1 + \frac{m_1}{2R}\right)^4 [(X^2 - Z^2) \cos \Omega T + XY \sin \Omega T], \\
g_{0Z} &= \frac{2m_2}{b^3} \sqrt{\frac{m}{b}} \left(1 - \frac{m_1}{2R}\right)^2 \left(1 + \frac{m_1}{2R}\right)^4 (Y \cos \Omega T - X \sin \Omega T) Z, \\
g_{ij} &= \left(1 + \frac{m_1}{2R}\right)^4 \left(\delta_{ij} + \frac{m_2}{b^3} [3(X \cos \Omega T + Y \sin \Omega T)^2 - R^2] \right. \\
&\quad \left. \times \left\{ \left[\left(1 + \frac{m_1}{2R}\right)^4 - \frac{2m_1^2}{R^2} \right] \delta_{ij} - \frac{2m_1}{R} \left(1 + \frac{m_1^2}{4R^2}\right) \frac{X^i X^j}{R^2} \right\} \right). \tag{2.42}
\end{aligned}$$

Expanding the components (2.42) in positive powers of m_1/R and R/b in the buffer zone $m_1 \ll R \ll b$ and keeping only lowest-order terms yields the local asymptotic rest frame metric:

$$\begin{aligned}
g_{00} &= -1 + \frac{2m_1}{R} + \frac{m_2}{b^3} [3(X \cos \Omega T + Y \sin \Omega T)^2 - R^2], \\
g_{0X} &= \frac{2m_2}{b^3} \sqrt{\frac{m}{b}} [(Z^2 - Y^2) \sin \Omega T - XY \cos \Omega T], \\
g_{0Y} &= \frac{2m_2}{b^3} \sqrt{\frac{m}{b}} [(X^2 - Z^2) \cos \Omega T + XY \sin \Omega T], \\
g_{0Z} &= \frac{2m_2}{b^3} \sqrt{\frac{m}{b}} (Y \cos \Omega T - X \sin \Omega T) Z, \\
g_{ij} &= \delta_{ij} \left\{ 1 + \frac{2m_1}{R} + \frac{m_2}{b^3} [3(X \cos \Omega T + Y \sin \Omega T)^2 - R^2] \right\}. \tag{2.43}
\end{aligned}$$

This metric includes the first black hole's (weak) gravitational field as well as the second black hole's tidal fields.

2.4 Distorted black hole metrics in corotating coordinates

The post-Newtonian metric (2.9), when expressed in internal coordinates (T, X, Y, Z) in the buffer zone around BH1, must take the form (2.43). The next step is to find explicitly the coordinate transformation in the buffer zone taking corotating post-Newtonian coordinates to these internal coordinates. Applying the inverse of this transformation to the internal metric (2.42) will put that metric in corotating coordinates (t, x, y, z) . An identical procedure will then be followed to obtain the metric near BH2 in corotating coordinates.

2.4.1 Buffer zone coordinate transformation

In this section, a series of coordinate transformations are performed on the metric (2.9) in the buffer zone of BH1 to bring it to the form (2.43). Composing these transformations gives the final transformation from corotating to internal coordinates. Throughout this process terms of $O(m^2)$ are dropped; justification for this will be given at the end of the section.

Begin with the near-zone metric (2.9) with terms of $O(m^2)$ removed. Restrict attention to the buffer zone $m_1 \ll r_1 \ll b$ since this is where the corotating coordinate system and internal coordinate system overlap. Center the coordinate grid on BH1 by shifting the origin to $(x, y, z) = (m_2 b/m, 0, 0)$. This is done by defining a new coordinate

$$\xi = x - \frac{m_2 b}{m}. \quad (2.44)$$

Next expand the metric in powers of the distance

$$r_1 = (\xi^2 + y^2 + z^2)^{1/2} \quad (2.45)$$

to the new origin. The expansion for r_2^{-1} is

$$\frac{1}{r_2} = [(b + \xi)^2 + y^2 + z^2]^{-1/2} = \frac{1}{b} - \frac{\xi}{b^2} + \frac{2\xi^2 - y^2 - z^2}{2b^3} + \dots \quad (2.46)$$

Positive powers of r_1 in the metric components come in the form $(r_1/b)^p$ with integer $p > 0$. Since $r_1 \ll b$ in the buffer zone, discard terms of $O[(r_1/b)^3]$ or higher. This results in the following metric:

$$\begin{aligned} ds^2 = & dt^2 [-1 + 2m_1/r_1 + (2m_2/b)(1 + m_2/2m) + (m_2/b^3)(2\xi^2 - y^2 - z^2) + (m/b^3)(\xi^2 + y^2)] \\ & - 2\omega y dt d\xi [1 + 2m_2/b + 2m_1/r_1 - 2m_2\xi/b^2] + 2\omega dt dy \left\{ (m_2/m)(b + 4m_1 + 2m_2) \right. \\ & \left. - 2\mu b/r_1 + \xi(1 + 2m_1/r_1 - 2\mu/b) + (m_2/b^2) [2m_1\xi^2/m - (1 + m_1/m)(y^2 + z^2)] \right\} \\ & + (d\xi^2 + dy^2 + dz^2) [1 + 2m_1/r_1 + 2m_2/b - 2m_2\xi/b^2 + (m_2/b^3)(2\xi^2 - y^2 - z^2)]. \quad (2.47) \end{aligned}$$

Now renormalize the time-coordinate by defining

$$t = \tilde{t} [1 + (m_2/b)(1 + m_2/2m)], \quad (2.48)$$

and then perform a partial Lorentz transformation by setting

$$\begin{aligned} \tilde{t} &= \tilde{t} + (m_2\omega/m)(b + 4m_1 + 3m_2 + m_2^2/2m)\tilde{y}, \\ \xi &= \tilde{x}, \quad y = \tilde{y}, \quad z = \tilde{z}. \end{aligned} \quad (2.49)$$

In the new coordinates $(\tilde{t}, \tilde{x}, \tilde{y}, \tilde{z})$, the metric (2.47) is

$$\begin{aligned} ds^2 = & d\tilde{t}^2 [-1 + 2m_1/\tilde{r} + (m_2/b^3)(3\tilde{x}^2 - \tilde{r}^2) + (m/b^3)(\tilde{x}^2 + \tilde{y}^2)] \\ & - 2\omega d\tilde{t} d\tilde{x} \left\{ \tilde{y} [1 + (m_2/2mb)(6m_1 + 7m_2) + 2m_1/\tilde{r}] - 2m_2\tilde{x}\tilde{y}/b^2 \right\} \\ & + 2\omega d\tilde{t} d\tilde{y} \left\{ \tilde{x} [1 + (m_2/2mb)(-2m_1 + 3m_2) + 2m_1/\tilde{r}] + (m_2/b^2)(3\tilde{x}^2 - \tilde{y}^2 - 2\tilde{z}^2) \right\} \end{aligned}$$

$$\begin{aligned}
& + (d\tilde{x}^2 + d\tilde{y}^2 + d\tilde{z}^2) [1 + 2m_1/\tilde{r} + 2m_2/b - 2m_2\tilde{x}/b^2 + (m_2/b^3)(3\tilde{x}^2 - \tilde{r}^2)] \\
& + (m_2/b)d\tilde{y} [(m_2/m + 2\tilde{x}/b)d\tilde{y} - (2\tilde{y}/b)d\tilde{x}]
\end{aligned} \tag{2.50}$$

where $\tilde{r} = (\tilde{x}^2 + \tilde{y}^2 + \tilde{z}^2)^{1/2}$ and terms of $O(m^2)$ have been dropped, as is done throughout this section.

Next clean up the spatial part of the metric by putting

$$\begin{aligned}
\tilde{t} &= \hat{t}, & \tilde{x} &= \hat{x}(1 - m_2/b) + (m_2/2b^2)(\hat{x}^2 + \hat{y}^2 - \hat{z}^2), \\
\tilde{y} &= \hat{y}[1 - (m_2/2mb)(2m_1 + 3m_2)], & \tilde{z} &= \hat{z}(1 - m_2/b) + (m_2/b^2)\hat{x}\hat{z}.
\end{aligned} \tag{2.51}$$

Transforming the metric (2.50) using Eq. (2.51) results in

$$\begin{aligned}
ds^2 &= d\hat{t}^2 [-1 + 2m_1/\hat{r} + (m_2/b^3)(3\hat{x}^2 - \hat{r}^2) + (m/b^3)(\hat{x}^2 + \hat{y}^2)] \\
&\quad - 2\omega d\hat{t}d\hat{x} [\hat{y}(1 + m_2/b + 2m_1/\hat{r}) - m_2\hat{x}\hat{y}/b^2] \\
&\quad + 2\omega d\hat{t}d\hat{y} \{ \hat{x}[1 - (m_2/mb)(3m_1 + m_2) + 2m_1/\hat{r}] + (m_2/2b^2)(7\hat{x}^2 - 3\hat{y}^2 - 5\hat{z}^2) \} \\
&\quad + 2(m_2\omega/b^2)\hat{y}\hat{z}d\hat{t}d\hat{z} + (d\hat{x}^2 + d\hat{y}^2 + d\hat{z}^2) [1 + 2m_1/\hat{r} + (m_2/b^3)(3\hat{x}^2 - \hat{r}^2)]
\end{aligned} \tag{2.52}$$

where $\hat{r} = (\hat{x}^2 + \hat{y}^2 + \hat{z}^2)^{1/2}$.

Consider the terms $2\omega d\hat{t} \{ \hat{x}d\hat{y} [1 - (m_2/mb)(3m_1 + m_2) + 2m_1/\hat{r}] - \hat{y}d\hat{x}(1 + m_2/b + 2m_1/\hat{r}) \}$ in Eq. (2.52). These terms contain information about the rotation of the coordinate axes. However, they are not yet in the form of the rotation terms $2\Omega(1 + 2m_1/\hat{r})d\hat{t}(\hat{x}d\hat{y} - \hat{y}d\hat{x})$ that result from rotating—at a constant rate Ω and in an active sense, i.e., using a pull-back map—the metric $ds^2 = d\hat{t}^2(-1 + 2m_1/\hat{r}) + (d\hat{x}^2 + d\hat{y}^2 + d\hat{z}^2)(1 + 2m_1/\hat{r})$, which is a fragment of Eq. (2.52). An additional coordinate transformation is required to bring the former terms into the latter form. With this goal in mind, look first for a gauge transformation taking the perturbation

$$\gamma = 2\omega d\hat{t} \{ \hat{x}d\hat{y} [1 - (m_2/mb)(3m_1 + m_2) + 2m_1/\hat{r}] - \hat{y}d\hat{x}(1 + m_2/b + 2m_1/\hat{r}) \} \tag{2.53}$$

on a flat background metric $ds^2 = -d\hat{t}^2 + d\hat{x}^2 + d\hat{y}^2 + d\hat{z}^2$ to the perturbation

$$\check{\gamma} = 2\Omega(1 + 2m_1/\hat{r})d\hat{t}(\hat{x}d\hat{y} - \hat{y}d\hat{x}). \tag{2.54}$$

In other words, look for a vector field $\boldsymbol{\eta}$ such that

$$\check{\gamma}_{\hat{\mu}\hat{\nu}} = \gamma_{\hat{\mu}\hat{\nu}} - 2\partial_{(\hat{\mu}}\eta_{\hat{\nu})}. \tag{2.55}$$

In order to solve Eq. (2.55), it suffices to consider $\boldsymbol{\eta}$ with only one nonzero component $\eta^{\hat{t}} =$

$\eta^{\hat{t}}(\hat{x}, \hat{y}, \hat{z})$. The perturbations (2.53) and (2.54) when put in Eq. (2.55) yield

$$-\Omega\hat{y}(1 + 2m_1/\hat{r}) = \check{\gamma}_{\hat{t}\hat{x}} = \gamma_{\hat{t}\hat{x}} + \partial\eta^{\hat{t}}/\partial\hat{x} = -\omega\hat{y}(1 + m_2/b + 2m_1/\hat{r}) + \partial\eta^{\hat{t}}/\partial\hat{x}, \quad (2.56)$$

$$\begin{aligned} \Omega\hat{x}(1 + 2m_1/\hat{r}) &= \check{\gamma}_{\hat{t}\hat{y}} = \gamma_{\hat{t}\hat{y}} + \partial\eta^{\hat{t}}/\partial\hat{y} \\ &= \omega\hat{x}[1 - (m_2/m_b)(3m_1 + m_2) + 2m_1/\hat{r}] + \partial\eta^{\hat{t}}/\partial\hat{y}. \end{aligned} \quad (2.57)$$

These two equations determine the rotation rate Ω as follows: the function $\eta^{\hat{t}}(\hat{x}, \hat{y}, \hat{z})$ must satisfy $\partial^2\eta^{\hat{t}}/\partial\hat{x}\partial\hat{y} = \partial^2\eta^{\hat{t}}/\partial\hat{y}\partial\hat{x}$. Taking $\partial/\partial\hat{y}$ of Eq. (2.56) and $\partial/\partial\hat{x}$ of Eq. (2.57), equating the mixed partials of $\eta^{\hat{t}}$, and ignoring terms of $O(m^2)$ yields the following equation for Ω :

$$\Omega - \omega[1 - (m_2/b)(1 + 2m_1/m)] = \omega(1 + m_2/b) - \Omega, \quad (2.58)$$

which has solution $\Omega = \omega[1 - \mu/b + O(\epsilon^3)]$. This is the rotation rate of the second black hole's tidal field as seen in the first black hole's local asymptotic rest frame; this value confirms the claim in Sec. 2.3.1 [see Eq. (2.31)]. With Ω in hand, Eqs. (2.56) and (2.57) now yield

$$\eta^{\hat{t}} = (m_2\omega/b)(1 + m_1/m)\hat{x}\hat{y}. \quad (2.59)$$

Gauge transformations can also be thought of as resulting from infinitesimal coordinate transformations. The coordinate transformation corresponding to the gauge transformation given in Eqs. (2.55) and (2.59) is

$$\begin{aligned} \hat{t} &= \check{t} - (m_2\omega/b)(1 + m_1/m)\check{x}\check{y}, \\ \hat{x} &= \check{x}, \quad \hat{y} = \check{y}, \quad \hat{z} = \check{z}. \end{aligned} \quad (2.60)$$

The metric (2.52) expressed in the new coordinates $(\check{t}, \check{x}, \check{y}, \check{z})$ is

$$\begin{aligned} ds^2 &= d\check{t}^2 [-1 + 2m_1/\check{r} + (m_2/b^3)(3\check{x}^2 - \check{r}^2) + (m/b^3)(\check{x}^2 + \check{y}^2)] \\ &\quad + 2\Omega(1 + 2m_1/\check{r})d\check{t}(\check{x}d\check{y} - \check{y}d\check{x}) + (m_2\omega/b^2)d\check{t}[2\check{x}\check{y}d\check{x} + (7\check{x}^2 - 3\check{y}^2 - 5\check{z}^2)d\check{y} + 2\check{y}\check{z}d\check{z}] \\ &\quad + (d\check{x}^2 + d\check{y}^2 + d\check{z}^2)[1 + 2m_1/\check{r} + (m_2/b^3)(3\check{x}^2 - \check{r}^2)], \end{aligned} \quad (2.61)$$

where $\check{r} = (\check{x}^2 + \check{y}^2 + \check{z}^2)^{1/2}$.

The next step is to undo the rotation of the coordinate system. But first some fine adjustment of coordinates is needed in order to obtain the local asymptotic rest frame metric (2.43). To find out what is required, the metric (2.43) can be put in coordinates rotating with angular velocity Ω .

It turns out that the fine adjustment needed is

$$\begin{aligned}\tilde{t} &= \bar{t} + (m_2\omega/2b^2)(3\bar{x}^2 - \bar{y}^2 - \bar{z}^2)\bar{y}, \\ \tilde{x} &= \bar{x}, \quad \tilde{y} = \bar{y}, \quad \tilde{z} = \bar{z}.\end{aligned}\tag{2.62}$$

In the new coordinates $(\tilde{t}, \tilde{x}, \tilde{y}, \tilde{z})$, the metric (2.61) is

$$\begin{aligned}ds^2 &= d\tilde{t}^2 [-1 + 2m_1/\bar{r} + (m_2/b^3)(3\bar{x}^2 - \bar{r}^2) + (m/b^3)(\bar{x}^2 + \bar{y}^2)] \\ &\quad + 2\Omega(1 + 2m_1/\bar{r})d\tilde{t}(\tilde{x}d\tilde{y} - \tilde{y}d\tilde{x}) + 4(m_2\omega/b^2)d\tilde{t}[-\tilde{x}\tilde{y}d\tilde{x} + (\tilde{x}^2 - \tilde{z}^2)d\tilde{y} + \tilde{y}\tilde{z}d\tilde{z}] \\ &\quad + (d\tilde{x}^2 + d\tilde{y}^2 + d\tilde{z}^2) [1 + 2m_1/\bar{r} + (m_2/b^3)(3\bar{x}^2 - \bar{r}^2)],\end{aligned}\tag{2.63}$$

where $\bar{r} = (\bar{x}^2 + \bar{y}^2 + \bar{z}^2)^{1/2}$. Now eliminate the rotation of coordinates by defining

$$\begin{aligned}\tilde{t} &= T, \quad \tilde{x} = X \cos \Omega T + Y \sin \Omega T, \\ \tilde{y} &= -X \sin \Omega T + Y \cos \Omega T, \quad \tilde{z} = Z.\end{aligned}\tag{2.64}$$

Transforming the metric (2.63) using Eq. (2.64) results in the local asymptotic rest frame metric (2.43).

The transformation from corotating post-Newtonian coordinates (t, x, y, z) to isotropic internal coordinates (T, X, Y, Z) can now be gotten by composing the transformations (2.44), (2.48), (2.49), (2.51), (2.60), (2.62), and (2.64). Inverting this composite map gives the following transformation from internal to corotating coordinates:

$$\begin{aligned}T &= t \left[1 - \frac{m_2}{b} \left(1 + \frac{m_2}{2m} \right) \right] - y \left[\frac{m_2}{\sqrt{mb}} + \frac{m_2}{b} \sqrt{\frac{m}{b}} \left(3 + \frac{m_1}{m} + \frac{m_2^2}{2m^2} \right) \right] \\ &\quad + \frac{m_2 y}{b^2} \sqrt{\frac{m}{b}} \left[\left(1 + \frac{m_1}{m} \right) \xi - \frac{1}{2b} (3\xi^2 - y^2 - z^2) \right], \\ X &= \Gamma \cos \Omega T - \Lambda \sin \Omega T, \\ Y &= \Gamma \sin \Omega T + \Lambda \cos \Omega T, \\ Z &= z \left(1 + \frac{m_2}{b} - \frac{m_2 \xi}{b^2} \right),\end{aligned}\tag{2.65}$$

where

$$\begin{aligned}\xi &= x - \frac{m_2 b}{m}, \quad \Gamma = \xi \left(1 + \frac{m_2}{b} \right) - \frac{m_2}{2b^2} (\xi^2 + y^2 - z^2), \\ \Lambda &= y \left[1 + \frac{m_2}{b} \left(1 + \frac{m_2}{2m} \right) \right], \quad \Omega = \omega \left(1 - \frac{\mu}{b} \right),\end{aligned}\tag{2.66}$$

and terms of $O(m^2)$ have been dropped. In terms of the coordinates (x, y, z) ,

$$R = (\Gamma^2 + \Lambda^2 + Z^2)^{1/2} \quad (2.67)$$

[cf. Eq. (2.21)].

There are two reasons why terms of $O(m^2)$ were dropped from the metric (2.9) at the beginning of this section. First, suppose that such terms were kept and were used to calculate higher-order deformation of the black hole. Since internal metric components are coupled to each other via the Einstein equations (in particular, the components of a black hole perturbation are coupled via the linearized Einstein equations), to be fully consistent, terms of $O(m^2)$ would have to be included in the spatial part g_{ij} of the metric (2.9). But these terms are of higher order than first post-Newtonian, and so have not been included in this paper.

Second, black-hole perturbations with asymptotic form $m^2 r_1^p / b^{p+2}$ ($p \geq 2$) in the buffer zone, which come from terms of $O(m^2)$ in g_{00} in Eq. (2.9), are actually smaller in the internal region than the perturbation with asymptotic form $m_2 r_1^3 / b^4$ in the buffer zone; the latter perturbation has been ignored in this paper. Once terms of $O(m^2)$ were dropped in Eq. (2.9), all terms of $O(m^2)$ were consistently discarded in this section.

2.4.2 Internal metric in corotating coordinates

In this section, the transformation (2.65) is applied to the internal metric (2.42) throughout region I (not just in the buffer zone). This puts the internal metric in corotating post-Newtonian coordinates (t, x, y, z) . In order to preserve finiteness of the perturbations (2.37)–(2.38) and (2.39)–(2.40) at the horizon of BH1, all terms must be kept when performing the transformation. The rotation in Eq. (2.65) can easily be performed on the metric (2.41) by first defining $\varphi = \phi - \Omega T$ and then setting $\Gamma = R \sin \theta \cos \varphi$, $\Lambda = R \sin \theta \sin \varphi$, and $Z = R \cos \theta$. To complete the transformation (2.65), define the functions $P_{\alpha\beta}(x, y, z)$ for $\alpha, \beta = 0, \dots, 3$ to be components of the internal metric in coordinates (T, Γ, Λ, Z) ; write the components as functions of (x, y, z) using Eqs. (2.65) and (2.66). Explicitly, the functions $P_{\alpha\beta}$ are

$$\begin{aligned} P_{00} &= - \left(\frac{1 - m_1/2R}{1 + m_1/2R} \right)^2 + \frac{m_2}{b^3} \left(1 - \frac{m_1}{2R} \right)^4 (3\Gamma^2 - R^2) \\ &\quad - \frac{4\epsilon m_2}{b^3} \Omega \Gamma \left(1 - \frac{m_1}{2R} \right)^2 \left(1 + \frac{m_1}{2R} \right)^4 (2Z^2 - R^2) \\ &\quad + \Omega^2 \left(1 + \frac{m_1}{2R} \right)^4 (\Gamma^2 + \Lambda^2) \left\{ 1 + \frac{m_2}{b^3} (3\Gamma^2 - R^2) \left[\left(1 + \frac{m_1}{2R} \right)^4 - \frac{2m_1^2}{R^2} \right] \right\}, \\ P_{01} &= P_{10} = - \frac{2\epsilon m_2}{b^3} \left(1 - \frac{m_1}{2R} \right)^2 \left(1 + \frac{m_1}{2R} \right)^4 \Gamma \Lambda \\ &\quad - \Omega \Lambda \left(1 + \frac{m_1}{2R} \right)^4 \left\{ 1 + \frac{m_2}{b^3} (3\Gamma^2 - R^2) \left[\left(1 + \frac{m_1}{2R} \right)^4 - \frac{2m_1^2}{R^2} \right] \right\}, \end{aligned}$$

$$\begin{aligned}
P_{02} &= P_{20} = \frac{2\epsilon m_2}{b^3} \left(1 - \frac{m_1}{2R}\right)^2 \left(1 + \frac{m_1}{2R}\right)^4 (\Gamma^2 - Z^2) \\
&\quad + \Omega \Gamma \left(1 + \frac{m_1}{2R}\right)^4 \left\{1 + \frac{m_2}{b^3} (3\Gamma^2 - R^2) \left[\left(1 + \frac{m_1}{2R}\right)^4 - \frac{2m_1^2}{R^2}\right]\right\}, \\
P_{03} &= P_{30} = \frac{2\epsilon m_2}{b^3} \left(1 - \frac{m_1}{2R}\right)^2 \left(1 + \frac{m_1}{2R}\right)^4 \Lambda Z, \\
P_{11} &= \left(1 + \frac{m_1}{2R}\right)^4 \left\{1 + \frac{m_2}{b^3} (3\Gamma^2 - R^2) \left[\left(1 + \frac{m_1}{2R}\right)^4 - \frac{2m_1^2}{R^2} - \frac{2m_1}{R^3} \left(1 + \frac{m_1^2}{4R^2}\right) \Gamma^2\right]\right\}, \\
P_{22} &= \left(1 + \frac{m_1}{2R}\right)^4 \left\{1 + \frac{m_2}{b^3} (3\Gamma^2 - R^2) \left[\left(1 + \frac{m_1}{2R}\right)^4 - \frac{2m_1^2}{R^2} - \frac{2m_1}{R^3} \left(1 + \frac{m_1^2}{4R^2}\right) \Lambda^2\right]\right\}, \\
P_{33} &= \left(1 + \frac{m_1}{2R}\right)^4 \left\{1 + \frac{m_2}{b^3} (3\Gamma^2 - R^2) \left[\left(1 + \frac{m_1}{2R}\right)^4 - \frac{2m_1^2}{R^2} - \frac{2m_1}{R^3} \left(1 + \frac{m_1^2}{4R^2}\right) Z^2\right]\right\}, \\
P_{12} &= P_{21} = -\frac{2m_1 m_2}{R^3 b^3} \left(1 + \frac{m_1}{2R}\right)^4 \left(1 + \frac{m_1^2}{4R^2}\right) (3\Gamma^2 - R^2) \Gamma \Lambda, \\
P_{13} &= P_{31} = -\frac{2m_1 m_2}{R^3 b^3} \left(1 + \frac{m_1}{2R}\right)^4 \left(1 + \frac{m_1^2}{4R^2}\right) (3\Gamma^2 - R^2) \Gamma Z, \\
P_{23} &= P_{32} = -\frac{2m_1 m_2}{R^3 b^3} \left(1 + \frac{m_1}{2R}\right)^4 \left(1 + \frac{m_1^2}{4R^2}\right) (3\Gamma^2 - R^2) \Lambda Z, \tag{2.68}
\end{aligned}$$

where $\epsilon = (m/b)^{1/2}$, $\Omega = \omega(1 - \mu/b)$, $R = (\Gamma^2 + \Lambda^2 + Z^2)^{1/2}$, and Γ , Λ , and Z are given in terms of (x, y, z) in Eqs. (2.65) and (2.66).

Next define the functions $K_\rho^\sigma(x, y, z)$ for $\rho, \sigma = 0, \dots, 3$ by $K_\rho^0 = \partial T / \partial x^\rho$, $K_\rho^1 = \partial \Gamma / \partial x^\rho$, $K_\rho^2 = \partial \Lambda / \partial x^\rho$, and $K_\rho^3 = \partial Z / \partial x^\rho$, where (T, Γ, Λ, Z) are to be expressed in terms of (t, x, y, z) using Eqs. (2.65) and (2.66). Explicitly, the functions K_ρ^σ are

$$\begin{aligned}
K_0^0 &= 1 - \frac{m_2}{b} \left(1 + \frac{m_2}{2m}\right), & K_1^0 &= \frac{\epsilon m_2 y}{b^2} \left(1 + \frac{m_1}{m} - \frac{3\xi}{b}\right), \\
K_2^0 &= -\epsilon \left[\frac{m_2}{m} + \frac{m_2}{b} \left(3 + \frac{m_1}{m} + \frac{m_2^2}{2m^2}\right)\right] + \frac{\epsilon m_2}{b^2} \left[\left(1 + \frac{m_1}{m}\right) \xi - \frac{1}{2b} (3\xi^2 - 3y^2 - z^2)\right], \\
K_3^0 &= \frac{\epsilon m_2}{b^3} yz, \\
K_0^1 &= 0, & K_1^1 &= 1 + \frac{m_2}{b} - \frac{m_2 \xi}{b^2}, & K_2^1 &= -\frac{m_2 y}{b^2}, & K_3^1 &= \frac{m_2 z}{b^2}, \\
K_0^2 &= 0, & K_1^2 &= 0, & K_2^2 &= 1 + \frac{m_2}{b} \left(1 + \frac{m_2}{2m}\right), & K_3^2 &= 0, \\
K_0^3 &= 0, & K_1^3 &= -\frac{m_2 z}{b^2}, & K_2^3 &= 0, & K_3^3 &= 1 + \frac{m_2}{b} - \frac{m_2 \xi}{b^2}, \tag{2.69}
\end{aligned}$$

where $\epsilon = (m/b)^{1/2}$ and $\xi = x - m_2 b / m$.

The metric in region I can now be written in terms of the functions $P_{\alpha\beta}$ and K_ρ^σ . It is given in corotating coordinates (t, x, y, z) by

$$g_{\mu\nu}(x, y, z) = \sum_{\alpha, \sigma=0}^3 P_{\alpha\sigma}(x, y, z) K_\mu^\alpha(x, y, z) K_\nu^\sigma(x, y, z) \tag{2.70}$$

with $P_{\alpha\beta}$ and K_ρ^σ as defined in Eqs. (2.68) and (2.69). Note that the metric components are explicitly

independent of time t . This metric is valid throughout region I (up to the first black hole's apparent horizon) and matches (to some finite order; see below) the post-Newtonian metric (2.9) at $r_1 = r_1^{in}$.

Errors in the internal metric (2.70) will only be analyzed in the weak-gravity buffer zone $m_1 \ll r_1 \ll b$. The largest errors come from inaccuracies in the coordinate transformation (2.65). Terms of the form $(m^2/b^2)(r_1/b)^p$ for integer $p \geq 1$ have been ignored in Eq. (2.65). This leads to errors $\delta g_{\mu\nu} \sim \epsilon^4$ for $r_1 \lesssim r_1^{in}$.

The match between the internal and post-Newtonian metrics at $r_1 = r_1^{in}$ is not perfect; there are discontinuities $[g_{\mu\nu}]$ in the metric components on that 3-surface. A term of the form m_1^3/r_1^3 in the internal metric component g_{00} [as given in Eq. (2.70)] is not matched in the post-Newtonian metric component g_{00} in Eq. (2.9); as a result, $[g_{00}] \sim \epsilon^3$ at $r_1 = r_1^{in}$. Similarly, a term of the form m_1^2/r_1^2 is not matched in g_{ij} , so $[g_{ij}] \sim \epsilon^2$. Lastly, a term of the form m_1^2/R^2 in the internal-coordinate metric component g_{00} in Eq. (2.42) gives via a (partial) Lorentz boost an unmatched term of the form $\epsilon m_1^2/r_1^2$ in the internal-metric component g_{0i} in corotating coordinates [given in Eq. (2.70)]; so $[g_{0i}] \sim \epsilon^3$.

The internal metric (2.70) contains terms of the form $(m_1/r_1)^p(m_2 r_1^2/b^3)$, $p \geq 1$, in the buffer zone. These terms represent the first black hole's multipole moments and the nonlinear interaction of internal and external gravitational fields. They are of $O(\epsilon^{p+4})$, $p \geq 1$, in the buffer zone and have not been matched to the post-Newtonian near-zone metric (2.9). At the level of accuracy achieved in this paper, the metric (2.9) need not be modified to include the near-zone gravitational effects of the black holes' deformation.

2.4.3 Metric near the second black hole

An identical procedure can now be followed to obtain the metric in corotating post-Newtonian coordinates in region II. However, it is not necessary to repeat all the steps. This metric can simply be gotten as follows: exchange $m_1 \leftrightarrow m_2$ in the internal metric (2.42) and in the transformation (2.65); take $x \rightarrow -x$ and $y \rightarrow -y$ in Eq. (2.65); then transform. In other words, the metric components in region II [denoted $g_{\mu\nu}^II(t, x, y, z)$] are related to those in region I [$g_{\mu\nu}^I(t, x, y, z)$] by $g_{\mu\nu}^II(t, x, y, z) = (-1)^p g_{\mu\nu}^I(t, -x, -y, z)$ (with $m_1 \leftrightarrow m_2$), where p is the number of the indices μ and ν that are equal to 1 or 2.

Define $\bar{P}_{\alpha\beta}$ to be $P_{\alpha\beta}$ with m_1 and m_2 exchanged, and similarly \bar{K}_ρ^σ to be K_ρ^σ with $m_1 \leftrightarrow m_2$. Then the metric in region II is given in corotating coordinates (t, x, y, z) by

$$g_{\mu\nu}(x, y, z) = (-1)^p \sum_{\alpha, \sigma=0}^3 \bar{P}_{\alpha\sigma}(-x, -y, z) \bar{K}_\mu^\alpha(-x, -y, z) \bar{K}_\nu^\sigma(-x, -y, z) \quad (2.71)$$

where p is, as above, the number of the indices μ and ν that are equal to 1 or 2. Again, the metric components are explicitly independent of time t . This metric is valid up to the second black hole's

apparent horizon and matches (to a finite order) the post-Newtonian metric (2.9) at $r_2 = r_2^{in}$. Error analysis for this metric is identical to the analysis above for the metric in region I.

2.5 Results and discussion

The result of this calculation is an approximate solution to Einstein's equations representing two widely separated nonrotating black holes in a circular orbit. The metric has been expressed in a single set of coordinates valid up to the black holes' apparent horizons; the coordinate system chosen is corotating coordinates (t, x, y, z) . In these coordinates, the metric components are explicitly independent of time t . The metric is specified in region I by Eq. (2.70), in region II by Eq. (2.71), in region III by Eq. (2.9), and in region IV by Eq. (2.18). At the boundaries $r_1 = r_1^{in}$, $r_2 = r_2^{in}$, and $r = r^{out}$ of these regions, there are discontinuities in the metric components that result from truncation of perturbative expansions and finite-order matching. The magnitudes of these discontinuities can be reduced by taking this calculation to higher orders.

The full 4-metric is summarized below:

$$g_{00} = \begin{cases} \sum_{\mu,\nu=0}^3 P_{\mu\nu}(x, y, z) K_0^\mu(x, y, z) K_0^\nu(x, y, z), & \text{in region I;} \\ \sum_{\mu,\nu=0}^3 \bar{P}_{\mu\nu}(-x, -y, z) \bar{K}_0^\mu(-x, -y, z) \bar{K}_0^\nu(-x, -y, z), & \text{in region II;} \\ -1 + \frac{2m_1}{r_1} + \frac{2m_2}{r_2} - 2 \left(\frac{m_1}{r_1} + \frac{m_2}{r_2} \right)^2 + \frac{3\mu}{b} \left(\frac{m_2}{r_1} + \frac{m_1}{r_2} \right) \\ \quad - \frac{\mu}{b} \left(\frac{m_2}{r_1^3} + \frac{m_1}{r_2^3} \right) y^2 - 7\mu\epsilon^2 \left(\frac{1}{r_1} - \frac{1}{r_2} \right) \frac{x}{b} \\ \quad - 2\mu\epsilon^2 \left(\frac{1}{r_1} + \frac{1}{r_2} \right) + \omega^2 \left(1 + \frac{2m_1}{r_1} + \frac{2m_2}{r_2} \right) (x^2 + y^2), & \text{in region III;} \\ -1 + \frac{2m}{r} \left(1 - \frac{\mu}{2b} \right) - \frac{2m^2}{r^2} + A + \frac{2\epsilon^2}{b} \mathcal{L}B - 2\epsilon\mathcal{M}D \\ \quad + \omega^2 (x^2 + y^2) E + \frac{\epsilon^4}{b^2} \mathcal{L}^2 N + \epsilon^2 \mathcal{M}^2 S - \frac{12\mu\epsilon^5}{r^2 b^2} \frac{\delta m}{m} \mathcal{L}^2 \mathcal{M}, & \text{in region IV.} \end{cases} \quad (2.72)$$

$$g_{0x} = \begin{cases} \sum_{\mu,\nu=0}^3 P_{\mu\nu}(x, y, z) K_0^\mu(x, y, z) K_1^\nu(x, y, z), & \text{in region I;} \\ -\sum_{\mu,\nu=0}^3 \bar{P}_{\mu\nu}(-x, -y, z) \bar{K}_0^\mu(-x, -y, z) \bar{K}_1^\nu(-x, -y, z), & \text{in region II;} \\ -\omega y \left(1 + \frac{2m_1}{r_1} + \frac{2m_2}{r_2} \right), & \text{in region III;} \\ \epsilon B \sin \omega r + bD \cos \omega r - \omega E y + \frac{\epsilon^3}{b} \mathcal{L}N \sin \omega r \\ \quad - \epsilon b \mathcal{M} S \cos \omega r + \frac{6\mu\epsilon^4}{r^2 b} \frac{\delta m}{m} \mathcal{L} (x \cos 2\omega r - y \sin 2\omega r), & \text{in region IV.} \end{cases} \quad (2.73)$$

$$g_{0y} = \begin{cases} \sum_{\mu,\nu=0}^3 P_{\mu\nu}(x, y, z) K_0^\mu(x, y, z) K_2^\nu(x, y, z), & \text{in region I;} \\ -\sum_{\mu,\nu=0}^3 \bar{P}_{\mu\nu}(-x, -y, z) \bar{K}_0^\mu(-x, -y, z) \bar{K}_2^\nu(-x, -y, z), & \text{in region II;} \\ \omega x \left(1 + \frac{2m_1}{r_1} + \frac{2m_2}{r_2} \right) - 4\mu\epsilon \left(\frac{1}{r_1} - \frac{1}{r_2} \right), & \text{in region III;} \\ \epsilon B \cos \omega r - bD \sin \omega r + \omega E x + \frac{\epsilon^3}{b} \mathcal{L}N \cos \omega r \\ \quad + \epsilon b \mathcal{M} S \sin \omega r - \frac{6\mu\epsilon^4}{r^2 b} \frac{\delta m}{m} \mathcal{L} (x \sin 2\omega r + y \cos 2\omega r), & \text{in region IV.} \end{cases} \quad (2.74)$$

$$g_{0z} = \begin{cases} \sum_{\mu,\nu=0}^3 P_{\mu\nu}(x, y, z) K_0^\mu(x, y, z) K_3^\nu(x, y, z), & \text{in region I;} \\ \sum_{\mu,\nu=0}^3 \bar{P}_{\mu\nu}(-x, -y, z) \bar{K}_0^\mu(-x, -y, z) \bar{K}_3^\nu(-x, -y, z), & \text{in region II;} \\ 0, & \text{in region III;} \\ 0, & \text{in region IV.} \end{cases} \quad (2.75)$$

$$g_{xx} = \begin{cases} \sum_{\mu,\nu=0}^3 P_{\mu\nu}(x, y, z) K_1^\mu(x, y, z) K_1^\nu(x, y, z), & \text{in region I;} \\ \sum_{\mu,\nu=0}^3 \bar{P}_{\mu\nu}(-x, -y, z) \bar{K}_1^\mu(-x, -y, z) \bar{K}_1^\nu(-x, -y, z), & \text{in region II;} \\ 1 + \frac{2m_1}{r_1} + \frac{2m_2}{r_2}, & \text{in region III;} \\ E + \frac{m^2 x^2}{r^4} + \epsilon^2 N \sin^2 \omega r + b^2 S \cos^2 \omega r + \frac{6\mu\epsilon^3}{r^2} \frac{\delta m}{m} \mathcal{L} \sin 2\omega r, & \text{in region IV.} \end{cases} \quad (2.76)$$

$$g_{yy} = \begin{cases} \sum_{\mu,\nu=0}^3 P_{\mu\nu}(x, y, z) K_2^\mu(x, y, z) K_2^\nu(x, y, z), & \text{in region I;} \\ \sum_{\mu,\nu=0}^3 \bar{P}_{\mu\nu}(-x, -y, z) \bar{K}_2^\mu(-x, -y, z) \bar{K}_2^\nu(-x, -y, z), & \text{in region II;} \\ 1 + \frac{2m_1}{r_1} + \frac{2m_2}{r_2}, & \text{in region III;} \\ E + \frac{m^2 y^2}{r^4} + \epsilon^2 N \cos^2 \omega r + b^2 S \sin^2 \omega r - \frac{6\mu\epsilon^3}{r^2} \frac{\delta m}{m} \mathcal{L} \sin 2\omega r, & \text{in region IV.} \end{cases} \quad (2.77)$$

$$g_{zz} = \begin{cases} \sum_{\mu,\nu=0}^3 P_{\mu\nu}(x, y, z) K_3^\mu(x, y, z) K_3^\nu(x, y, z), & \text{in region I;} \\ \sum_{\mu,\nu=0}^3 \bar{P}_{\mu\nu}(-x, -y, z) \bar{K}_3^\mu(-x, -y, z) \bar{K}_3^\nu(-x, -y, z), & \text{in region II;} \\ 1 + \frac{2m_1}{r_1} + \frac{2m_2}{r_2}, & \text{in region III;} \\ E + \frac{m^2 z^2}{r^4}, & \text{in region IV.} \end{cases} \quad (2.78)$$

$$g_{xy} = \begin{cases} \sum_{\mu,\nu=0}^3 P_{\mu\nu}(x, y, z) K_1^\mu(x, y, z) K_2^\nu(x, y, z), & \text{in region I;} \\ \sum_{\mu,\nu=0}^3 \bar{P}_{\mu\nu}(-x, -y, z) \bar{K}_1^\mu(-x, -y, z) \bar{K}_2^\nu(-x, -y, z), & \text{in region II;} \\ 0, & \text{in region III;} \\ \frac{m^2}{r^4} xy + \frac{1}{2}(\epsilon^2 N - b^2 S) \sin 2\omega r + \frac{6\mu\epsilon^3}{r^2} \frac{\delta m}{m} \mathcal{L} \cos 2\omega r, & \text{in region IV.} \end{cases} \quad (2.79)$$

$$g_{xz} = \begin{cases} \sum_{\mu,\nu=0}^3 P_{\mu\nu}(x, y, z) K_1^\mu(x, y, z) K_3^\nu(x, y, z), & \text{in region I;} \\ -\sum_{\mu,\nu=0}^3 \bar{P}_{\mu\nu}(-x, -y, z) \bar{K}_1^\mu(-x, -y, z) \bar{K}_3^\nu(-x, -y, z), & \text{in region II;} \\ 0, & \text{in region III;} \\ \frac{m^2}{r^4} xz, & \text{in region IV.} \end{cases} \quad (2.80)$$

$$g_{yz} = \begin{cases} \sum_{\mu,\nu=0}^3 P_{\mu\nu}(x, y, z) K_2^\mu(x, y, z) K_3^\nu(x, y, z), & \text{in region I;} \\ -\sum_{\mu,\nu=0}^3 \bar{P}_{\mu\nu}(-x, -y, z) \bar{K}_2^\mu(-x, -y, z) \bar{K}_3^\nu(-x, -y, z), & \text{in region II;} \\ 0, & \text{in region III;} \\ \frac{m^2}{r^4} yz, & \text{in region IV.} \end{cases} \quad (2.81)$$

In the expressions above, $m = m_1 + m_2$, $\mu = m_1 m_2 / m$, $\delta m = m_1 - m_2$, $\epsilon = (m/b)^{1/2}$, $\omega = (m/b^3)^{1/2}$, $r_1 = [(x - m_2 b/m)^2 + y^2 + z^2]^{1/2}$, $r_2 = [(x + m_1 b/m)^2 + y^2 + z^2]^{1/2}$, $\mathcal{L} = x \cos \omega r - y \sin \omega r$, and $\mathcal{M} = x \sin \omega r + y \cos \omega r$. Region I is specified by $r_1 < (m_1 b)^{1/2}$ and region II by $r_2 < (m_2 b)^{1/2}$ (but these regions do not extend inside the black holes' apparent horizons). Region III is specified by $r_1 > (m_1 b)^{1/2}$, $r_2 > (m_2 b)^{1/2}$, and $r < b/2\epsilon$; and region IV by $r > b/2\epsilon$. The functions A , B , D , E , N , and S are defined in Eq. (2.19). The functions $P_{\alpha\beta}$ and K_ρ^σ are defined in Eqs. (2.68) and (2.69). The functions $\bar{P}_{\alpha\beta}$ and \bar{K}_ρ^σ are obtained from $P_{\alpha\beta}$ and K_ρ^σ respectively by exchanging m_1 and m_2 .

The errors and discontinuities in the metric components are summarized in Table 2.1. The discontinuities should be smoothed out before initial data are extracted from the metric. In addition, initial data taken should be relaxed numerically to approach more closely an exact solution of the constraint equations. It is expected that higher-order versions of this calculation will differ by smaller amounts from an exact solution of the Einstein equations.

	Region I or II	disc. at	Region III			disc. at $r = r^{out}$	Region IV	
	$r_1 \lesssim r_1^{in}$ or $r_2 \lesssim r_2^{in}$	$r_1 = r_1^{in}$ or $r_2 = r_2^{in}$	$r_1 \gtrsim r_1^{in}$ or $r_2 \gtrsim r_2^{in}$	$r_1 \sim b$ and $r_2 \sim b$	$r \lesssim r^{out}$		$r \gtrsim r^{out}$	$r \sim b/\epsilon^2$
g_{00}	4	3	3	6	5	5	7	8
g_{0i}	4	3	3	5	5	5	7	8
g_{ij}	4	2	2	4	5	5	7	8

Table 2.1: Errors and discontinuities in the metric components in corotating coordinates. Numbers denote orders in $\epsilon = (m/b)^{1/2}$; e.g., 4 denotes $O(\epsilon^4)$. The last two columns contain normalized errors.

Acknowledgments

I would like to thank Kip Thorne for suggesting this research project and for his guidance during its completion. This research was supported in part by NASA grant NAG5-6840 and by NSF grant AST-9731698.

2.6 Bibliography

- [1] P. R. Brady, J. D. E. Creighton, and K. S. Thorne, Phys. Rev. D **58**, 061501 (1998).
- [2] F. K. Manasse, J. Math. Phys. **4**, 746 (1963).
- [3] P. D. D'Eath, Phys. Rev. D **11**, 1387 (1975).
- [4] P. D. D'Eath, Phys. Rev. D **12**, 2183 (1975).
- [5] L. Blanchet, G. Faye, and B. Ponsot, Phys. Rev. D **58**, 124002 (1998).
- [6] C. M. Will and A. G. Wiseman, Phys. Rev. D **54**, 4813 (1996).
- [7] L. Blanchet, T. Damour, and B. R. Iyer, Phys. Rev. D **51**, 5360 (1995).
- [8] K. S. Thorne and J. B. Hartle, Phys. Rev. D **31**, 1815 (1985).
- [9] L. G. Fishbone, Astrophys. J. **185**, 43 (1973).
- [10] J.-A. Marck, Proc. R. Soc. Lond. A **385**, 431 (1983).
- [11] F. K. Manasse and C. W. Misner, J. Math. Phys. **4**, 735 (1963).

- [12] *Black Holes: The Membrane Paradigm*, edited by K. S. Thorne, R. H. Price, and D. A. MacDonald (Yale University Press, New Haven, 1986).
- [13] K. S. Thorne, private communication.
- [14] T. Regge and J. A. Wheeler, *Phys. Rev.* **108**, 1063 (1957).
- [15] J. B. Hartle, *Phys. Rev. D* **8**, 1010 (1973).

Chapter 3

Ingoing coordinates for binary black holes

Abstract

In Chapter 2, a binary black hole 4-metric was presented in a post-Newtonian corotating coordinate system valid only up to the holes' apparent horizons. In this chapter, I define an ingoing coordinate transformation that extends this corotating coordinate system through the holes' horizons and into their interiors. The motivation for using ingoing coordinates is that numerical simulations of black holes require the computational grid to extend inside the horizons. The coordinate transformation presented here makes the binary black hole 4-metric suitable as a source of initial data for numerical simulations.

3.1 Introduction

In this chapter, I write the binary black hole 4-metric from Chapter 2 in coordinates that are corotating and post-Newtonian in the radiation and near zones and smoothly become ingoing near the black holes. This coordinate system is valid through the holes' horizons and covers the holes' interiors as well as the near and radiation zones. The metric components in this coordinate system are explicitly nonsingular on the black hole horizons. The metric presented here is promising as a source of initial data for numerical simulations of binary black holes. Since these simulations require the computational grid to extend inside the holes' horizons, the coordinate system used near the black holes in Chapter 2 is not suitable for numerical relativity.

Let us begin with the metric near the first black hole, that is, in region I in the terminology of Chapter 2 (see Fig. 1 in Chapter 2). This metric is the Schwarzschild metric plus electric-type and magnetic-type tidal perturbations due to the second black hole, and is given in isotropic coordinates in Eq. (3.22) of Chapter 2. The second black hole's tidal field rotates with angular velocity Ω as seen by inertial observers in the first black hole's local asymptotic rest frame. However, the tidal perturbation's angular dependence $\phi - \Omega \tilde{t}$ as given in Eq. (3.22) of Chapter 2 (*I have replaced*

T in that equation with \tilde{t}) is singular at the first black hole's horizon. The reason is that the Schwarzschild time coordinate \tilde{t} , though suitable for matched asymptotic expansions in the buffer zone around the black hole, is badly behaved at the horizon. Since our goal in this chapter is to come up with coordinates valid through the horizon and inside the black hole, we must use a time coordinate T with the property that the hypersurfaces of constant time coincide with Schwarzschild time slices in the buffer zone but smoothly transition into ingoing Eddington-Finkelstein time slices which penetrate the horizon. The singular angular dependence $\phi - \Omega\tilde{t}$ can be simply replaced by the nonsingular $\phi - \Omega T$, with T as described above; this is discussed in further detail below.

It turns out that isotropic coordinates are not a good starting point for an ingoing transformation. The analog of the ingoing Eddington-Finkelstein transformation, which is based on ingoing null geodesics of the Schwarzschild spacetime, is unsuccessful when applied to isotropic coordinates: the coordinate system remains singular at the horizon¹. Indeed, the isotropic radial coordinate is only defined outside the black hole. However, isotropic coordinates were used in Chapter 2 to match a tidally perturbed Schwarzschild metric to the post-Newtonian near zone metric. It is therefore necessary to define a new radial coordinate that is equal to the (tidally distorted) isotropic radial coordinate in the buffer zone but transitions smoothly into the (tidally distorted) Schwarzschild radial coordinate near the black hole.

3.2 Ingoing coordinates

Following the notation in Chapter 2, I denote the black holes' masses by m_1 and m_2 , and their coordinate separation in post-Newtonian harmonic coordinates by b . Let $m = m_1 + m_2$, $\epsilon = (m/b)^{1/2}$, and $\Omega = (1 - m_1 m_2 / mb)(m/b^3)^{1/2}$. By assumption, $\epsilon \ll 1$.

Let us begin with the region I metric given in isotropic coordinates in Eq. (3.22) of Chapter 2. Note that, in this chapter, T and R denote the nonsingular time and radial coordinates described in Sec. 3.1, while in the previous chapter, they denoted the isotropic time and radial coordinates. Set $\Omega = 0$ in Eq. (3.22) of Chapter 2 and transform to Schwarzschild coordinates $(\tilde{t}, \tilde{r}, \theta, \phi)$. This yields the metric $\tilde{\mathbf{g}} = \mathbf{g}_S + \tilde{\mathbf{h}}$; the Schwarzschild metric \mathbf{g}_S and the stationary tidal perturbation $\tilde{\mathbf{h}}$ are given in Schwarzschild coordinates by

$$\begin{aligned} \mathbf{g}_S &= - \left(1 - \frac{2m_1}{\tilde{r}}\right) d\tilde{t}^2 + \left(1 - \frac{2m_1}{\tilde{r}}\right)^{-1} d\tilde{r}^2 + \tilde{r}^2 (d\theta^2 + \sin^2 \theta d\phi^2), \\ \tilde{\mathbf{h}} &= - \frac{4m_2}{b^3} \sqrt{\frac{m}{b}} \left(1 - \frac{2m_1}{\tilde{r}}\right) \tilde{r}^3 dt [\cos \theta \sin \phi d\theta + \sin \theta \cos(2\theta) \cos \phi d\phi] \\ &\quad + \frac{m_2 \tilde{r}^2}{b^3} [3 \sin^2 \theta \cos^2 \phi - 1] \left[\left(1 - \frac{2m_1}{\tilde{r}}\right)^2 dt^2 + d\tilde{r}^2 \right] \end{aligned} \quad (3.1)$$

¹I thank M. Vallisneri for pointing this out.

$$+ (\tilde{r}^2 - 2m_1^2)(d\theta^2 + \sin^2 \theta d\phi^2) \Big]. \quad (3.2)$$

In this notation, $d\tilde{t}$, $d\tilde{r}$, $d\theta$, and $d\phi$ are coordinate one-forms and $d\tilde{t}^2$ denotes the tensor product $d\tilde{t} \otimes d\tilde{t}$.

Let ζ_1 and ζ_2 be two numbers satisfying $2 < \zeta_1 < \zeta_2 < (b/m_1)^{1/2}$. Define the new ingoing coordinates (T, R, θ, ϕ) by

$$\tilde{t} = T - 2m_1 \ln \left(\frac{R}{2m_1} - 1 \right) \psi(R), \quad (3.3)$$

$$\tilde{r} = R + m_1 \left(1 + \frac{m_1}{4R} \right) \eta(R). \quad (3.4)$$

The functions $\psi(R)$ and $\eta(R)$ must satisfy the following properties: (i) for $R \geq \zeta_2 m_1$, $\psi(R) = 0$ and $\eta(R) = 1$ so the coordinates are isotropic; (ii) for $R \leq \zeta_1 m_1$, $\psi(R) = 1$ and $\eta(R) = 0$ so the time coordinate is Eddington-Finkelstein and the radial coordinate is Schwarzschild; and (iii) for $\zeta_1 m_1 < R < \zeta_2 m_1$, $\psi(R)$ and $\eta(R)$ smoothly and monotonically vary between their constant values outside this interval. The transition points $R = \zeta_1 m_1$ and $R = \zeta_2 m_1$ and the functions $\psi(R)$ and $\eta(R)$ can be chosen freely as long as the above properties are satisfied. Since $d\tilde{r}/dR = 1 + (m_1 + m_1^2/4R)\eta'(R) - m_1^2\eta(R)/4R^2 \geq 1 - m_1^2/4R^2$, we have $d\tilde{r}/dR > 0$ for $R > 2m_1$, and so Eqs. (3.3) and (3.4) define a valid coordinate transformation.

Transforming (3.1) and (3.2) using (3.3) and (3.4), we obtain

$$\mathbf{g}_S = -f(dT^2 - 2\Psi dT dR + \Psi^2 dR^2) + \frac{H^2}{f} dR^2 + \tilde{r}^2(d\theta^2 + \sin^2 \theta d\phi^2), \quad (3.5)$$

$$\begin{aligned} \tilde{\mathbf{h}} = & -\frac{4\epsilon m_2}{b^3} f \tilde{r}^3 (dT - \Psi dR) [\cos \theta \sin \phi d\theta + \sin \theta \cos(2\theta) \cos \phi d\phi] \\ & + \frac{m_2}{b^3} \tilde{r}^2 (3 \sin^2 \theta \cos^2 \phi - 1) [f^2 (dT^2 - 2\Psi dT dR + \Psi^2 dR^2) + H^2 dR^2 \\ & + (\tilde{r}^2 - 2m_1^2)(d\theta^2 + \sin^2 \theta d\phi^2)], \end{aligned} \quad (3.6)$$

where

$$\Psi(R) = 2m_1 \left[R^{-1} \left(1 - \frac{2m_1}{R} \right)^{-1} \psi(R) + \psi'(R) \ln \left(\frac{R}{2m_1} - 1 \right) \right], \quad (3.7)$$

$$H(R) = 1 + m_1 \left(1 + \frac{m_1}{4R} \right) \eta'(R) - \frac{m_1^2}{4R^2} \eta(R), \quad (3.8)$$

$$f(R) = 1 - \frac{2m_1}{\tilde{r}(R)}, \quad (3.9)$$

and \tilde{r} is given in terms of R in (3.4). Since the linearized Einstein Eq. is a tensor Eq. (see, e.g., Eq. (7.5.15) in [1]) and we have only performed a coordinate transformation, $\tilde{\mathbf{h}}$ remains a solution to this Eq. on the background \mathbf{g}_S . However, the ϕ -dependence of the perturbation $\tilde{\mathbf{h}}$ does not correspond to

the second black hole's rotating tidal field—we set $\Omega = 0$ above. To remedy this, we simply change ϕ to $\phi - \Omega T$ in the components of $\tilde{\mathbf{h}}$, which yields a new perturbation \mathbf{h} . Note that this replacement is not a coordinate transformation; a new tensor \mathbf{h} is defined. Also note that T becomes an ingoing coordinate near the horizon, so the time dependence $\phi - \Omega T$ causes no problems on the horizon. This simple remedy works for the following reason: if we solve the linearized Einstein Eq. order by order in ϵ , then time derivatives of the components of \mathbf{h} produce factors of $m_1 \Omega \sim \epsilon^3$ and can thus be neglected. The perturbation \mathbf{h} is given by

$$\begin{aligned} \mathbf{h} = & -\frac{4\epsilon m_2}{b^3} f \tilde{r}^3 (dT - \Psi dR) [\cos \theta \sin(\phi - \Omega T) d\theta + \sin \theta \cos(2\theta) \cos(\phi - \Omega T) d\phi] \\ & + \frac{m_2}{b^3} \tilde{r}^2 [3 \sin^2 \theta \cos^2(\phi - \Omega T) - 1] [f^2 (dT^2 - 2\Psi dT dR + \Psi^2 dR^2) + H^2 dR^2 \\ & + (\tilde{r}^2 - 2m_1^2)(d\theta^2 + \sin^2 \theta d\phi^2)]. \end{aligned} \quad (3.10)$$

We have now arrived at a metric $\mathbf{g} = \mathbf{g}_S + \mathbf{h}$, where \mathbf{g}_S is given in (3.5) and \mathbf{h} in (3.10), which is valid from the black hole's interior up into and through the buffer zone around the hole, and is written in coordinates that are well behaved throughout this region.

3.3 Transformation to corotating coordinates

The next step is to transform the metric \mathbf{g} to corotating post-Newtonian coordinates (t, x, y, z) using the transformation given in Eqs. (4.22) and (4.23) of Chapter 2. This transformation contains a rotation that can be performed by first defining $\varphi = \phi - \Omega T$ and then setting $\Gamma = R \sin \theta \cos \varphi$, $\Lambda = R \sin \theta \sin \varphi$, and $Z = R \cos \theta$. To complete the transformation, define the functions $P_{\alpha\beta}(x, y, z)$ for $\alpha, \beta = 0, \dots, 3$ to be components of the metric \mathbf{g} in coordinates (T, Γ, Λ, Z) ; write these components as functions of (x, y, z) using Eqs. (4.22) and (4.23) in Chapter 2. The functions $P_{\alpha\beta}$ are given by

$$\begin{aligned} P_{00} &= -f + \frac{\tilde{r}^2}{R^2} \Omega^2 (\Gamma^2 + \Lambda^2) - \frac{4\epsilon m_2 \tilde{r}^3}{b^3 R^3} (2Z^2 - R^2) f \Omega \Gamma \\ &\quad + \frac{m_2 \tilde{r}^2}{b^3 R^2} (3\Gamma^2 - R^2) \left[f^2 + \frac{\Omega^2}{R^2} (\tilde{r}^2 - 2m_1^2) (\Gamma^2 + \Lambda^2) \right], \\ P_{01} &= P_{10} = \frac{\Gamma}{R} f \Psi - \frac{\tilde{r}^2}{R^2} \Omega \Lambda - \frac{2\epsilon m_2 \tilde{r}^3}{b^3 R^3} f \left[\Gamma \Lambda - \frac{\Omega}{R} \Psi \Gamma^2 (2Z^2 - R^2) \right] \\ &\quad + \frac{m_2 \tilde{r}^2}{b^3 R^2} (3\Gamma^2 - R^2) \left[-\frac{\Gamma}{R} f^2 \Psi - \frac{\Omega \Lambda}{R^2} (\tilde{r}^2 - 2m_1^2) \right], \\ P_{02} &= P_{20} = \frac{\Lambda}{R} f \Psi + \frac{\tilde{r}^2}{R^2} \Omega \Gamma - \frac{2\epsilon m_2 \tilde{r}^3}{b^3 R^3} f \left[Z^2 - \Gamma^2 - \frac{\Omega}{R} \Psi \Gamma \Lambda (2Z^2 - R^2) \right] \\ &\quad + \frac{m_2 \tilde{r}^2}{b^3 R^2} (3\Gamma^2 - R^2) \left[-\frac{\Lambda}{R} f^2 \Psi + \frac{\Omega \Gamma}{R^2} (\tilde{r}^2 - 2m_1^2) \right], \\ P_{03} &= P_{30} = \frac{Z}{R} f \Psi - \frac{2\epsilon m_2 \tilde{r}^3}{b^3 R^3} f \left[-\Lambda Z - \frac{\Omega}{R} \Psi \Gamma Z (2Z^2 - R^2) \right] \end{aligned}$$

$$\begin{aligned}
& + \frac{m_2 \tilde{r}^2}{b^3 R^2} (3\Gamma^2 - R^2) \left(-\frac{Z}{R} f^2 \Psi \right), \\
P_{11} &= \frac{\Gamma^2}{R^2} \left(-f \Psi^2 + \frac{H^2}{f} - \frac{\tilde{r}^2}{R^2} \right) + \frac{\tilde{r}^2}{R^2} + \frac{4\epsilon m_2 \tilde{r}^3}{b^3 R^4} f \Psi \Gamma^2 \Lambda \\
& + \frac{m_2 \tilde{r}^2}{b^3 R^2} (3\Gamma^2 - R^2) \left[\frac{\Gamma^2}{R^2} (f^2 \Psi^2 + H^2) + R^{-2} (\tilde{r}^2 - 2m_1^2) \left(1 - \frac{\Gamma^2}{R^2} \right) \right], \\
P_{22} &= \frac{\Lambda^2}{R^2} \left(-f \Psi^2 + \frac{H^2}{f} - \frac{\tilde{r}^2}{R^2} \right) + \frac{\tilde{r}^2}{R^2} + \frac{4\epsilon m_2 \tilde{r}^3}{b^3 R^4} f \Psi \Lambda (Z^2 - \Gamma^2) \\
& + \frac{m_2 \tilde{r}^2}{b^3 R^2} (3\Gamma^2 - R^2) \left[\frac{\Lambda^2}{R^2} (f^2 \Psi^2 + H^2) + R^{-2} (\tilde{r}^2 - 2m_1^2) \left(1 - \frac{\Lambda^2}{R^2} \right) \right], \\
P_{33} &= \frac{Z^2}{R^2} \left(-f \Psi^2 + \frac{H^2}{f} - \frac{\tilde{r}^2}{R^2} \right) + \frac{\tilde{r}^2}{R^2} - \frac{4\epsilon m_2 \tilde{r}^3}{b^3 R^4} f \Psi Z^2 \Lambda \\
& + \frac{m_2 \tilde{r}^2}{b^3 R^2} (3\Gamma^2 - R^2) \left[\frac{Z^2}{R^2} (f^2 \Psi^2 + H^2) + R^{-2} (\tilde{r}^2 - 2m_1^2) \left(1 - \frac{Z^2}{R^2} \right) \right], \\
P_{12} &= P_{21} = \frac{\Gamma \Lambda}{R^2} \left(-f \Psi^2 + \frac{H^2}{f} - \frac{\tilde{r}^2}{R^2} \right) + \frac{2\epsilon m_2 \tilde{r}^3}{b^3 R^4} f \Psi \Gamma (-\Gamma^2 + \Lambda^2 + Z^2) \\
& + \frac{m_2 \tilde{r}^2}{b^3 R^4} (3\Gamma^2 - R^2) [f^2 \Psi^2 + H^2 - R^{-2} (\tilde{r}^2 - 2m_1^2)] \Gamma \Lambda, \\
P_{13} &= P_{31} = \frac{\Gamma Z}{R^2} \left(-f \Psi^2 + \frac{H^2}{f} - \frac{\tilde{r}^2}{R^2} \right) \\
& + \frac{m_2 \tilde{r}^2}{b^3 R^4} (3\Gamma^2 - R^2) [f^2 \Psi^2 + H^2 - R^{-2} (\tilde{r}^2 - 2m_1^2)] \Gamma Z, \\
P_{23} &= P_{32} = \frac{\Lambda Z}{R^2} \left(-f \Psi^2 + \frac{H^2}{f} - \frac{\tilde{r}^2}{R^2} \right) + \frac{2\epsilon m_2 \tilde{r}^3}{b^3 R^4} f \Psi Z (-\Gamma^2 - \Lambda^2 + Z^2) \\
& + \frac{m_2 \tilde{r}^2}{b^3 R^4} (3\Gamma^2 - R^2) [f^2 \Psi^2 + H^2 - R^{-2} (\tilde{r}^2 - 2m_1^2)] \Lambda Z,
\end{aligned} \tag{3.11}$$

where $\epsilon = (m/b)^{1/2}$, $\Omega = (1 - m_1 m_2 / mb)(m/b^3)^{1/2}$, $R = (\Gamma^2 + \Lambda^2 + Z^2)^{1/2}$, and Γ , Λ , and Z are to be expressed in terms of (x, y, z) via Eqs. (4.22) and (4.23) in Chapter 2. The functions $\tilde{r}(R)$, $\Psi(R)$, $H(R)$, and $f(R)$ are given in Eqs. (3.4), (3.7), (3.8), and (3.9).

The remainder of the coordinate transformation from black hole coordinates (T, R, θ, ϕ) to corotating post-Newtonian coordinates (t, x, y, z) can be done exactly as in Chapter 2. The final metric in region I (see Fig. 1 in Chapter 2) is given by Eq. (4.27) of Chapter 2, but with $P_{\alpha\beta}$ taken from Eq. (3.11) above. Define $\bar{P}_{\alpha\beta}$ to be $P_{\alpha\beta}$ (as given in (3.11)) with m_1 and m_2 exchanged. Then the metric in region II (that is, near the second black hole; see Fig. 1 in Chapter 2) is given by Eq. (4.28) in Chapter 2, but with $\bar{P}_{\alpha\beta}$ taken from here. Note that the final metric components are everywhere explicitly independent of time t .

To summarize, *the expressions for the metric components given in Sec. V of Chapter 2 are valid in ingoing coordinates if $P_{\alpha\beta}$ (and $\bar{P}_{\alpha\beta}$) are taken from Eq. (3.11) and the functions $\tilde{r}(R)$, $\Psi(R)$, $H(R)$, and $f(R)$ are taken from Eqs. (3.4), (3.7), (3.8), and (3.9) with $\psi(R)$ and $\eta(R)$ having properties (i)–(iii) given below Eq. (3.4).* In order to show explicitly that these components are

nonsingular at the black holes' horizons, I write out $P_{\alpha\beta}$ for $R \leq \zeta_1 m_1$. In this region, $\psi = 1$, $\Psi(R) = 2m_1 R^{-1}(1 - 2m_1/R)^{-1}$, $\eta = 0$, $H = 1$, $\tilde{r} = R$, and $f(R) = 1 - 2m_1/R$. Therefore, for $R \leq \zeta_1 m_1$, $P_{\alpha\beta}$ are given by

$$\begin{aligned}
P_{00} &= -1 + \frac{2m_1}{R} + \Omega^2(\Gamma^2 + \Lambda^2) - \frac{4\epsilon m_2}{b^3} \left(1 - \frac{2m_1}{R}\right) (2Z^2 - R^2)\Omega\Gamma \\
&\quad + \frac{m_2}{b^3}(3\Gamma^2 - R^2) \left[\left(1 - \frac{2m_1}{R}\right)^2 + \Omega^2 \left(1 - \frac{2m_1^2}{R^2}\right) (\Gamma^2 + \Lambda^2) \right], \\
P_{01} &= P_{10} = \frac{2m_1}{R^2}\Gamma - \Omega\Lambda - \frac{2\epsilon m_2}{b^3} \left[\left(1 - \frac{2m_1}{R}\right) \Gamma\Lambda - \frac{2m_1}{R^2}\Omega\Gamma^2(2Z^2 - R^2) \right] \\
&\quad - \frac{m_2}{b^3}(3\Gamma^2 - R^2) \left[\frac{2m_1}{R^2} \left(1 - \frac{2m_1}{R}\right) \Gamma + \Omega\Lambda \left(1 - \frac{2m_1^2}{R^2}\right) \right], \\
P_{02} &= P_{20} = \frac{2m_1}{R^2}\Lambda + \Omega\Gamma - \frac{2\epsilon m_2}{b^3} \left[\left(1 - \frac{2m_1}{R}\right) (Z^2 - \Gamma^2) - \frac{2m_1}{R^2}\Omega\Gamma\Lambda(2Z^2 - R^2) \right] \\
&\quad - \frac{m_2}{b^3}(3\Gamma^2 - R^2) \left[\frac{2m_1}{R^2} \left(1 - \frac{2m_1}{R}\right) \Lambda - \Omega\Gamma \left(1 - \frac{2m_1^2}{R^2}\right) \right], \\
P_{03} &= P_{30} = \frac{2m_1}{R^2}Z + \frac{2\epsilon m_2}{b^3} \left[\left(1 - \frac{2m_1}{R}\right) \Lambda Z + \frac{2m_1}{R^2}\Omega\Gamma Z(2Z^2 - R^2) \right] \\
&\quad - \frac{2m_1 m_2}{b^3 R^2} (3\Gamma^2 - R^2) \left(1 - \frac{2m_1}{R}\right) Z, \\
P_{11} &= 1 + \frac{2m_1 \Gamma^2}{R^3} + \frac{8\epsilon m_1 m_2}{b^3 R^2} \Gamma^2 \Lambda + \frac{m_2}{b^3} (3\Gamma^2 - R^2) \left[1 - \frac{2m_1^2}{R^2} \left(1 - \frac{3\Gamma^2}{R^2}\right) \right], \\
P_{22} &= 1 + \frac{2m_1 \Lambda^2}{R^3} + \frac{8\epsilon m_1 m_2}{b^3 R^2} \Lambda (Z^2 - \Gamma^2) + \frac{m_2}{b^3} (3\Gamma^2 - R^2) \left[1 - \frac{2m_1^2}{R^2} \left(1 - \frac{3\Lambda^2}{R^2}\right) \right], \\
P_{33} &= 1 + \frac{2m_1 Z^2}{R^3} - \frac{8\epsilon m_1 m_2}{b^3 R^2} Z^2 \Lambda + \frac{m_2}{b^3} (3\Gamma^2 - R^2) \left[1 - \frac{2m_1^2}{R^2} \left(1 - \frac{3Z^2}{R^2}\right) \right], \\
P_{12} &= P_{21} = \frac{2m_1 \Gamma \Lambda}{R^3} + \frac{4\epsilon m_1 m_2}{b^3 R^2} \Gamma (R^2 - 2\Gamma^2) + \frac{6m_1^2 m_2}{b^3 R^4} (3\Gamma^2 - R^2) \Gamma \Lambda, \\
P_{13} &= P_{31} = \frac{2m_1 \Gamma Z}{R^3} + \frac{6m_1^2 m_2}{b^3 R^4} (3\Gamma^2 - R^2) \Gamma Z, \\
P_{23} &= P_{32} = \frac{2m_1 \Lambda Z}{R^3} + \frac{4\epsilon m_1 m_2}{b^3 R^2} Z (2Z^2 - R^2) + \frac{6m_1^2 m_2}{b^3 R^4} (3\Gamma^2 - R^2) \Lambda Z, \tag{3.12}
\end{aligned}$$

where $\epsilon = (m/b)^{1/2}$, $\Omega = (1 - m_1 m_2 / mb)(m/b^3)^{1/2}$, $R = (\Gamma^2 + \Lambda^2 + Z^2)^{1/2}$, and Γ , Λ , and Z are to be expressed in terms of (x, y, z) via Eqs. (4.22) and (4.23) in Chapter 2. Note that the quantities $P_{\alpha\beta}$ in Eq. (3.12) are all finite at the horizon $R = 2m_1$.

Acknowledgments

I thank Lee Lindblom, Mark Scheel, Kip Thorne, and Michele Vallisneri for useful discussions. This research was supported in part by NSF grant PHY-9900776.

3.4 Bibliography

- [1] R. M. Wald, *General Relativity* (University of Chicago Press, Chicago, 1984).

Chapter 4

Energy and angular momentum flow into a black hole in a binary

Published as K. Alvi, Phys. Rev. D **64**, 104020 (2001).

Abstract

As a black hole in a binary spirals in gradually from large separation, energy and angular momentum flow not only to infinity but also into or out of the hole. In addition, the hole's horizon area increases slowly during this process. In this paper, the changes in the black hole's mass, spin, and horizon area during inspiral are calculated for a hole in a circular binary with a companion body of possibly comparable mass. When the binary is composed of equal-mass black holes that have spins aligned with the orbital angular momentum and are rapidly rotating (with spins 99.8 percent of their maximal values), it is found that the fractional increase in the surface area of each hole's horizon is one percent by the time the binary spirals down to a separation b of $6M$ (where M is the binary's total mass), and seven percent down to $b = 2M$. The flow of energy and angular momentum into the black holes' horizons changes the number of gravitational-wave cycles in the LIGO band by no more than a tenth of a cycle by the time the binary reaches $b = 2M$. The results obtained in this paper are relevant for the detection and analysis of gravitational waves from binary systems containing a black hole.

4.1 Introduction

Binary black holes are expected to be among the primary sources of gravitational waves for interferometric detectors [1]. Since we do not have exact solutions of Einstein's equations that represent binary black holes in sufficient generality, we must study these systems perturbatively and/or numerically. One regime in which the evolution of binary black holes is well understood is the early inspiral phase. In this phase, the holes' separation is still much larger than the binary's total mass,

and post-Newtonian expansions can be used to analyze the system. Eventually radiation reaction drives the holes together and the post-Newtonian approximation fails. The binary's subsequent evolution must be studied numerically.

While the flow of energy and angular momentum to infinity during inspiral has been calculated to high post-Newtonian order, to date the flow into or out of the black holes' horizons has not been computed except in the extreme-mass-ratio limit; and in that limit, it has been done to very high post-Newtonian order [2] (for numerical work, see, e.g., [3]). Absorption (or emission) of energy and angular momentum by the holes' horizons, while much smaller than emission to infinity, might still be important because extraction of weak gravitational signals from noisy detector output using matched filtering requires knowledge of the orbital evolution to very high accuracy, and black hole absorption/emission might affect the evolution at that level. Two purposes of this paper are to calculate black hole absorption/emission of energy and angular momentum to leading order in a circular binary with holes of possibly comparable mass, and to investigate whether it is relevant for detection and analysis of gravitational waves.

A third purpose of this paper is to provide some information on the interface between the inspiral and merger phases of binary evolution. Numerical simulations of binary black holes typically begin computing at this interface and need initial data representing holes that have spiraled in from infinity, i.e., initial data tied to the inspiral phase and to the post-Newtonian expansions used to describe it. One approach to obtaining such initial data is given in [4]. Since initial data of this sort are not yet being used, one needs to relate the masses, spins, and horizon areas of the black holes present in currently used initial data to the corresponding quantities when the holes were infinitely separated. For this purpose, it is necessary to know how these quantities change during inspiral. In this paper, I calculate the leading-order changes in the holes' masses, spins, and horizon areas during inspiral for a circular binary.

Recently, Price and Whelan [5] have emphasized the role of angular momentum absorption or emission by rapidly rotating black holes at the end of inspiral, when the holes are beginning to merge. Here I focus on the earlier stages of inspiral, when the holes are widely (or moderately) separated and their gravitational effects on each other can be described using black hole perturbation theory.

The results obtained in this paper are actually valid for a black hole in a binary with any companion body (e.g., a neutron star) that is well separated from the hole. The formulas for the changes in black hole quantities presented here depend only on the companion body's mass and not on its internal structure. These formulas therefore remain valid when the companion is not a black hole.

4.2 Framework

I follow the field-theory-in-flat-spacetime notation used in the literature on post-Newtonian expansions (e.g., [6, 7]) and denote 3-vectors by bold-face letters. A centered dot between 3-vectors denotes the usual inner product in flat 3-space; a hatted 3-vector represents the unit vector in that direction.

Consider a black hole binary undergoing circular motion with the separation b between the holes much larger than their total mass $M = M_1 + M_2$, where M_B denotes the mass of the B th hole. Define $\mu = M_1 M_2 / M$ and $\eta = \mu / M$. Label the holes BH1 and BH2, and denote their spins by \mathbf{S}_B and horizon areas by A_B for $B = 1, 2$. Let $S_B = (\mathbf{S}_B \cdot \mathbf{S}_B)^{1/2}$ be the spin magnitudes, and define the parameters χ_B by $S_B = \chi_B M_B^2$ ($B = 1, 2$). Throughout this paper I assume $\chi_B \leq 0.998$ ($B = 1, 2$); this restriction is based on the analysis in [8].

Define each black hole's horizon radius $r_{HB} = M_B [1 + (1 - \chi_B^2)^{1/2}]$, angular velocity $\Omega_{HB} = \chi_B (2r_{HB})^{-1}$, and surface gravity $\kappa_B = (1 - \chi_B^2)^{1/2} (2r_{HB})^{-1}$ ($B = 1, 2$). Introduce the following Newtonian quantities for the binary: the orbital angular momentum \mathbf{L}_N , the orbital angular velocity $\Omega_N = (M/b^3)^{1/2}$, and the relative velocity $v = (M/b)^{1/2}$. By assumption, $v \ll 1$.

Since the black holes are widely separated, each hole has a surrounding region that satisfies the following properties: (i) it is far enough from the hole that gravity is weak there; (ii) it does not extend so far that the companion hole's tidal field varies appreciably in the region [9]. We can place in this region an inertial coordinate system in which the hole is (momentarily) at rest. This region and its local coordinates are referred to as the black hole's local asymptotic rest frame (LARF) [9]. Label the two regions around the holes LARF1 and LARF2.

Usually mass and angular momentum are only defined globally in general relativity, using fields at infinity, since precise local definitions are not available. However, for a black hole well separated from its companion, one can define the hole's mass and angular momentum using fields measured in the hole's LARF; these definitions are inherently ambiguous [9–12]. (For further discussion of the ambiguities, see Sec. 4.6.) I refer to these definitions when discussing a black hole's mass and angular momentum in this paper. I calculate the rates of change of these quantities as measured in the LARF—that is, with respect to time t measured by an inertial observer in the LARF. When integrated over the duration of inspiral, these rates of change should give results exceeding the ambiguities in the definitions of mass and angular momentum, in order to be relevant to the analysis of initial data at the interface between inspiral and merger. This issue will be discussed further in Sec. 4.6.

I also consider slices of constant time t that begin in the LARF and extend into the black hole, intersecting the horizon in 2-surfaces that correspond to constant ingoing-time slices of a Kerr black hole's horizon. (Alternatively, one can consider slices that intersect a “stretched horizon” as discussed in [13] and references therein.) The rate of area increase of these 2-surfaces can be calculated using

the results of Hawking and Hartle [14] combined with black hole perturbation theory [15, 16]. The quantities dM_B/dt and dS_B/dt can then be obtained from dA_B/dt using the first law of black hole mechanics $dM = (\kappa/8\pi)dA + \Omega_H dJ$ and the relation $\omega dJ = m dM$ for black hole perturbation modes of angular frequency ω and azimuthal angular number m [13, 16, 17]. (Here J refers to the black hole's angular momentum.)

Throughout this paper, I focus on BH1 and the changes in its parameters. The corresponding formulas for BH2 are simply obtained by exchanging the subscripts $1 \leftrightarrow 2$ in the final results [e.g., Eqs. (4.11)]. In Sec. 4.3, I consider the special situation in which BH2 is held stationary with respect to BH1. The results from this artificial scenario are used in Sec. 4.4 to analyze a circular binary with black hole spins aligned or anti-aligned with \mathbf{L}_N . The more general case of spins not fully aligned or anti-aligned with \mathbf{L}_N is treated in Sec. 4.5.

4.3 Stationary companion

In this section, I calculate the tidal distortion BH1 suffers when BH2 is held stationary. This involves solving for the Weyl tensor component ψ_0 , which contains complete information about the gravitational perturbation on BH1, using the Teukolsky formalism [15]. With ψ_0 in hand, the rates of change of BH1 parameters can be calculated using the results of Hawking and Hartle [14] and Teukolsky and Press [16].

The first step in this process is to calculate BH2's tidal field as seen in LARF1. I will consider only the lowest-order Newtonian tidal field, which is approximately constant throughout LARF1. To calculate this field and its effect on BH1, consider first a fictitious Euclidean 3-space containing a single stationary body of mass M_2 at coordinate location (b, θ_0, ϕ_0) in a spherical polar coordinate system. The Newtonian gravitational potential at the field point (r, θ, ϕ) is given in these coordinates by

$$\Phi(r, \theta, \phi) = -4\pi \frac{M_2}{b} \sum_{l=0}^{\infty} \sum_{m=-l}^l (2l+1)^{-1} \left(\frac{r}{b}\right)^l Y_{lm}^*(\theta_0, \phi_0) Y_{lm}(\theta, \phi) \quad (4.1)$$

for $r < b$.

We are interested in the gravitational field only in a small neighborhood of the origin satisfying $r \ll b$. In particular, we would like to evaluate the body's tidal field at the origin, so only the $l = 2$ part $\Phi^{(2)}$ of Φ is relevant. The (electric-type) tidal field is given by $\mathcal{E}_{ij} = \Phi_{,ij}^{(2)}$ in Cartesian coordinates. Taking these derivatives in spherical coordinates and evaluating in the usual spherical orthonormal basis yields the tidal field components $\mathcal{E}_{\hat{\theta}\hat{\theta}}, \mathcal{E}_{\hat{\theta}\hat{\phi}}, \mathcal{E}_{\hat{\phi}\hat{\phi}}$ near the origin $r = 0$. The particular combination of relevance to us (see below) is in this way determined to be

$$\mathcal{E}_{\hat{\phi}\hat{\phi}} - \mathcal{E}_{\hat{\theta}\hat{\theta}} - 2i\mathcal{E}_{\hat{\theta}\hat{\phi}} = \frac{8\pi\sqrt{6}M_2}{5b^3} \sum_{m=-2}^2 {}_2Y_{2m}(\theta, \phi) Y_{2m}^*(\theta_0, \phi_0). \quad (4.2)$$

Here the functions ${}_2Y_{2m}(\theta, \phi)$ are spin-weighted spherical harmonics [18].

Return now to the black hole binary. The region near BH1, including LARF1, can be described as a perturbed Kerr black hole, and so can be covered by Boyer-Lindquist coordinates (t, r, θ, ϕ) . We would like to solve the Teukolsky equation [15] in this region for the Weyl tensor component $\psi_0(r, \theta, \phi)$. If we were considering a single perturbed Kerr black hole as the entire spacetime, the asymptotic form of ψ_0 as $r/M_1 \rightarrow \infty$ would be the combination $\mathcal{E}_{\hat{\phi}\hat{\phi}} - \mathcal{E}_{\hat{\theta}\hat{\theta}} - 2i\mathcal{E}_{\hat{\theta}\hat{\phi}}$ of the external tidal field [13], since ψ_0 vanishes for an unperturbed black hole. In our binary system, ψ_0 acquires this asymptotic form for $M_1 \ll r \ll b$, i.e., in LARF1, with the tidal field \mathcal{E}_{ij} being that of BH2. To lowest order, this tidal field is exactly the Newtonian field of a body of mass M_2 at separation b , which was calculated above; in particular, the angular dependence of ψ_0 in LARF1 is given by Eq. (4.2), but with θ and ϕ now representing Boyer-Lindquist coordinates, and θ_0 and ϕ_0 now representing BH2's angular coordinates as seen in LARF1. Therefore, to solve for the perturbation ψ_0 on BH1, we impose the LARF1 boundary condition

$$\psi_0 \rightarrow \frac{8\pi\sqrt{6}M_2}{5b^3} \sum_{m=-2}^2 {}_2Y_{2m}(\theta, \phi) Y_{2m}^*(\theta_0, \phi_0) \quad (4.3)$$

for $M_1 \ll r \ll b$.

It now remains to solve the Teukolsky equation for ψ_0 with the boundary condition (4.3) and an appropriate no-outgoing-wave boundary condition at the black hole horizon [15]. We express ψ_0 as a sum of modes

$$\psi_0 = \sum_{m=-2}^2 {}_2Y_{2m}(\theta, \phi) R_m(r) \quad (4.4)$$

and solve the radial Teukolsky equation for $R_m(r)$ subject to the no-outgoing-wave boundary condition at the horizon. This yields the radial functions (Eq. (5.7) in Ch. VI of [19])

$$R_m(r) = C_m x^{\gamma_m - 2} (1+x)^{-\gamma_m - 2} F(-4, 1, -1 + 2\gamma_m, -x) \quad (4.5)$$

for $m \neq 0$. Here

$$\gamma_m = \frac{im\chi_1}{2(1 - \chi_1^2)^{1/2}}, \quad x = \frac{r - r_{H1}}{2M_1(1 - \chi_1^2)^{1/2}}, \quad (4.6)$$

and F is a hypergeometric function. The $m = 0$ mode can be treated separately; since a full treatment reveals that this mode does not contribute to the rates of change of black hole parameters, I ignore it here. The constants C_m are determined by imposing the LARF1 boundary condition (4.3); we obtain

$$C_m = \frac{8\pi M_2}{5b^3\sqrt{6}} \gamma_m (\gamma_m + 1) (4\gamma_m^2 - 1) Y_{2m}^*(\theta_0, \phi_0). \quad (4.7)$$

The leading-order tidal distortion of BH1 due to the presence of a stationary companion of mass

M_2 has now been determined. This information allows us to calculate the rates of change of BH1 quantities using the results of Hawking and Hartle [14]. In fact, given the modal decomposition (4.4), we can easily obtain the relevant rates using explicit formulas provided by Teukolsky and Press [16]. The results are $dM_1/dt = 0$ and

$$\begin{aligned}\frac{dA_1}{dt} &= \frac{64\pi M_1^5 M_2^2 \chi_1^2 \sin^2 \theta_0}{5b^6 (1 - \chi_1^2)^{1/2}} \left(1 - \frac{3}{4}\chi_1^2 + \frac{15}{4}\chi_1^2 \sin^2 \theta_0 \right), \\ \frac{dS_1}{dt} &= -\frac{(1 - \chi_1^2)^{1/2}}{8\pi\chi_1} \frac{dA_1}{dt} = -\frac{8M_1^5 M_2^2}{5b^6} \chi_1 \sin^2 \theta_0 \left(1 - \frac{3}{4}\chi_1^2 + \frac{15}{4}\chi_1^2 \sin^2 \theta_0 \right).\end{aligned}\tag{4.8}$$

Here θ_0 is BH2's θ -coordinate—that is, its polar angle with respect to \mathbf{S}_1 —as measured in LARF1.

Since the effects of only the leading-order tidal field were taken into account above, the expressions (4.8) are actually valid for any companion body of mass M_2 , not just a black hole. The rates (4.8) of area increase and spin-down have already been derived by Teukolsky [19] in the extreme-mass-ratio limit, i.e., for $M_2 \ll M_1$. The derivation I have presented above establishes the validity of the expressions (4.8) for comparable-mass black holes as well. Hartle and collaborators [13, 14, 20, 21] have shown that the spin-down of a black hole by an external tidal field is analogous to the Newtonian tidal friction process in a planet-moon system.

The results (4.8) will be used in the next sections to obtain the corresponding formulas for a binary undergoing circular motion.

4.4 Equatorial orbits

In this section I study special configurations of the binary in which the black holes are in a circular orbit and have their spins aligned or anti-aligned with the orbital angular momentum \mathbf{L}_N . In these scenarios there is no precession of the angular momenta: the spins remain aligned or anti-aligned with \mathbf{L}_N . As a result, the companion to each of the holes orbits in the hole's equatorial plane; more precisely, the external tidal field seen by each of the holes rigidly rotates about an axis parallel or antiparallel to the hole's spin axis.

In Boyer-Lindquist coordinates (t, r, θ, ϕ) centered on BH1, with \mathbf{S}_1 along $\theta = 0$, the t - and ϕ -dependence of the companion's tidal field enter in the combination $\phi - \Omega t$. The rotation rate Ω of the tidal field as seen in LARF1 is to leading order $\Omega = (\hat{\mathbf{L}}_N \cdot \hat{\mathbf{S}}_1)\Omega_N$, where $\hat{\mathbf{L}}_N \cdot \hat{\mathbf{S}}_1 = +1$ (-1) for a prograde (retrograde) orbit. The first correction to this expression for Ω is $O(v^2)$ higher (see Eq. (3.12) in [4]), and will be ignored in this paper.

4.4.1 Instantaneous rates

In the rigid ϕ -rotation case, simple formulas given in Eqs. (7.21) of [13] (and reproduced below) specify the rates of change of black hole quantities in terms of a horizon integral I that depends on the particular perturbing gravitational fields present:

$$\begin{aligned} \frac{dS_1}{dt} &= (\Omega - \Omega_{H1})I, & \frac{dM_1}{dt} &= \Omega \frac{dS_1}{dt} = \Omega(\Omega - \Omega_{H1})I, \\ \frac{\kappa_1}{8\pi} \frac{dA_1}{dt} &= (\Omega - \Omega_{H1}) \frac{dS_1}{dt} = (\Omega - \Omega_{H1})^2 I. \end{aligned} \tag{4.9}$$

In terms of ingoing Kerr coordinates $(V, r, \theta, \tilde{\phi})$ (see, e.g., [22] for a definition), I is an integral of a function of θ and $(\tilde{\phi} - \Omega V)$ over a constant- V slice of the horizon. Since $\tilde{\phi}$ -rotations are isometries of the horizon metric, I is independent of V .

Consider an expansion of I in powers of $M_1\Omega$, which is $O(v^3)$ and hence much smaller than 1. The zeroth-order part $I_0 = I|_{\Omega=0}$ is independent of Ω and, in our situation of binary black holes, can be easily obtained from the results for a stationary companion. From Eqs. (4.9), we have $\dot{S}_1|_{\Omega=0} = -\Omega_{H1}I_0$, where an overdot indicates a time derivative. But $\Omega = 0$ corresponds to a stationary companion, and in this case we have an explicit expression for \dot{S}_1 in Eqs. (4.8). Equating \dot{S}_1 in Eqs. (4.8) to $-\Omega_{H1}I_0$ yields

$$I_0(\theta_0) = \frac{16r_{H1}}{5b^6} M_1^5 M_2^2 \sin^2 \theta_0 \left(1 - \frac{3}{4}\chi_1^2 + \frac{15}{4}\chi_1^2 \sin^2 \theta_0 \right), \tag{4.10}$$

where $\theta_0 = \pi/2$ for the equatorial orbits considered in this section. The general expression (4.10) with a wider range of values for θ_0 will be used for non-equatorial orbits in the next section. Since the first correction to I_0 in the expansion of I in powers of $M_1\Omega$ is $O(M_1\Omega) = O(v^3)$, I will approximate I by I_0 throughout this paper.

Note that Eqs. (4.9) are, strictly speaking, valid only for constant rotation rates Ω . In our situation, radiation reaction drives the binary together and so Ω changes during inspiral. However, the timescale for these changes is the inspiral timescale $\tau_{\text{ins}} \sim bv^{-6}$, where “ \sim ” means “is of the order of”; this is to be compared to the timescale κ_1^{-1} on which the divergence and shear of the null generators of the horizon probe the future [13, 14, 17]. By assumption, χ_1 is less than or equal to 0.998; this implies $\kappa_1^{-1} < 34M_1$, so κ_1^{-1} is much smaller than τ_{ins} . Therefore Eqs. (4.9) are valid in our binary system to a very good approximation. The various timescales of interest to us will be discussed in more detail below.

Note also that Eqs. (4.9) [and, in addition, Eqs. (4.11), (4.21), and (4.22) below] are valid only when integrated over time intervals much longer than κ_1^{-1} (see the discussion in Sec. VI.C.11 of [13]). In this paper, I am interested in integrating these equations over the entire inspiral—that is, over

time intervals of order τ_{ins} —so this condition is certainly satisfied.

After putting $I_0(\pi/2)$ and $\Omega = (\hat{\mathbf{L}}_N \cdot \hat{\mathbf{S}}_1)\Omega_N$ into Eqs. (4.9), we obtain the following rates of change of BH1 quantities for a circular orbit with spins aligned or anti-aligned with \mathbf{L}_N :

$$\begin{aligned}
\frac{dS_1}{dt} &= (\Omega - \Omega_{H1})I_0(\pi/2) \\
&= \left(\frac{dJ}{dt}\right)_N \frac{v^5}{4} \left(\frac{M_1}{M}\right)^3 (1 + 3\chi_1^2) \left\{ -\chi_1 + 2(\hat{\mathbf{L}}_N \cdot \hat{\mathbf{S}}_1) \left[1 + (1 - \chi_1^2)^{1/2} \right] \frac{M_1}{M} v^3 \right\}, \\
\frac{dM_1}{dt} &= \Omega(\Omega - \Omega_{H1})I_0(\pi/2) \\
&= \left(\frac{dE}{dt}\right)_N \frac{v^5}{4} \left(\frac{M_1}{M}\right)^3 (1 + 3\chi_1^2) \left\{ -(\hat{\mathbf{L}}_N \cdot \hat{\mathbf{S}}_1)\chi_1 + 2 \left[1 + (1 - \chi_1^2)^{1/2} \right] \frac{M_1}{M} v^3 \right\}, \\
\frac{dA_1}{dt} &= 8\pi\kappa_1^{-1}(\Omega - \Omega_{H1})^2 I_0(\pi/2) \\
&= \frac{64\pi M_1^5 M_2^2 (1 + 3\chi_1^2)}{5b^6 (1 - \chi_1^2)^{1/2}} \left\{ \chi_1 - 2(\hat{\mathbf{L}}_N \cdot \hat{\mathbf{S}}_1) \left[1 + (1 - \chi_1^2)^{1/2} \right] \frac{M_1}{M} v^3 \right\}^2.
\end{aligned} \tag{4.11}$$

In these formulas, the Newtonian quadrupole expressions for energy and angular momentum flow to infinity are [23, 24]

$$\left(\frac{dE}{dt}\right)_N = \frac{32}{5}\eta^2 v^{10}, \quad \left(\frac{dJ}{dt}\right)_N = \frac{32}{5}\eta^2 M v^7, \tag{4.12}$$

where $v = (M/b)^{1/2}$ and $\eta = M_1 M_2 / M^2$. Note that energy and angular momentum absorption/emission by a rotating (nonrotating) black hole is 2.5 (4) post-Newtonian orders below the quadrupole emission (4.12) to infinity, as first derived in the extreme-mass-ratio limit by Poisson and Sasaki [25] and Tagoshi, Mano, and Takasugi [2]. The rates of change for BH2 are obtained by exchanging the subscripts $1 \leftrightarrow 2$ in the formulas (4.11).

The energy absorption/emission rate \dot{M}_1 given above agrees in the limit $M_2/M \rightarrow 0$ with the lowest-order expression obtained by Tagoshi, Mano, and Takasugi [2]. Those authors have calculated this rate in the extreme-mass-ratio limit, for a circular equatorial orbit, to much higher order in v than I have done here. However, their results are not applicable to comparable-mass binaries, while the formulas (4.11) are.

The expressions (4.11) are valid even if BH1's companion is not a black hole, provided the companion's mass is substituted for M_2 .

4.4.2 Total changes during inspiral

In this subsection, I integrate Eqs. (4.11) to calculate the total changes in M_1 , S_1 , and A_1 during inspiral. I take into account only the leading-order Newtonian effects of radiation reaction when

computing orbital decay; given this approximation, the orbital separation b evolves as [22, 24]

$$b(t) = b_0(1 - t/\tau_0)^{1/4}, \quad (4.13)$$

where $\tau_0 = (5/256)b_0^4(\mu M^2)^{-1}$. I also ignore all post-Newtonian corrections to the orbital angular velocity Ω_N .

It is convenient to parametrize the orbit by separation b instead of time t . The total change in a parameter, say S_1 , from infinite separation to separation b is denoted $\Delta S_1(b)$ and is calculated by integrating Eqs. (4.11). As a first approximation, the quantities M_B and S_B ($B = 1, 2$) on the right-hand sides of Eqs. (4.11) can be considered constants during inspiral. The reason is that the timescales for evolution of M_B and S_B are much longer than the inspiral timescale $\tau_{\text{ins}} \sim bv^{-6}$. Indeed, the timescale for evolution of the masses is $\tau_M \sim M_B/\dot{M}_B \sim bv^{-13}$, and for the spins is $\tau_S \sim S_B/\dot{S}_B \sim bv^{-10}$. So $\tau_M \gg \tau_S \gg \tau_{\text{ins}}$ and we can safely treat M_B and S_B ($B = 1, 2$) as constants on the right-hand sides of Eqs. (4.11) when integrating over inspiral.

With these approximations, the normalized changes in BH1 parameters from infinite separation to separation b are

$$\begin{aligned} \frac{\Delta S_1}{M_1^2}(b) &= \frac{\eta M_1}{4M} (1 + 3\chi_1^2) \left\{ -\frac{\chi_1}{4} \left(\frac{M}{b}\right)^2 + (\hat{\mathbf{L}}_N \cdot \hat{\mathbf{S}}_1) \left[1 + (1 - \chi_1^2)^{1/2}\right] \frac{2M_1}{7M} \left(\frac{M}{b}\right)^{7/2} \right\}, \\ \frac{\Delta M_1}{M_1}(b) &= \frac{\eta}{4} \left(\frac{M_1}{M}\right)^2 (1 + 3\chi_1^2) \left\{ -(\hat{\mathbf{L}}_N \cdot \hat{\mathbf{S}}_1) \frac{\chi_1}{7} \left(\frac{M}{b}\right)^{7/2} + \left[1 + (1 - \chi_1^2)^{1/2}\right] \frac{M_1}{5M} \left(\frac{M}{b}\right)^5 \right\}, \\ \frac{\Delta A_1}{A_1}(b) &= \frac{\eta M_1^2 (1 + 3\chi_1^2)}{8M r_{H1} (1 - \chi_1^2)^{1/2}} \left[\frac{\chi_1^2}{2} \left(\frac{M}{b}\right)^2 - (\hat{\mathbf{L}}_N \cdot \hat{\mathbf{S}}_1) \frac{8\chi_1}{7} \frac{r_{H1}}{M} \left(\frac{M}{b}\right)^{7/2} \right. \\ &\quad \left. + \frac{4}{5} \left(\frac{r_{H1}}{M}\right)^2 \left(\frac{M}{b}\right)^5 \right], \end{aligned} \quad (4.14)$$

where $r_{H1} = M_1[1 + (1 - \chi_1^2)^{1/2}]$. To evaluate these changes, one can put into the formulas (4.14) the values of M_1 , S_1 , and A_1 at infinite separation or, for that matter, at any separation much larger than M , because the changes in these quantities during inspiral are small. Once again, the changes for BH2 are obtained by exchanging the subscripts $1 \leftrightarrow 2$ in the expressions (4.14).

The normalized parameter changes (4.14), evaluated at different stages during inspiral, are displayed in Tables 4.1-4.3 for an equal-mass binary ($M_1 = M_2$) with $\hat{\mathbf{L}}_N \cdot \hat{\mathbf{S}}_1 = 1$. Since a binary composed of slowly rotating black holes is expected to be undergoing a transition from inspiral to merger by the time it reaches $b = 6M$, the endpoint of integration is chosen to be $b = 6M$ when $\chi_1 = 0$ and 0.5. For rapidly rotating holes ($\chi_1 = \chi_2 = 0.998$), the endpoint is chosen to be $b = 2M$. The assumption $M \ll b$ is not valid at and near these endpoints. The results presented here are

χ_1	$b/M = 100$	$b/M = 20$	$b/M = 6$	$b/M = 2$
0	$9. \times 10^{-10}$	$2. \times 10^{-7}$	$2. \times 10^{-5}$	
0.5	$-7. \times 10^{-7}$	$-2. \times 10^{-5}$	$-2. \times 10^{-4}$	
0.998	$-3. \times 10^{-6}$	$-8. \times 10^{-5}$	$-8. \times 10^{-4}$	$-6. \times 10^{-3}$

Table 4.1: Normalized change $\Delta S_1/M_1^2$ in spin evaluated at $b/M=100, 20,$ and 6 for an equal-mass binary with $\hat{\mathbf{L}}_N \cdot \hat{\mathbf{S}}_1 = 1$. For rapidly rotating holes ($\chi_1 = \chi_2 = 0.998$), this change is also evaluated at $b/M = 2$.

χ_1	$b/M = 100$	$b/M = 20$	$b/M = 6$	$b/M = 2$
0	$3. \times 10^{-13}$	$1. \times 10^{-9}$	$4. \times 10^{-7}$	
0.5	$-2. \times 10^{-10}$	$-5. \times 10^{-8}$	$-3. \times 10^{-6}$	
0.998	$-9. \times 10^{-10}$	$-2. \times 10^{-7}$	$-2. \times 10^{-5}$	$-6. \times 10^{-4}$

Table 4.2: Normalized change $\Delta M_1/M_1$ in mass evaluated at $b/M=100, 20,$ and 6 for an equal-mass binary with $\hat{\mathbf{L}}_N \cdot \hat{\mathbf{S}}_1 = 1$. For rapidly rotating holes ($\chi_1 = \chi_2 = 0.998$), this change is also evaluated at $b/M = 2$.

most accurate in the early stages of inspiral, when the black holes are widely separated, and are a rough estimate of the true parameter changes in the late stages of inspiral.

4.4.3 Effect on orbital evolution

The orbital evolution of binary black holes is affected by the absorption/emission of energy and angular momentum by the holes. In particular, the number of orbits—and hence the number of gravitational-wave cycles emitted to infinity—changes when black hole absorption/emission is accounted for. To estimate this effect, let us consider a circular, nearly Newtonian binary, with spins aligned or anti-aligned with \mathbf{L}_N , that is losing orbital energy and angular momentum to infinity via Newtonian quadrupole radiation (4.12), and to the black holes via tidal interaction as specified

χ_1	$b/M = 100$	$b/M = 20$	$b/M = 6$	$b/M = 2$
0	$6. \times 10^{-13}$	$2. \times 10^{-9}$	$8. \times 10^{-7}$	
0.5	$2. \times 10^{-7}$	$5. \times 10^{-6}$	$4. \times 10^{-5}$	
0.998	$5. \times 10^{-5}$	$1. \times 10^{-3}$	$1. \times 10^{-2}$	$7. \times 10^{-2}$

Table 4.3: Normalized change $\Delta A_1/A_1$ in horizon area evaluated at $b/M=100, 20,$ and 6 for an equal-mass binary with $\hat{\mathbf{L}}_N \cdot \hat{\mathbf{S}}_1 = 1$. For rapidly rotating holes ($\chi_1 = \chi_2 = 0.998$), this change is also evaluated at $b/M = 2$.

$M(M_\odot)$	$M_1/M_2 = 1$	$M_1/M_2 = 2$	$M_1/M_2 = 4$
5	0.07 (0.07)	0.11 (0.11)	0.23 (0.24)
20	0.05 (0.07)	0.07 (0.10)	0.16 (0.22)
50	0.03 (0.06)	0.05 (0.08)	0.11 (0.18)

Table 4.4: Change ΔN in the number of gravitational-wave cycles due to black hole absorption/emission, for various values of total mass M and mass ratio M_1/M_2 . The initial separation is such that the wave frequency is 10 Hz and the spins satisfy $\chi_1 = \chi_2 = 0.998$ and $\hat{\mathbf{L}}_N \cdot \hat{\mathbf{S}}_1 = \hat{\mathbf{L}}_N \cdot \hat{\mathbf{S}}_2 = 1$. The numbers without parentheses are for a final separation b_f of $6M$; those with parentheses are for b_f equal to the larger of $2M$ or the separation at which the wave frequency is 1000 Hz.

by Eqs. (4.11). Since $\dot{M}_B = \Omega \dot{S}_B = (\hat{\mathbf{L}}_N \cdot \hat{\mathbf{S}}_B) \Omega_N \dot{S}_B$ ($B = 1, 2$), circular, nearly Newtonian orbits remain circular. Therefore the evolution of the separation $b(t)$ is determined by setting the rate of change of Newtonian orbital energy (given by $E_{\text{orb}} = -M_1 M_2 / 2b$) to the rate of energy loss to infinity and to the holes:

$$\frac{dE_{\text{orb}}}{dt} = \frac{M_1 M_2}{2b^2} \frac{db}{dt} = - \left(\frac{dE}{dt} \right)_N - \frac{dM_1}{dt} - \frac{dM_2}{dt}, \quad (4.15)$$

where $(dE/dt)_N$ is given in Eqs. (4.12) and \dot{M}_1 in Eqs. (4.11) [with \dot{M}_2 obtained by exchanging the subscripts $1 \leftrightarrow 2$ in Eqs. (4.11)].

The number of gravitational-wave cycles N_1 emitted to infinity from initial time t_i to final time t_f (corresponding to separations b_i and b_f) is given by

$$N = \int_{t_i}^{t_f} dt \frac{\Omega_N}{\pi} = \frac{1}{\pi} \int_{b_i}^{b_f} db \frac{dt}{db} \left(\frac{M}{b^3} \right)^{1/2}, \quad (4.16)$$

where dt/db is determined from Eq. (4.15). This number is to be compared with the number of cycles N_2 obtained by ignoring black hole absorption/emission of energy and angular momentum, i.e., by setting \dot{E}_{orb} equal to $-(dE/dt)_N$. The difference $\Delta N = N_1 - N_2$ measures the effect of black hole absorption/emission on the binary's orbital evolution.

The values of ΔN obtained by setting b_i to be the separation at which the gravitational-wave frequency is 10 Hz (the low-frequency end of the LIGO band), χ_1 and χ_2 to be 0.998, and the spins to be aligned with \mathbf{L}_N (i.e., $\hat{\mathbf{L}}_N \cdot \hat{\mathbf{S}}_1 = \hat{\mathbf{L}}_N \cdot \hat{\mathbf{S}}_2 = 1$) are displayed in Table 4.4 for various choices of total mass M (in units of a solar mass M_\odot) and mass ratio M_1/M_2 . In the table, the numbers without parentheses are obtained by setting $b_f = 6M$, and those with parentheses by setting b_f to be the larger of $2M$ or the separation at which the wave frequency is 1000 Hz (the high-frequency end of the LIGO band). For nonrotating black holes ($\chi_1 = \chi_2 = 0$), the corresponding values of ΔN (with $b_f = 6M$) are all less than 10^{-2} .

The values of ΔN in Table 4.4 indicate that black hole absorption/emission of energy and angular momentum during inspiral may not be an important effect for the detection (by LIGO and VIRGO) and analysis of gravitational waves from comparable-mass black holes. Indeed, post-Newtonian corrections to the equations of motion and energy loss have far greater influence on the number of wave cycles emitted by the binary [6, 7]. It should be noted, however, that black hole absorption/emission could have a much larger impact on the orbital evolution of rapidly rotating holes when they are beginning to merge, as suggested by Price and Whelan [5]. They have presented models in which the tidal torque that results from black hole absorption/emission of angular momentum plays a crucial role in the late stages of binary evolution (see Fig. 1 in [5]). The perturbative methods used in this paper (based on wide separation of the binary) are not valid in the close limit analyzed in [5].

It has been pointed out by Hughes [3] that in the extreme-mass-ratio limit, black hole absorption/emission can strongly influence the binary's orbital evolution and is an important effect for LISA.

4.5 Non-equatorial orbits

In general, binary black holes are not expected to have spins aligned with the orbital angular momentum \mathbf{L}_N . This misalignment causes the spins and orbit to precess in a complicated way due to spin-orbit and spin-spin coupling [7, 26]. Each black hole's companion is not in general confined to the hole's equatorial plane, and so the formulas in the previous section are not applicable. However, for orbits suitably close to the equatorial plane (see below for details), one can imagine using an approximation scheme in which at each instant the companion's θ -velocity is ignored; that is, the companion is taken to be rigidly rotating in the ϕ -direction at each point on the orbit. The changes in black hole parameters can then be calculated by putting the instantaneous ϕ -velocity into the rigid ϕ -rotation formulas (4.9) at each point on the orbit. In this section, I construct such an approximation scheme.

4.5.1 Description of orbit

The evolutions of the spins and orbit are described by the equations [7, 26]

$$\dot{\mathbf{S}}_B = \boldsymbol{\Omega}_{\text{spin}}^{(B)} \times \mathbf{S}_B, \quad \dot{\mathbf{L}}_N = \boldsymbol{\Omega}_{\text{orb}} \times \mathbf{L}_N - \frac{32}{5} \eta^2 M v^7 \hat{\mathbf{L}}_N, \quad (4.17)$$

for $B = 1, 2$. The orders of magnitude of the precession frequencies are $\Omega_{\text{spin}} \sim v^3 b^{-1}$ and $\Omega_{\text{orb}} \sim v^4 b^{-1}$. Since the Newtonian angular velocity is $\Omega_N \sim v b^{-1}$, both Ω_{spin} and Ω_{orb} are much smaller than Ω_N . This means that, over a few orbital periods, $\mathbf{L}_N(t)$ and $\mathbf{S}_B(t)$ do not change much due to precession. Thus, the companion's orbit as seen in LARF1 is to a good approximation confined to a

single plane with normal vector $\mathbf{n} = \hat{\mathbf{L}}_N(t)$ along the instantaneous direction of the orbital angular momentum, on timescales of a few orbital periods.

In this subsection, I analyze the trajectory of a particle in a planar, circular orbit of arbitrary orientation in a fictitious Euclidean 3-space in terms of spherical coordinates. This information will be used to specify the rotation rate and orientation of the companion's tidal field as seen in LARF1. Denote the particle's radial coordinate by b , its constant (non-negative) angular velocity by ω , and the normal to its orbital plane by \mathbf{n} . The angle of inclination of the normal with respect to the z -axis is denoted θ_n ; so $\cos \theta_n = \mathbf{n} \cdot \mathbf{e}_z = n_z$. Assume the orbit is centered on the origin, so the particle's position $\mathbf{X}(t)$ at time t is given by a rotation $R(\mathbf{n}, \omega t)$ about \mathbf{n} , by an angle ωt , of the initial position \mathbf{X}_0 .

In Cartesian coordinates, the particle's trajectory is given by $\mathbf{X}(t) = \mathbf{X}_0 \cos \omega t + (\mathbf{n} \times \mathbf{X}_0) \sin \omega t$. In terms of the particle's angular coordinates $\theta(t)$ and $\phi(t)$, $\mathbf{X}(t)$ is equal to $b[\sin \theta(t) \cos \phi(t), \sin \theta(t) \sin \phi(t), \cos \theta(t)]$. I choose the initial position to be in the equatorial plane, i.e., $Z_0 = \mathbf{X}_0 \cdot \mathbf{e}_z = 0$. This choice does not affect the orbit-averaged quantities I calculate later in this section.

The angular functions $\theta(t)$ and $\phi(t)$ can now be expressed in terms of \mathbf{n} and ω using the relations above. The quantities of interest are $\sin^2 \theta(t)$ and $\dot{\phi}(t)$, which are determined to be

$$\sin^2 \theta(t) = 1 - \sin^2 \theta_n \sin^2 \omega t, \quad \dot{\phi}(t) = \frac{\omega \cos \theta_n}{\sin^2 \theta(t)}. \quad (4.18)$$

4.5.2 Approximation scheme

Return now to our black hole binary, and go to Boyer-Lindquist coordinates (t, r, θ, ϕ) in LARF1. The companion's trajectory as seen in LARF1 will be described (to lowest order in v) by angular functions $\theta(t)$ and $\phi(t)$ given by the expressions (4.18) with ω replaced by Ω_N and θ_n now referring to the angle of inclination of $\mathbf{L}_N(t)$ with respect to $\mathbf{S}_1(t)$, that is, $\cos \theta_n = \hat{\mathbf{L}}_N(t) \cdot \hat{\mathbf{S}}_1(t)$. After these substitutions, we have

$$\sin^2 \theta(t) = 1 - \left(1 - \left[\hat{\mathbf{L}}_N(t) \cdot \hat{\mathbf{S}}_1(t)\right]^2\right) \sin^2 \Omega_N t, \quad \dot{\phi}(t) = \frac{\Omega_N \hat{\mathbf{L}}_N(t) \cdot \hat{\mathbf{S}}_1(t)}{\sin^2 \theta(t)}. \quad (4.19)$$

Since θ_n is now time dependent, these expressions are meaningful only when used to calculate orbit-averaged quantities.

Consider the regime in which $\sin^2 \theta(t)$ and $\dot{\phi}(t)$ are slowly varying; more precisely, require them to be approximately constant on the timescale κ_1^{-1} associated with the horizon. As noted before, this is the timescale on which the null generators of the horizon probe the future [13, 14, 17]. The teleological behavior of the horizon is, however, exponentially limited; that is, the influence of future events on the horizon decays exponentially in time, with decay rate κ_1 (see, e.g., the discussion of teleological Green functions in [13]). We thus require $\left|\dot{\phi}/\ddot{\phi}\right|$ and $\left|(1/\sin^2 \theta)d(\sin^2 \theta)/dt\right|^{-1}$ [which

are the same to leading order by Eqs. (4.19)] to be only several times larger than κ_1^{-1} , rather than orders of magnitude larger.

By assumption, $\chi_1 \leq 0.998$, so κ_1^{-1} is less than $34M_1$. Our requirement can then be expressed as

$$34\alpha M_1 \Omega_N \leq \frac{\sin^2 \theta(t)}{\sin^2 \theta_n |\sin 2\Omega_N t|} \quad (4.20)$$

for all t , where α is a number roughly in the range 2-4. A sufficient condition for this constraint to be satisfied is $\cot^2 \theta_n \geq 34\alpha M_1 \Omega_N$. This requires $\hat{\mathbf{L}}_N(t)$ to be near one of the polar axes $\pm \hat{\mathbf{S}}_1(t)$, which correspond to $\theta = 0, \pi$; or, equivalently, the orbital plane must be near the equatorial plane.

We are interested in separations as small as $b = 6M$, so Ω_N can be as large as $(6^{3/2}M)^{-1}$. For this reason, I impose the constraint $\cot^2 \theta_n \geq 34\alpha 6^{-3/2}$ and set α to be approximately 3, obtaining the approximate constraints $0 \leq \theta_n \lesssim \pi/9$ or $8\pi/9 \lesssim \theta_n \leq \pi$. In other words, $\hat{\mathbf{L}}_N(t)$ is within 20-degree cones around the polar axes, or, equivalently, the inclination angle of the orbit with respect to the equatorial plane is less than or (approx.) equal to 20 degrees.

For the approximation scheme in this section to be valid, we require further that in the horizon's reference frame, the external tidal field should rotate primarily in the ϕ -direction and not significantly in the θ -direction. More precisely, we require $|\dot{\theta}| \ll |\dot{\phi} - \Omega_{H1}|$. The rates of change presented in Eqs. (4.21) and (4.22) below are subject to this condition. For most values of χ_1 , this condition is automatically satisfied throughout inspiral (down to $b = 6M$). Even if it is not satisfied at some point during inspiral, the restriction on θ_n discussed above ensures that the effect of the θ -motion, when integrated over inspiral, is negligible compared to that of the ϕ -motion, for almost all values of χ_1 .

With the above restriction on θ_n , we can at each instant take $\sin^2 \theta(t)$ and $\dot{\phi}(t)$ to be constant relative to the horizon timescale κ_1^{-1} , and apply the rigid ϕ -rotation formulas (4.9) with the instantaneous values $\theta(t)$ and $\dot{\phi}(t)$ put in. This yields

$$\begin{aligned} \frac{dS_1}{dt} &= [\dot{\phi}(t) - \Omega_{H1}] I_0[\theta(t)], & \frac{dM_1}{dt} &= \dot{\phi}(t) [\dot{\phi}(t) - \Omega_{H1}] I_0[\theta(t)], \\ \frac{\kappa_1}{8\pi} \frac{dA_1}{dt} &= [\dot{\phi}(t) - \Omega_{H1}]^2 I_0[\theta(t)], \end{aligned} \quad (4.21)$$

where $\theta(t)$ and $\dot{\phi}(t)$ are given by Eqs. (4.19) and I_0 by Eq. (4.10).

4.5.3 Orbit-averaged quantities

Next I would like to average these rates of change over an orbit assuming the binary's masses, spins, separation, and orbital angular momentum are approximately constant over an orbital period. This assumption is justified by the following ordering of the relevant timescales: $\Omega_N^{-1} \ll \Omega_{\text{spin}}^{-1}, \Omega_{\text{orb}}^{-1} \ll$

$\tau_{\text{ins}} \ll \tau_S \ll \tau_M$. We can therefore take all the quantities on the right-hand sides of Eqs. (4.21) except $\theta(t)$ and $\dot{\phi}(t)$ to be constant, to a good approximation, when averaging over an orbit. Denote orbit averages by angular brackets $\langle \rangle$; so, for example, $\langle \dot{S}_1 \rangle = (\Omega_N/2\pi) \int_0^{2\pi/\Omega_N} \dot{S}_1 dt$. Plugging the expressions (4.19) into Eqs. (4.21) and performing the orbit averages (as defined above) yields

$$\begin{aligned}
\left\langle \frac{dS_1}{dt} \right\rangle &= \frac{r_{H1}}{10b^6} M_1^5 M_2^2 \left(16(1 + 3\chi_1^2) \left\{ 2\Omega_N \mathcal{N}_1(t) - \Omega_{H1} [\mathcal{N}_1^2(t) + 1] \right\} \right. \\
&\quad \left. + 15\chi_1^2 [\mathcal{N}_1^2(t) - 1] \left\{ 4\Omega_N \mathcal{N}_1(t) - \Omega_{H1} [3\mathcal{N}_1^2(t) + 1] \right\} \right), \\
\left\langle \frac{dM_1}{dt} \right\rangle &= \frac{2r_{H1}}{5b^6} M_1^5 M_2^2 \Omega_N \mathcal{N}_1(t) \left(2\Omega_N (4 - 3\chi_1^2) \text{sign}[\mathcal{N}_1(t)] - 8\Omega_{H1} (1 + 3\chi_1^2) \right. \\
&\quad \left. + 15\chi_1^2 \left\{ 2\Omega_N \mathcal{N}_1(t) + \Omega_{H1} [1 - \mathcal{N}_1^2(t)] \right\} \right), \\
\left\langle \frac{dA_1}{dt} \right\rangle &= \frac{8\pi r_{H1}^2 M_1^5 M_2^2}{5b^6 (1 - \chi_1^2)^{1/2}} \left((16 - 12\chi_1^2) \left\{ \Omega_{H1}^2 [\mathcal{N}_1^2(t) + 1] - 4\Omega_{H1} \Omega_N \mathcal{N}_1(t) \right. \right. \\
&\quad \left. \left. + 2\Omega_N^2 |\mathcal{N}_1(t)| \right\} + 15\chi_1^2 \left\{ \Omega_{H1}^2 [3\mathcal{N}_1^4(t) + 2\mathcal{N}_1^2(t) + 3] \right. \right. \\
&\quad \left. \left. - 8\Omega_{H1} \Omega_N \mathcal{N}_1(t) [\mathcal{N}_1^2(t) + 1] + 8\Omega_N^2 \mathcal{N}_1^2(t) \right\} \right),
\end{aligned} \tag{4.22}$$

where $\mathcal{N}_B(t) = \hat{\mathbf{L}}_N(t) \cdot \hat{\mathbf{S}}_B(t)$ for $B = 1, 2$. The corresponding expressions for BH2 can be obtained by exchanging the subscripts $1 \leftrightarrow 2$ in Eqs. (4.22). Note that these equations are valid only for $\mathcal{N}_B(t)$ suitably close to ± 1 , as discussed above. The formulas (4.22) can be applied to a black hole in a binary with any companion body (e.g., a neutron star) that has mass M_2 and is well separated from the hole.

Numerical integration of Eqs. (4.22) using the 2.5 post-Newtonian equations of motion for spinning bodies ([7] and references therein) yields results comparable to those in Tables 4.1-4.3.

4.6 Discussion

Having obtained the leading-order changes in a black hole's mass and spin during inspiral [see Eqs. (4.14)], we must check whether these changes exceed the ambiguities inherent in the definitions of mass and spin [9]. Denote by δM and δS the magnitudes of the mass and spin ambiguities. From Eqs. (1.8) in [9],

$$\delta M \sim \frac{ML^2}{\mathcal{R}^2}, \quad \delta S \sim \frac{M^3 L}{\mathcal{R}^2}, \tag{4.23}$$

where M and L are the mass and size of the (isolated) body in question, and \mathcal{R} is the external universe's radius of curvature. For a black hole in a binary, say BH1, $L \sim M_1$ and $\mathcal{R}^2 \sim b^3/M_2$.

This implies

$$\frac{\delta M_1}{M_1} \sim \frac{\delta S_1}{M_1^2} \sim \eta \frac{M_1}{M} \left(\frac{M}{b}\right)^3. \quad (4.24)$$

From Eqs. (4.14), the changes ΔM_1 and ΔS_1 from infinite separation to separation b are

$$\frac{\Delta M_1}{M_1} \sim \eta \left(\frac{M_1}{M}\right)^2 \left(\frac{M}{b}\right)^{7/2}, \quad \frac{\Delta S_1}{M_1^2} \sim \eta \frac{M_1}{M} \left(\frac{M}{b}\right)^2. \quad (4.25)$$

So, at separation b , we have

$$\frac{\Delta M_1}{\delta M_1} \sim \frac{M_1}{M} \left(\frac{M}{b}\right)^{1/2}, \quad \frac{\Delta S_1}{\delta S_1} \sim \frac{b}{M}. \quad (4.26)$$

We conclude that $|\Delta S_1|$ exceeds the ambiguity δS_1 in the definition of spin, but $|\Delta M_1|$ does not rise above δM_1 . Note that the concept of tidal work is unambiguous [10–12].

When analyzing initial data that contain a black hole and represent the interface between inspiral and merger, one can define and calculate the hole’s mass and spin in different ways, giving different answers corresponding to the ambiguities δM and δS discussed above. Since δM is larger than $|\Delta M|$, the hole’s mass can be considered constant during inspiral to the same level of accuracy as used in defining mass. On the other hand, $|\Delta S|$ exceeds δS , so the hole’s spin cannot be considered constant; however, as Table 4.1 indicates, the changes in spin are small during inspiral.

The results of this work—in particular, Eqs. (4.14) and (4.22)—can be used to relate the spin and horizon area of a black hole in a particular initial data set to the spin and horizon area the hole had when infinitely separated from its companion.

Acknowledgments

I am grateful to Kip Thorne for helpful discussions and advice, and to Scott Hughes for useful comments on the manuscript. This research was supported in part by NSF grant PHY-0099568 and NASA grant NAG5-10707.

4.7 Bibliography

- [1] S. F. P. Zwart and S. L. W. McMillan, *Astrophys. J.* **528**, L17 (2000); astro-ph/9910061.
- [2] H. Tagoshi, S. Mano, and E. Takasugi, *Prog. Theor. Phys.* **98**, 829 (1997); gr-qc/9711072.
- [3] S. A. Hughes, gr-qc/0104041.
- [4] K. Alvi, *Phys. Rev. D* **61**, 124013 (2000); gr-qc/9912113.

- [5] R. H. Price and J. T. Whelan, gr-qc/0107029.
- [6] L. Blanchet *et al.*, Phys. Rev. Lett. **74**, 3515 (1995); gr-qc/9501027.
- [7] L. E. Kidder, Phys. Rev. D **52**, 821 (1995); gr-qc/9506022.
- [8] K. S. Thorne, Astrophys. J. **191**, 507 (1974).
- [9] K. S. Thorne and J. B. Hartle, Phys. Rev. D **31**, 1815 (1985).
- [10] P. Purdue, Phys. Rev. D **60**, 104054 (1999); gr-qc/9901086.
- [11] I. S. Booth and J. D. E. Creighton, Phys. Rev. D **62**, 067503 (2000); gr-qc/0003038.
- [12] M. Favata, Phys. Rev. D **63**, 064013 (2001); gr-qc/0008061.
- [13] *Black Holes: The Membrane Paradigm*, edited by K. S. Thorne, R. H. Price, and D. A. Macdonald (Yale University Press, New Haven, 1986).
- [14] S. W. Hawking and J. B. Hartle, Commun. Math. Phys. **27**, 283 (1972).
- [15] S. A. Teukolsky, Astrophys. J. **185**, 635 (1973).
- [16] S. A. Teukolsky and W. H. Press, Astrophys. J. **193**, 443 (1974).
- [17] B. Carter, in *General Relativity: An Einstein Centenary Survey*, edited by S. W. Hawking and W. Israel (Cambridge University Press, New York, 1979), p. 294.
- [18] J. N. Goldberg *et al.*, J. Math. Phys. **8**, 2155 (1967).
- [19] S. A. Teukolsky, Ph.D. thesis, California Institute of Technology, 1973 (unpublished).
- [20] J. B. Hartle, Phys. Rev. D **8**, 1010 (1973).
- [21] J. B. Hartle, Phys. Rev. D **9**, 2749 (1974).
- [22] C. W. Misner, K. S. Thorne, and J. A. Wheeler, *Gravitation* (Freeman, San Francisco, 1973).
- [23] P. C. Peters and J. Mathews, Phys. Rev. **131**, 435 (1963).
- [24] P. C. Peters, Phys. Rev. **136**, B1224 (1964).
- [25] E. Poisson and M. Sasaki, Phys. Rev. D **51**, 5753 (1995); gr-qc/9412027.
- [26] T. A. Apostolatos, C. Cutler, G. J. Sussman, and K. S. Thorne, Phys. Rev. D **49**, 6274 (1994).

Chapter 5

First-order symmetrizable hyperbolic formulations of Einstein's equations including lapse and shift as dynamical fields

Submitted for publication to *Classical and Quantum Gravity*.

Abstract

First-order hyperbolic systems are promising as a basis for numerical integration of Einstein's equations. In previous work, the lapse and shift have typically not been considered part of the hyperbolic system and have been prescribed independently. This can be expensive computationally, especially if the prescription involves solving elliptic equations. Therefore, including the lapse and shift in the hyperbolic system could be advantageous for numerical work. In this paper, two first-order symmetrizable hyperbolic systems are presented that include the lapse and shift as dynamical fields and have only physical characteristic speeds.

5.1 Introduction

There has been considerable interest recently in first-order hyperbolic systems for Einstein's equations ([1–3] and references therein). These systems have been used in the past to prove that general relativity has a well-posed initial value formulation [4, 5]. Much of the recent interest is based on the advantages that hyperbolic formulations offer to numerical simulations [6, 7]. The main advantage is that imposing physical boundary conditions is much easier in the framework of a hyperbolic system than a non-hyperbolic one. This is especially true for boundary conditions inside a black hole horizon [6, 7]. Indeed, if the hyperbolic system has only physical characteristic speeds—that is, if the characteristic fields propagate only on the light cones of spacetime or normal to the time

slices—then the boundary condition inside the horizon on fields propagating into the numerical grid has no effect on the dynamics outside the horizon. Therefore, in this case, any convenient boundary condition can be imposed inside the horizon. This is a significant advantage when simulating black holes.

It is particularly important to come up with stable numerical schemes to evolve black holes since simulations of black hole collisions have an important role to play in the detection and analysis of gravitational waves. These simulations will be used in several stages of data analysis for gravitational wave detectors such as the Laser Interferometer Gravitational-Wave Observatory. First, the simulations are expected to yield a bank of gravitational waveforms that will be used to detect the presence of a gravitational signal in the detector output. Once a signal has been detected, numerical simulations will be used to extract binary parameters such as masses from the signal, to test general relativity, and to do other interesting physics.

Previous numerical work has generally been restricted to systems that do not treat the lapse and shift as dynamical fields, but rather take them to be external to the system and prescribe them independently. Freedom in choosing these gauge fields corresponds to freedom in choosing coordinates for spacetime. This freedom can be used for a variety of purposes, e.g., to prevent the occurrence of coordinate singularities and reduce coordinate shear [8], and to adapt the coordinate system to the particular problem under consideration. When simulating black holes, it is helpful to choose the shift so that numerical grid points do not fall into the holes. When simulating binary black holes, it may be advantageous to implement gauge conditions which generate corotating coordinates [9, 10].

Some of the favored gauge choices in numerical relativity [8, 10] require solution of elliptic equations for the lapse and shift, which is expensive computationally. It would be more efficient to evolve the gauge fields as part of the hyperbolic system. However, it is important to keep some freedom in choosing the gauge in order to allow the coordinates to be adapted to fit specific needs. The purpose of this paper is to present two first-order symmetrizable hyperbolic systems which include the lapse and shift as dynamical fields and allow four functions of spacetime to be specified freely in the gauge prescription.

Previous work in this direction includes [11], in which the authors present a weakly hyperbolic system¹ that incorporates the gauge fields in the system, and [12], in which the authors present a new class of dynamical gauge conditions which are not, however, part of a first-order hyperbolic system.

The first hyperbolic system presented in this paper is based on the work of Fischer and Marsden [4]; it uses generalized harmonic coordinates and evolves 50 fields. It is promising as a basis for

¹I refer to the full system including lapse and shift as dynamical fields; if the shift is considered a fixed spacetime function and not a dynamical field, then the system becomes strongly hyperbolic.

numerical work. The second system is based on the work of Kidder, Scheel, and Teukolsky [3] and Lindblom and Scheel [13]; it evolves 70 fields. This system is not practical for numerical implementation. Its main use is theoretical: it allows one to show that any solution to Einstein's equations in any gauge can be obtained using hyperbolic evolution of the entire metric, including the gauge fields. Both systems have only physical characteristic speeds.

In this paper, Greek indices range over 0, 1, 2, 3 and Latin indices over 1, 2, 3. The sign conventions are those of [14] with $G = c = 1$. The analysis of this paper is done within the framework of a 3+1 split of spacetime (see, e.g., [14, 15]). In this framework, the spacetime metric is expressed as

$$g_{\mu\nu} = \begin{pmatrix} -\alpha^2 + \beta_k \beta^k & \beta_j \\ \beta_i & \gamma_{ij} \end{pmatrix}, \quad (5.1)$$

and the inverse 4-metric as

$$g^{\mu\nu} = \frac{1}{\alpha^2} \begin{pmatrix} -1 & \beta^j \\ \beta^i & \alpha^2 \gamma^{ij} - \beta^i \beta^j \end{pmatrix}, \quad (5.2)$$

where α is the lapse, β^i is the shift, γ_{ij} is the spatial 3-metric with inverse γ^{ij} , and $\beta_i = \gamma_{ij} \beta^j$. The unit normal to the time slices is denoted by n^μ .

I restrict attention in this paper to the vacuum Einstein equations.

5.2 System I

5.2.1 Fischer-Marsden system

Let us first briefly review the Fischer-Marsden system [4] for Einstein's equations. They employ the 50 fields $g_{\mu\nu}$, $\tilde{k}_{\mu\nu} = \partial_t g_{\mu\nu}$, and $d_{i\mu\nu} = \partial_i g_{\mu\nu}$. Using harmonic coordinates, they reduce the vacuum Einstein equations $R_{\mu\nu} = 0$ to the following first-order symmetric hyperbolic system:

$$\begin{aligned} \partial_t g_{\mu\nu} &= \tilde{k}_{\mu\nu}, \\ -g^{00} \partial_t \tilde{k}_{\mu\nu} - 2g^{0i} \partial_i \tilde{k}_{\mu\nu} - g^{ij} \partial_i d_{j\mu\nu} &= -2\tilde{H}_{\mu\nu}, \\ g^{ij} \partial_t d_{j\mu\nu} - g^{ij} \partial_j \tilde{k}_{\mu\nu} &= 0, \end{aligned} \quad (5.3)$$

where $\tilde{H}_{\mu\nu}$ is a function of the fields $g_{\mu\nu}, \tilde{k}_{\mu\nu}, d_{i\mu\nu}$ only and not their derivatives. This system is obtained by setting to zero a reduced form of the Ricci tensor that is equal to the full Ricci tensor in harmonic coordinates. Using earlier work of Choquet-Bruhat ([16] and references therein), Fischer and Marsden show that if the initial data for (5.3) satisfy the harmonic coordinate condition and

the constraint equations, then the solution of (5.3) corresponding to these initial data continues to satisfy the harmonic coordinate condition off the initial hypersurface. Therefore, a solution of (5.3) is also a solution of the vacuum Einstein equations.

The Fischer-Marsden system (5.3) has two drawbacks when considered as a basis for numerical integration of Einstein's equations. The first is the restriction to harmonic coordinates: this eliminates the freedom to choose coordinates best suited for the physical problem at hand. While harmonic coordinates have been used successfully in some previous work ([17] and references therein) and are being strongly advocated for a wide variety of applications [17], it has not yet been established whether they are useful for simulating black hole collisions, for example.

The second drawback is that the Fischer-Marsden system has nonphysical characteristic speeds. As discussed above, systems with only physical characteristic speeds are better suited for numerical relativity, especially for black hole simulations [6, 7]. The characteristic speeds of the Fischer-Marsden system can be calculated as follows: first write (5.3) in the form

$$\partial_t u + A^i(t, x^j, u) \partial_i u = F(t, x^j, u), \quad (5.4)$$

where u is a column vector composed of the fields ($u = (g_{\mu\nu}, \tilde{k}_{\mu\nu}, d_{i\mu\nu})^T$ for the Fischer-Marsden system), and the matrices A^i and column vector F can depend on space and time and on the fields but not their derivatives. Pick a unit spatial covector ξ_i (i.e., $\gamma^{ij} \xi_i \xi_j = 1$) and compute the eigenvalues λ of the matrix $A^i \xi_i$; λ are the characteristic speeds in the direction ξ_i . For physical characteristic speeds, we require $\lambda = -\beta^i \xi_i, -\beta^i \xi_i \pm \alpha$ (see, e.g., [3]). However, the Fischer-Marsden system has $\lambda = 0, -\beta^i \xi_i \pm \alpha$.

5.2.2 Generalized harmonic coordinates

In this paper, I modify the Fischer-Marsden system to eliminate nonphysical characteristic speeds and generalize it to include a broader range of coordinate systems. Let us begin by defining $\Gamma^\mu = g^{\alpha\beta} \Gamma^\mu_{\alpha\beta}$ and $\Gamma_\mu = g_{\mu\nu} \Gamma^\nu$, where $\Gamma^\sigma_{\alpha\beta}$ are the Christoffel symbols associated with the metric $g_{\mu\nu}$ and the coordinates x^μ . The Ricci tensor can be written as [18]

$$R_{\mu\nu} = \tilde{R}_{\mu\nu} + \nabla_{(\mu} \Gamma_{\nu)}, \quad (5.5)$$

where

$$\tilde{R}_{\mu\nu} = -\frac{1}{2} g^{\alpha\beta} \partial_\alpha \partial_\beta g_{\mu\nu} + H_{\mu\nu}(g, \partial g), \quad (5.6)$$

and

$$H_{\mu\nu} = g^{\alpha\beta} g^{\rho\sigma} (\partial_\alpha g_{\mu\rho}) (\partial_\beta g_{\nu\sigma}) - g^{\rho\alpha} g^{\sigma\beta} \Gamma_{\mu\rho\sigma} \Gamma_{\nu\alpha\beta}. \quad (5.7)$$

I generalize harmonic coordinates using Friedrich's gauge source functions [5, 6] by setting

$$\Gamma^\mu \equiv -\nabla_\alpha \nabla^\alpha x^\mu = f^\mu(t, x^j), \quad (5.8)$$

where the coordinates x^μ are treated as scalar fields in the expression $\nabla_\alpha \nabla^\alpha x^\mu$, and f^μ are arbitrary but predetermined functions of space and time. These functions can be used to tailor the coordinates to fit specific needs.

Consider the reduced equations obtained by setting

$$\tilde{R}_{\mu\nu} + \nabla_{(\mu} f_{\nu)} = 0, \quad (5.9)$$

where $f_\mu = g_{\mu\nu} f^\nu$. Equation (5.9) will be used to write down a first-order symmetrizable hyperbolic system in section 5.2.3. Hence we must show that a solution to (5.9) yields a solution to the vacuum Einstein equations $R_{\mu\nu} = 0$ under appropriate conditions. I follow an argument due to Friedrich [5, 6] which is based on earlier work by Choquet-Bruhat ([16] and references therein).

Let $g_{\mu\nu}$ be a solution to (5.9). Compute Γ^μ and $R_{\mu\nu}$ from $g_{\mu\nu}$, and let $h^\mu = \Gamma^\mu - f^\mu$. Then $R_{\mu\nu} = \tilde{R}_{\mu\nu} + \nabla_{(\mu} \Gamma_{\nu)} = \nabla_{(\mu} h_{\nu)}$ where $h_\mu = \Gamma_\mu - f_\mu$. The Einstein tensor is

$$G_{\mu\nu} = R_{\mu\nu} - \frac{R}{2} g_{\mu\nu} = \nabla_{(\mu} h_{\nu)} - \frac{1}{2} g_{\mu\nu} \nabla_\alpha h^\alpha, \quad (5.10)$$

and the contracted Bianchi identities $\nabla^\mu G_{\mu}{}^\nu = 0$ imply

$$\nabla^\mu \nabla_\mu h^\nu + R^\nu{}_\mu h^\mu = 0, \quad (5.11)$$

which is the subsidiary equation derived by Friedrich [5, 6]. Since this is a linear homogeneous wave equation for h^μ , we conclude that if $h^\mu = 0$ and $\nabla_\nu h^\mu = 0$ on the initial hypersurface, then $h^\mu = 0$ in a neighborhood of the initial hypersurface. This implies $R_{\mu\nu} = \nabla_{(\mu} h_{\nu)} = 0$ in this neighborhood. So $g_{\mu\nu}$ is a solution to the vacuum Einstein equations in a neighborhood of the initial hypersurface. This solution is obtained in coordinates satisfying $\Gamma^\mu = f^\mu$.

We therefore need to ensure

$$[\Gamma^\mu - f^\mu]_{t=0} = 0, \quad (5.12)$$

$$[\nabla_\nu (\Gamma^\mu - f^\mu)]_{t=0} = 0, \quad (5.13)$$

where the time slice $t = 0$ represents the initial hypersurface. Given a spatial 3-metric γ_{ij} and an extrinsic curvature K_{ij} that satisfy the constraint equations, we will construct initial data for our system such that (5.12) is satisfied. Equation (5.13) will then follow from the constraint equations.

This will be discussed in detail in section 5.2.4.

5.2.3 System I

Define the fields

$$k_{\mu\nu} = \partial_t g_{\mu\nu} - \beta^j \partial_j g_{\mu\nu}, \quad (5.14)$$

$$d_{i\mu\nu} = \partial_i g_{\mu\nu}. \quad (5.15)$$

Here and throughout this section, β^i will be considered convenient shorthand for $-g^{0i}/g^{00}$, and similarly α for $(-g^{00})^{-1/2}$. The new field $k_{\mu\nu}$ is a replacement for $\tilde{k}_{\mu\nu}$ and has been introduced to eliminate nonphysical characteristic speeds.

The first-order symmetrizable hyperbolic system presented in this section is based on the 50 fields $g_{\mu\nu}$, $k_{\mu\nu}$, and $d_{i\mu\nu}$. The definition (5.14) yields an expression for $\partial_t g_{\mu\nu}$ in terms of the 50 fields and their first spatial derivatives. An expression for $\partial_t d_{i\mu\nu}$ is obtained through equality of mixed partials: $\partial_t d_{i\mu\nu} = \partial_i \partial_t g_{\mu\nu} = \partial_i (k_{\mu\nu} + \beta^j d_{j\mu\nu})$. Finally, an expression for $\partial_t k_{\mu\nu}$ is obtained from the reduced equation (5.9). To summarize, we have the first-order system

$$\partial_t g_{\mu\nu} + \frac{g^{0i}}{g^{00}} \partial_i g_{\mu\nu} = k_{\mu\nu}, \quad (5.16)$$

$$\partial_t k_{\mu\nu} + \frac{g^{0i}}{g^{00}} \partial_i k_{\mu\nu} + \frac{\gamma^{ij}}{g^{00}} \partial_i d_{j\mu\nu} = -\frac{\gamma^{ij}}{g^{00}} g^{0\alpha} d_{i\mu\nu} k_{\alpha j} + \frac{2}{g^{00}} [H_{\mu\nu} + \partial_{(\mu} f_{\nu)} - \Gamma^\alpha{}_{\mu\nu} f_\alpha], \quad (5.17)$$

$$\partial_t d_{i\mu\nu} + \frac{g^{0j}}{g^{00}} \partial_j d_{i\mu\nu} - \partial_i k_{\mu\nu} = \frac{\gamma^{jk}}{g^{00}} g^{0\alpha} d_{j\mu\nu} d_{i\alpha k}, \quad (5.18)$$

where $\gamma^{ij} = (g^{00})^{-2}(g^{00}g^{ij} - g^{0i}g^{0j})$ is the inverse of the 3-metric γ_{ij} . In (5.17), $H_{\mu\nu}$ is to be expressed via (5.7) in terms of the fields only and not their derivatives [using (5.14) and (5.15)]. In addition, in (5.16)–(5.18), the inverse 4-metric is considered to be a function of $g_{\mu\nu}$ and not a fundamental field. In deriving these expressions, I have used the relation

$$\partial_\alpha g^{\mu\nu} = -g^{\mu\theta} g^{\nu\lambda} \partial_\alpha g_{\theta\lambda}. \quad (5.19)$$

The system (5.16)–(5.18) will be called system I.

5.2.4 Initial data

It remains to specify how to set initial data for system I to ensure (5.12) and (5.13) are satisfied. Begin with a solution (γ_{ij}, K_{ij}) of the constraint equations, where K_{ij} represents the extrinsic curvature of the initial hypersurface. First set $g_{ij} = \gamma_{ij}$. We are free to choose $g_{0\mu}$ on the initial hypersurface as long as $g_{00} < g_{0i}g_{0j}\gamma^{ij}$. This requirement is equivalent to $\alpha^2 > 0$ and implies $g^{00} < 0$. Freedom

in choosing $g_{0\mu}$ corresponds to freedom in choosing the lapse and shift at $t = 0$.

We now have $g_{\mu\nu}|_{t=0}$. Next set $d_{i\mu\nu} = \partial_i g_{\mu\nu}|_{t=0}$. The final step is to fill in $k_{\mu\nu}$ from K_{ij} and the requirement (5.12). The extrinsic curvature can be expressed as

$$K_{ij} = -\frac{1}{2\alpha}(\partial_t \gamma_{ij} - \beta^k \partial_k \gamma_{ij} - 2\gamma_{k(i} \partial_{j)} \beta^k). \quad (5.20)$$

From this we deduce

$$k_{ij} = -2\alpha K_{ij} + 2g_{k(i} \partial_{j)} \beta^k, \quad (5.21)$$

which can be used to fill in k_{ij} at $t = 0$.

The quantities $k_{0\mu}$ are obtained from the requirement (5.12). Writing out Γ^μ in terms of the metric and its first derivatives, we obtain

$$\Gamma^0 = -\alpha^{-3}(\partial_t \alpha - \beta^i \partial_i \alpha + \alpha^2 K), \quad (5.22)$$

$$\Gamma^i = -\alpha^{-2}(\partial_t \beta^i - \beta^j \partial_j \beta^i) + \alpha^{-3}(\partial_t \alpha - \beta^j \partial_j \alpha + \alpha^2 K) \beta^i - \alpha^{-1} \gamma^{ij} \partial_j \alpha + {}^{(3)}\Gamma^i_{jk} \gamma^{jk}, \quad (5.23)$$

where $K = \gamma^{ij} K_{ij}$, and ${}^{(3)}\Gamma^i_{jk}$ are the Christoffel symbols associated with the 3-metric γ_{ij} and the spatial coordinates x^j . Setting $\Gamma^\mu = f^\mu$ gives us expressions for $\partial_t \alpha$ and $\partial_t \beta^i$ which we use to fill in $k_{0\mu}$ at $t = 0$:

$$k_{0i} = B_i + \beta^j k_{ij}, \quad (5.24)$$

$$k_{00} = 2\alpha^3(\alpha f^0 + K) + 2\beta^i B_i + \beta^i \beta^j k_{ij}, \quad (5.25)$$

where

$$B_i = -\alpha^2(g_{i\mu} f^\mu + \alpha^{-1} \partial_i \alpha - {}^{(3)}\Gamma_{ijk} \gamma^{jk}). \quad (5.26)$$

The initial data for system I is now complete and satisfies the constraint equations

$$G_{\mu\nu} n^\nu|_{t=0} = 0 \quad (5.27)$$

and the requirement (5.12). This in fact implies that the requirement (5.13) is satisfied. The argument follows earlier work [16] on the reduction of Einstein's equations using harmonic coordinates. From (5.10) and (5.27), we deduce

$$2n^\nu \nabla_{(\mu} h_{\nu)} - n_\mu \nabla_\alpha h^\alpha = 0. \quad (5.28)$$

Here and in the remainder of the paragraph, all quantities are evaluated at $t = 0$. We know $h^\mu \equiv \Gamma^\mu - f^\mu = 0$ on the initial hypersurface, so $v^\nu \nabla_\nu h^\mu = 0$ for any spatial vector v^μ (i.e., for

v^μ satisfying $v^\mu n_\mu = 0$). It remains to show $n^\nu \nabla_\nu h^\mu = 0$. By contracting (5.28) with v^μ , we obtain $v^\mu n^\nu \nabla_\nu h_\mu = 0$. Furthermore, $\nabla_\alpha h^\alpha = -n^\mu n^\nu \nabla_\mu h_\nu$. Contracting (5.28) with n^μ , we obtain $n^\mu n^\nu \nabla_\mu h_\nu = 0$. It follows that $n^\nu \nabla_\nu h^\mu = 0$ and so (5.13) is satisfied.

Therefore, a solution $(g_{\mu\nu}, k_{\mu\nu}, d_{i\mu\nu})$ to system I with initial data as constructed above yields a solution $g_{\mu\nu}$ to the vacuum Einstein equations.

5.2.5 Hyperbolicity of system I

System I is symmetrizable hyperbolic. To see this, let $u = (g_{\mu\nu}, k_{\mu\nu}, d_{1\mu\nu}, d_{2\mu\nu}, d_{3\mu\nu})^T$ and write equations (5.16)-(5.18) in the form (5.4). This determines the 50×50 matrices A^i to be

$$A^i = \begin{pmatrix} -\beta^i I & 0 & 0 & 0 & 0 \\ 0 & -\beta^i I & -\alpha^2 \gamma^{i1} I & -\alpha^2 \gamma^{i2} I & -\alpha^2 \gamma^{i3} I \\ 0 & -\delta_1^i I & -\beta^i I & 0 & 0 \\ 0 & -\delta_2^i I & 0 & -\beta^i I & 0 \\ 0 & -\delta_3^i I & 0 & 0 & -\beta^i I \end{pmatrix}. \quad (5.29)$$

Here and in equation (5.30), 0 is the 10×10 zero matrix and I is the 10×10 identity matrix. It can be checked easily that the positive definite symmetric 50×50 matrix

$$H = \begin{pmatrix} I & 0 & 0 & 0 & 0 \\ 0 & \alpha^{-2} I & 0 & 0 & 0 \\ 0 & 0 & \gamma^{11} I & \gamma^{12} I & \gamma^{13} I \\ 0 & 0 & \gamma^{12} I & \gamma^{22} I & \gamma^{23} I \\ 0 & 0 & \gamma^{13} I & \gamma^{23} I & \gamma^{33} I \end{pmatrix}, \quad (5.30)$$

is a symmetrizer for the system, i.e., HA^i are symmetric matrices.

Moreover, system I has only physical characteristic speeds; that is, the eigenvalues of $A^i \xi_i$ are $\lambda_+ = -\beta^i \xi_i + \alpha$, $\lambda_0 = -\beta^i \xi_i$, and $\lambda_- = -\beta^i \xi_i - \alpha$. Let $\xi^i = \gamma^{ij} \xi_j$. A complete set of eigenvectors for $A^i \xi_i$ is: (i) the 10 eigenvectors $-\alpha k_{\mu\nu} + \sum_{i=1}^3 \xi_i d_{i\mu\nu}$, each with eigenvalue λ_+ ; (ii) the 10 eigenvectors $g_{\mu\nu}$, the 10 eigenvectors $\xi^3 d_{1\mu\nu} - \xi^1 d_{3\mu\nu}$, and the 10 eigenvectors $\xi^2 d_{1\mu\nu} - \xi^1 d_{2\mu\nu}$, each with eigenvalue λ_0 ; and (iii) the 10 eigenvectors $\alpha k_{\mu\nu} + \sum_{i=1}^3 \xi_i d_{i\mu\nu}$, each with eigenvalue λ_- .

5.3 System II

In this section, all indices are lowered and raised by the spatial 3-metric γ_{ij} and its inverse γ^{ij} . The second system presented in this paper is based on a hyperbolic system in [3], which is in turn based on the ADM equations [19]. The system in [3], called system 1, employs the 30 fields γ_{ij} , K_{ij} , and

$$d_{kij} = \partial_k \gamma_{ij}. \quad (5.31)$$

It is obtained by densitizing the lapse and adding multiples of the constraint equations to the evolution equations. The relevant constraints are the Hamiltonian constraint

$$C = \frac{1}{2}({}^{(3)}R - K_{ij}K^{ij} + K^2) = 0, \quad (5.32)$$

the momentum constraints

$$C_i = D_j K_i^j - D_i K = 0, \quad (5.33)$$

and the constraint

$$C_{ijkl} = \partial_{[i} d_{j]kl} = 0, \quad (5.34)$$

where ${}^{(3)}R$ and D_i are the Ricci scalar and covariant derivative associated with γ_{ij} , and $K = \gamma^{ij} K_{ij}$.

System 1 has five free parameters that govern how to densitize the lapse and how much of the constraints to add; these parameters determine the system's hyperbolicity. In fact, it has been shown [13] that for a certain range of these parameters, system 1 is symmetrizable hyperbolic and has only physical characteristic speeds.

Here I construct a first-order symmetrizable hyperbolic system based on system 1 that includes the lapse and shift in the system. Let us begin by defining the densitized lapse

$$Q = \ln(\alpha \gamma^{-1/2}), \quad (5.35)$$

where $\gamma = \det(\gamma_{ij})$. Next define the new fields

$$\begin{aligned} Q_i &= \partial_i Q, & Q_{ij} &= \partial_i \partial_j Q, \\ b_i^j &= \partial_i \beta^j, & b_{ij}^k &= \partial_i \partial_j \beta^k. \end{aligned} \quad (5.36)$$

Note that $Q_{ij} = Q_{(ij)}$ and $b_{ij}^k = b_{(ij)}^k$. The hyperbolic system presented in this section is based on the 70 fields γ_{ij} , K_{ij} , d_{kij} , Q , Q_i , Q_{ij} , β^i , b_i^j , b_{ij}^k .

Expressions for time derivatives of these fields are obtained as follows. First, $\partial_t \gamma_{ij}$ is obtained

from (5.20):

$$\partial_t \gamma_{ij} - \beta^k \partial_k \gamma_{ij} = -2\alpha K_{ij} + 2\gamma_{k(i} b_j)^k. \quad (5.37)$$

This is one of the ADM evolution equations with the new fields (5.36) substituted in. Here and henceforth, it is understood that α is to be rewritten in terms of Q using (5.35). Following [3], I add $\zeta_1 \alpha \gamma_{ij} C$ and $\zeta_2 \alpha \gamma^{mn} C_{m(ij)n}$ to the second ADM evolution equation (which is equation (2.9) in [3]), where ζ_1 and ζ_2 are free parameters. Rewriting this equation in terms of the new fields (5.36), we obtain

$$\begin{aligned} \partial_t K_{ij} &= \beta^k \partial_k K_{ij} - \frac{1}{2} \alpha \gamma^{mn} [\partial_m d_{nij} + 2\partial_{(i} d_{j)mn} - (1 - \zeta_2) \partial_{(i} d_{|mn|j)} - (1 + \zeta_2) \partial_m d_{(ij)n} \\ &\quad - \zeta_1 \gamma_{ij} \gamma^{kl} (\partial_m d_{kln} - \partial_k d_{lmn})] + 2K_{k(i} b_j)^k - \alpha [2K_{im} K^m_j - K K_{ij} + Q_{ij} \\ &\quad + (d_{(ij)m} - \frac{1}{2} d_{mij}) (\tilde{d}^m - d^m - Q^m) + d^{mn}{}_i d_{[nm]j} - \frac{3}{4} d_{imn} d_j{}^{mn} + Q_i Q_j \\ &\quad + Q_{(i} d_{j)} + \frac{1}{4} \tilde{d}_i d_j] + \frac{1}{2} \zeta_1 \alpha \gamma_{ij} (\tilde{d}_m d^m - \tilde{d}_m \tilde{d}^m - \frac{1}{4} d_m d^m - \frac{1}{2} d_{klm} d^{mkl} \\ &\quad + \frac{3}{4} d_{klm} d^{klm} - K_{mn} K^{mn} + K^2), \end{aligned} \quad (5.38)$$

where $d_i = \gamma^{jk} d_{ijk}$ and $\tilde{d}_i = \gamma^{jk} d_{jki}$.

Using equality of mixed partials, we have $\partial_t d_{kij} = \partial_k \partial_t \gamma_{ij}$ which, together with a spatial derivative of (5.37), yields an evolution equation for d_{kij} . Following [3], I add $\zeta_3 \alpha \gamma_{k(i} C_{j)}$ and $\zeta_4 \alpha \gamma_{ij} C_k$ to this equation and use (5.36) to obtain

$$\begin{aligned} \partial_t d_{kij} &= \beta^m \partial_m d_{kij} + \alpha \gamma^{mn} [\zeta_3 (\gamma_{k(i} \partial_{|m} K_{n|j)}) - \gamma_{k(i} \partial_{j)} K_{mn}) + \zeta_4 \gamma_{ij} (\partial_m K_{nk} - \partial_k K_{mn})] \\ &\quad - 2\alpha \partial_k K_{ij} + 2\gamma_{m(i} b_j)^m + d_{mij} b_k{}^m + 2d_{km(i} b_j)^m \\ &\quad - \alpha K_{ij} (2Q_k + d_k) + \alpha \zeta_4 \gamma_{ij} [K_{km} (\frac{1}{2} d^m - \tilde{d}^m) + \frac{1}{2} K^{mn} d_{kmn}] \\ &\quad + \alpha \zeta_3 [\gamma_{k(i} K_{j)m} (\frac{1}{2} d^m - \tilde{d}^m) + \frac{1}{2} K^{mn} \gamma_{k(i} d_{j)mn}], \end{aligned} \quad (5.39)$$

where ζ_3 and ζ_4 are free parameters. The parameters $(\zeta_1, \zeta_2, \zeta_3, \zeta_4)$ in the above equations correspond to the parameters $(\gamma, \zeta, \eta, \chi)$ in [3]. The parameter σ in [3] has been set to 1/2 by the definition (5.35).

The next step is to specify evolution equations for the lapse density and shift. Spatial derivatives of these equations will then yield evolution equations for the fields (5.36). I consider a particular form for the lapse density and shift evolution equations, a form that results in a symmetrizable hyperbolic system but yet allows four functions of spacetime to be freely specified. The equations are

$$\partial_t Q - \beta^i \partial_i Q = \psi^0(t, x^j; Q), \quad (5.40)$$

$$\partial_t \beta^i - \beta^j \partial_j \beta^i = \psi^i(t, x^k; Q, \beta^m), \quad (5.41)$$

where ψ^μ are arbitrary but predetermined functions of space, time, and lapse density (and of shift in the case of ψ^i).

Evolution equations for the fields (5.36) are obtained by taking spatial derivatives of (5.40) and (5.41), and using equality of mixed partials. For example, $\partial_t Q_i = \partial_i \partial_t Q = \partial_i (\beta^j \partial_j Q + \psi^0)$. We obtain

$$\partial_t Q_i - \beta^j \partial_j Q_i = Q_j b_i^j + \partial_i \psi^0, \quad (5.42)$$

$$\partial_t Q_{ij} - \beta^k \partial_k Q_{ij} = 2Q_{k(i} b_{j)}^k + Q_k b_{ij}^k + \partial_i \partial_j \psi^0, \quad (5.43)$$

$$\partial_t \beta_i^j - \beta^k \partial_k \beta_i^j = b_i^k b_k^j + \partial_i \psi^j, \quad (5.44)$$

$$\partial_t b_{ij}^k - \beta^m \partial_m b_{ij}^k = 2b_{(i}^m b_{j)}^k + b_{ij}^m b_m^k + \partial_i \partial_j \psi^k, \quad (5.45)$$

where it is understood that the spatial derivatives of ψ^μ are to be written, using (5.36), in terms of fields only and not derivatives of fields.

When the system (5.37)-(5.45), called system II, is put in the form (5.4) with $u = (\gamma_{ij}, K_{ij}, d_{kij}, Q, Q_i, Q_{ij}, \beta^i, b_i^j, b_{ij}^k)^T$, the 70×70 matrices A^i have the block diagonal form

$$A^i = \begin{pmatrix} \tilde{A}_{30 \times 30}^i & 0_{30 \times 40} \\ 0_{40 \times 30} & -\beta^i I_{40 \times 40} \end{pmatrix}. \quad (5.46)$$

The nontrivial parts \tilde{A}^i of A^i come from the evolution equations (5.37)-(5.39) for the 30 fields $\gamma_{ij}, K_{ij}, d_{kij}$. Since the principal parts of these equations are identical (after relabeling the free parameters as indicated above) to the principal parts of the system I evolution equations for $\gamma_{ij}, K_{ij}, d_{kij}$ given in [3], the matrices \tilde{A}^i are identical to the corresponding matrices in [3]. This implies that if system I is symmetrizable, so is system II. Indeed, the matrix

$$H = \begin{pmatrix} \tilde{H}_{30 \times 30} & 0_{30 \times 40} \\ 0_{40 \times 30} & I_{40 \times 40} \end{pmatrix}, \quad (5.47)$$

where $\tilde{H}_{30 \times 30}$ symmetrizes system I, is a symmetrizer for system II. In other words, if the 30×30 matrices $\tilde{H} \tilde{A}^i$ are symmetric, then so are the 70×70 matrices $H A^i$. In addition, it is clear from (5.46) that $Q, Q_i, Q_{ij}, \beta^i, b_i^j, b_{ij}^k$ are eigenvectors of $A^i \xi_i$, all with eigenvalue $\lambda = -\beta^i \xi_i$, i.e., they all propagate normal to the time slices.

It has been shown [13] that system I in [3] is symmetrizable and has only physical characteristic

speeds when the free parameters are chosen as follows:

$$\zeta_3 = \frac{-8}{5 + 10\zeta_1 + 7\zeta_2 + 6\zeta_1\zeta_2}, \quad \zeta_4 = -\frac{4 + 10\zeta_1 + 4\zeta_2 + 6\zeta_1\zeta_2}{5 + 10\zeta_1 + 7\zeta_2 + 6\zeta_1\zeta_2},$$

$$-5/3 < \zeta_2 < 0, \quad 5 + 10\zeta_1 + 7\zeta_2 + 6\zeta_1\zeta_2 \neq 0. \quad (5.48)$$

We conclude that for the same choice of parameters, system II is symmetrizable and has only physical characteristic speeds.

System II is not practical for numerical implementation. Since the lapse density and shift evolution equations (5.40) and (5.41) decouple from the rest of the system, they can be evolved separately to obtain the lapse density and shift as spacetime functions. These functions can then be substituted into system I in [3]. Therefore, the full seventy-field system II does not need to be evolved; the thirty-field system I suffices.

However, system II is useful from a theoretical point of view. Consider a solution of Einstein's equations in an arbitrary gauge. Using the densitized lapse and shift from this solution, compute the left-hand sides of equations (5.40) and (5.41). Set the spacetime functions ψ^μ equal to these computed quantities. Take initial values for the fields in system II from the spacetime metric under consideration. System II can now be used, with these initial values and with ψ^μ as defined above, to obtain the entire metric by evolving hyperbolic equations that are part of a symmetrizable system with only physical characteristic speeds. So system II can be used to obtain any solution of Einstein's equations in any gauge using hyperbolic evolution for the entire metric, including the densitized lapse and shift. Note, however, that the lapse is not evolved directly in this system; it is obtained from the densitized lapse via equation (5.35).

5.4 Future directions

An important future research direction is to study and understand the stability of numerical implementations of system I. It has been shown in previous work [3] that some hyperbolic systems are more stable than others when used to simulate black holes in three spatial dimensions. The reasons for this behavior are not yet understood. Another future research direction is to explore how to use the free functions f^μ in system I to control the coordinate system.

Acknowledgments

I am grateful to Lee Lindblom and Mark Scheel for valuable discussions and for sharing their results before publication, and to Olivier Sarbach, Kip Thorne, and Manuel Tiglio for useful comments on the manuscript. This research was supported in part by NSF grant PHY-9900776.

5.5 Bibliography

- [1] H. Friedrich and A. D. Rendall, *Lect. Notes Phys.* **540**, 127 (2000).
- [2] O. A. Reula, *Living Rev. Relativity* **1** (1998), [Online article]: cited on 23 Apr 2002, URL <http://www.livingreviews.org/Articles/Volume1/1998-3reula/>.
- [3] L. E. Kidder, M. A. Scheel, and S. A. Teukolsky, *Phys. Rev. D* **64**, 064017 (2001).
- [4] A. E. Fischer and J. E. Marsden, *Commun. Math. Phys.* **28**, 1 (1972).
- [5] H. Friedrich, *Commun. Math. Phys.* **100**, 525 (1985).
- [6] H. Friedrich, *Class. Quantum Grav.* **13**, 1451 (1996).
- [7] A. Anderson and J. W. York, *Phys. Rev. Lett.* **82**, 4384 (1999).
- [8] L. Smarr and J. W. York, *Phys. Rev. D* **17**, 2529 (1978).
- [9] P. R. Brady, J. D. E. Creighton, and K. S. Thorne, *Phys. Rev. D* **58**, 061501 (1998).
- [10] D. Garfinkle, C. Gundlach, J. Isenberg, and N. ÓMurchadha, *Class. Quantum Grav.* **17**, 3899 (2000).
- [11] C. Bona, J. Massó, E. Seidel, and J. Stela, *Phys. Rev. Lett.* **75**, 600 (1995).
- [12] M. Alcubierre, B. Brügmann, D. Pollney, E. Seidel, and R. Takahashi, *Phys. Rev. D* **64**, 061401(R) (2001).
- [13] L. Lindblom and M. Scheel, in preparation.
- [14] C. W. Misner, K. S. Thorne, and J. A. Wheeler, *Gravitation* (Freeman, San Francisco, 1973).
- [15] J. W. York, in *Sources of Gravitational Radiation*, edited by L. L. Smarr (Cambridge University Press, Cambridge, 1979), p. 83.
- [16] Y. Bruhat, in *Gravitation: an Introduction to Current Research*, edited by L. Witten (Wiley, New York, 1962), p. 130.
- [17] D. Garfinkle, *Phys. Rev. D* **65**, 044029 (2002).
- [18] V. Fock, *The Theory of Space, Time and Gravitation* (MacMillan, New York, 1964).
- [19] R. Arnowitt, S. Deser, and C. W. Misner, in *Gravitation: an Introduction to Current Research*, edited by L. Witten (Wiley, New York, 1962), p. 227.